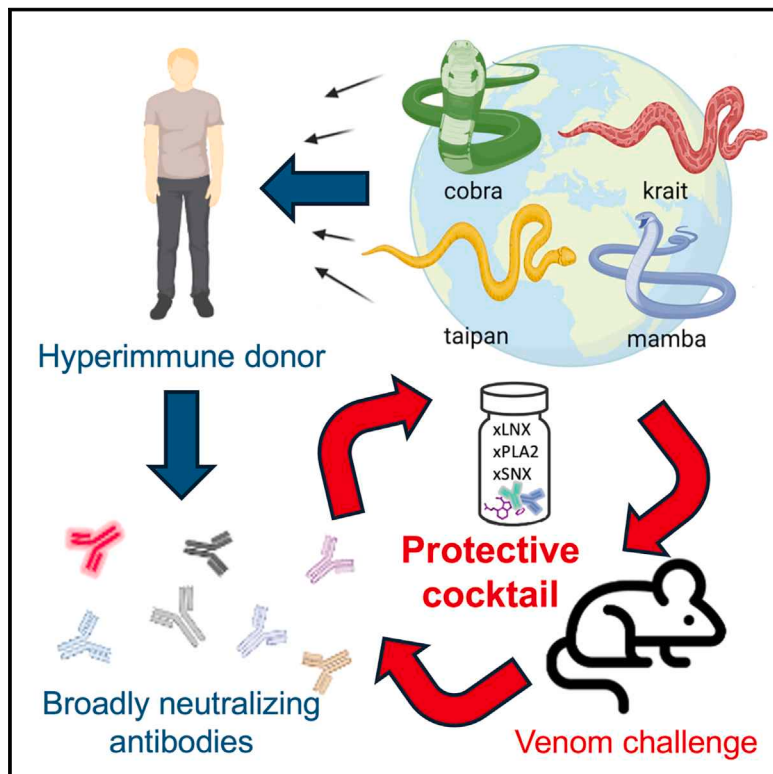


# Snake venom protection by a cocktail of varespladib and broadly neutralizing human antibodies

## Graphical abstract



## Authors

Jacob Glanville, Mark Bellin,  
Sergei Pletnev, ..., Hannah Hirou,  
Tracy Liu, Peter D. Kwong

## Correspondence

jake@centivax.com (J.G.),  
pdk3@cumc.columbia.edu (P.D.K.)

## In brief

To combat snake bites from diverse species, this work identifies broadly neutralizing antibodies from a donor hyperimmune to snake venom, and it demonstrates that a combination of two of the identified antibodies with an inhibitory drug can protect mice from envenomation by medically important snakes found around the world.

## Highlights

- We report a systematic method for the construction of a broad-spectrum snake antivenom
- Broadly neutralizing antitoxin antibodies were identified from a venom-immune subject
- Broad toxin neutralization involved recognition of conserved toxin-receptor interfaces
- A 3-agent cocktail blocked envenomation by 19 diverse WHO Category 1 and Category 2 snakes

Article

# Snake venom protection by a cocktail of varespladib and broadly neutralizing human antibodies

Jacob Glanville,<sup>1,4,5,\*</sup> Mark Bellin,<sup>1,4</sup> Sergei Pletnev,<sup>2,4</sup> Baoshan Zhang,<sup>2,4</sup> Joel Christian Andrade,<sup>1</sup> Sangil Kim,<sup>1</sup> David Tsao,<sup>1</sup> Raffaello Verardi,<sup>2</sup> Rishi Bedi,<sup>1</sup> Sindy Liao,<sup>1</sup> Raymond Newland,<sup>1</sup> Nicholas L. Bayless,<sup>1</sup> Sawsan Youssef,<sup>1</sup> Ena S. Tully,<sup>2</sup> Tatiana Bylund,<sup>2</sup> Sujeong Kim,<sup>1</sup> Hannah Hirou,<sup>1</sup> Tracy Liu,<sup>2</sup> and Peter D. Kwong<sup>2,3,\*</sup>

<sup>1</sup>Centivax, Inc., 1 Tower Place, Suite 800, South San Francisco, CA 94080, USA

<sup>2</sup>Vaccine Research Center, National Institute of Allergy and Infectious Diseases, National Institutes of Health, Bethesda, MD 20892, USA

<sup>3</sup>Aaron Diamond AIDS Research Center, Columbia University Vagelos College of Physicians and Surgeons, and Department of Biochemistry and Molecular Biophysics, Columbia University, New York, NY 10032, USA

<sup>4</sup>These authors contributed equally

<sup>5</sup>Lead contact

\*Correspondence: [jake@centivax.com](mailto:jake@centivax.com) (J.G.), [pdk3@cumc.columbia.edu](mailto:pdk3@cumc.columbia.edu) (P.D.K.)

<https://doi.org/10.1016/j.cell.2025.03.050>

## SUMMARY

Snake envenomation is a neglected tropical disease, with 600 species causing over 100,000 deaths and 300,000 permanent disabilities in humans annually. Broadly neutralizing antibodies and broad chemical inhibitors have been proposed as solutions, but how to develop a therapeutically effective cocktail and the number of required components have been unclear. To address this gap, we iteratively recovered two broadly neutralizing antivenom antibodies from the memory B cells of a hyperimmune human donor with extensive snake venom exposure. The antibodies recognized conserved neutralizing epitopes on prevalent long and short snake neurotoxins, with crystal structures revealing antibody mimicry of the interfaces between these neurotoxins and their host target, the nicotinic acetylcholine receptor. We combined and tested these antibodies and the phospholipase inhibitor varespladib. A 3-component cocktail rescued animals from whole-venom challenge of all species in a 19-member WHO Category 1 and Category 2 elapid diversity set, with complete protection against most snakes observed.

## INTRODUCTION

Snake-bite envenoming, which was added to the World Health Organization (WHO) list of neglected tropical diseases in 2017,<sup>1</sup> causes 81,000–138,000 deaths and 300,000–400,000 permanent disabilities annually.<sup>2,3</sup> For over a century, the standard treatment has been antivenom—a polyclonal serum derived from animals immunized with venom from one or more species of snakes.<sup>4</sup>

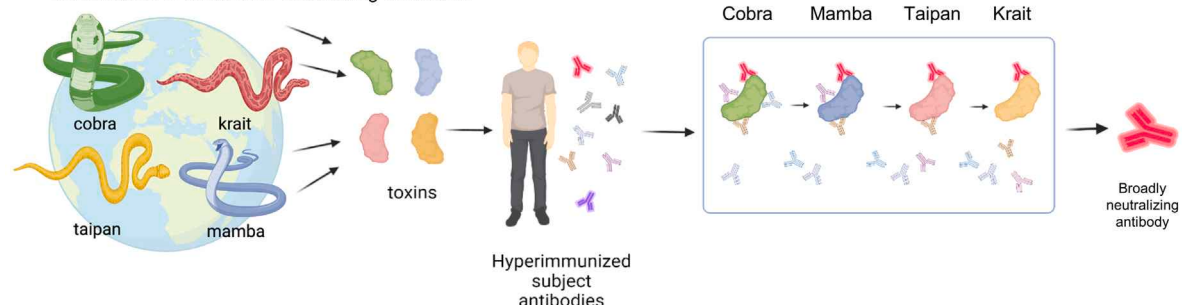
Antivenom serotherapies, although often effective, face significant challenges. The diversity of venom toxins across 600 venomous snake species means antivenoms typically work only against a single or a few related snakes. As a result, most snake species lack a specific antivenom, and efficacy can vary widely even within a species due to geographic genetic variations. Correctly identifying the snake, to provide the appropriate antivenom, is often difficult for victims or healthcare workers.<sup>5,6</sup> Treatments derived from non-human serum can cause adverse reactions like serum sickness and anaphylaxis, with increased risks if used again in the same patient.<sup>7</sup> While the modern practice of digesting antivenom immunoglobulin G (IgG) to antigen-binding fragments (Fabs) reduces reactogenicity, it also shortens half-life, requiring frequent dosing. The potency of current anti-

venom is further reduced by contamination with 5%–22% non-antibody proteins, and a low reported proportion (estimated at 9%–15%) of venom-specific antibodies in the case of polyvalent polyclonal antivenoms.<sup>5,8,9</sup> Research into improved antivenoms is hampered by venom heterogeneity, low market incentives in developing regions, and fragmented markets due to species-specific antivenoms.<sup>10</sup>

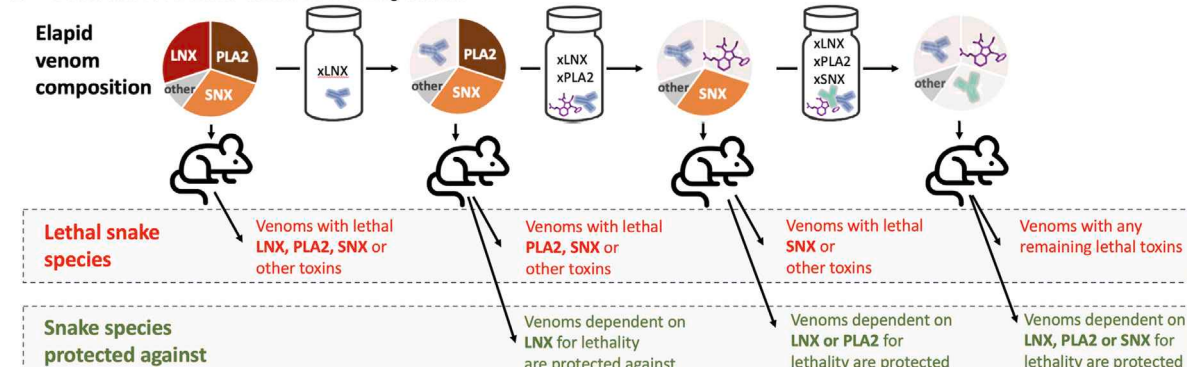
A single broad-spectrum antivenom has not been achieved, primarily due to the complexity of snake venom and the diversity of snake species. Globally, over 600 genetically diverse venomous snake species exist, spanning 167 million years of *Toxicofera* evolution.<sup>11</sup> Among these, 85 species are of highest medical relevance to humans—31 classified as WHO Category 1 and 54 as Category 2. The rest are either potentially lethal but rare, like coral snakes, or have less potent venom.<sup>12</sup> Each snake produces 5–70 unique protein toxins with significant polymorphism, even within a single species.<sup>13</sup> Consequently, even if antivenom agents were found for every toxin, combining them into a single antivenom would be impractical, as the required dose would far exceed safe administration levels for humans.<sup>14–16</sup>

In principle, a cocktail of broadly neutralizing agents against common snake toxins could provide a path to a universal

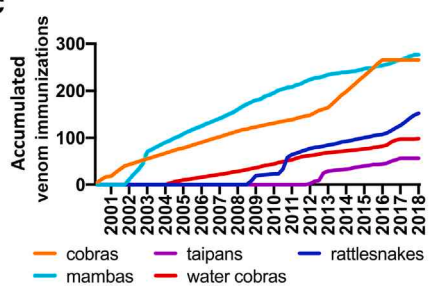
**A Identification of broad toxin-neutralizing antibodies**



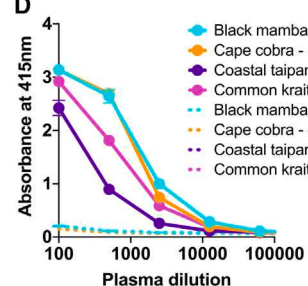
**B Delineation of a broad venom-neutralizing cocktail**



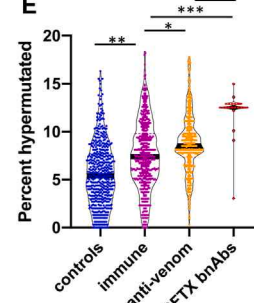
**C**



**D**



**E**



**F Heavy chain**

D09 -EVQLVEGGGVQPGGSLRLSCAASGFTFSNFDMWVROSPGKGLEWVSGLDHSGGAHYAGSVKQRFTISREDAKNSLQLQMNLLRVDVTAVYFCVRGTLHYHTGSYYSDAFD1WGQGTLTVTSS  
EVQLVEGGGVQPGGSLRLSCAASGFTFSNFDMWVROSPGKGLEWVSGLDHSGGAHYAGSVKQRFTISREAGKHSLLDQMNSLRVDDTAVYFCVRGTLHYHTGSYYSDAFD1WGQGTLTVTSS  
QVQLQSGGGLVQPGGSLRLSCAASGFTFSNFDMWVROSPGKGLEWVSGLDHSGGAHYAGSVKQRFTISREDAKNSLQLQMNLLRVDVTAVYFCVRGTLHYHTGSYYSDAFD1WGQGTLTVTSS  
QVQLQSGGGVVQPGGSLRLSCAASGFTFSNFDMWVROSPGKGLEWVSGLDHSGGAHYAGSVKQRFTISREDAKNSLQLQMNLLRVDVTAVYFCVRGTLHYHTGSYYSDAFD1WGQGTTVTVSS  
QVQLQSGGGLVQPGGSLRLSCAASGFTFSNFDMWVROSPGKGLEWVSGLDHSGGAHYAGSVKQRFTISREDAKNSLQLQMNLLRVDVTAVYFCVRGTLHYHTGSYYSDAFD1WGQGTLTVTSS

5 10 15 20 25 30 35 40 45 50 55 60 65 70 75 80 82C 87 92 97 100A 100F 101 106 111 non-templated region

**Light chain**

D09 -EIVLTQSPSSLASVGDRVTITCRASQISDNLYQQKPGKAPKLIIYASSLSGPSPRSFGSGSGTDFTLTISSQQPEDFATYYCQOANSFPYTFCGGTKEIKR  
DVVMTQSPSSLFAVGDRVTITCRASQDIRNDLGWYQQKPGKAPKLIIYGASTLQSGPSPRSFGSGSGVADFTLTISSQQPEDFATYYCQOQSITPLTFCGGTKEIKR  
DIQMTQSPSSLASVGDRVTITCRASQISSSYLWYQQKPGKAPKLIIYASSLSGPSPRSFGSGSGTDFTLTISSQQPEDFATYYCQOQSITPLTFCGGTKEIKR  
DIQMTQSPSSLASVGDRVTITCRASQISSSYLWYQQKPGKAPKLIIYASSLSGPSPRSFGSGSGTDFTLTISSQQPEDFATYYCQOQSITPLTFCGGTKEIKR  
DIQMTQSPSSLASVGDRVTITCRASQISSSFLWYQQKPGKAPKLIIYASSLSGPSPRSFGSGSGTDFTLTISSQQPEDFATYYCQOQSITPLTFCGGTKEIKR  
DIVMTQSPSSLASVGDRVTITCRASQISSSWLWYQQKPGKAPKLIIYASSNLONGVPSPRSFGSGSGTDFTLTISSQQPEDFATYYCQOQSITPLTFCGGTKEIKR  
EIVLTQSPSSLASVGDRVTITCRASQISSSWLWYQQKPGKAPKLIIYASSLSGPSPRSFGSGSGTDFTLTISSQQPEDFATYYCQOQSITPLTFCGGTKEIKR  
DIVMTQSPSSLASVGDRVTITCRASQGISDNLYQQKPGKAPKLIIYASTLQSGPSPRSFGSGSGTDFTLTISSQQPEDFATYYCQOANSFPYTFCGGTKEIKR  
EIVLTQSPSSLASVGDRVTITCRASQGISSSWLWYQQKPGKAPKLIIYASSLSGPSPRSFGSGSGTDFTLTISSQQPEDFATYYCQOANSFPYTFCGGTKEIKR  
EIVLTQSPSSLASVGDRVTITCRASQGISSSWLWYQQKPGKAPKLIIYASSLSGPSPRSFGSGSGTDFTLTISSQQPEDFATYYCQOANSFPYTFCGGTKEIKR

5 10 15 20 25 30 35 40 45 50 55 60 65 70 75 80 85 90 95 100 105

(legend on next page)

antivenom. Small-molecule inhibitors have been identified for some enzymatic toxins,<sup>17</sup> suggesting they could be of utility. Historical efforts to isolate therapeutic antibodies against individual toxins have yielded limited, species-specific efficacy,<sup>18,19</sup> but recent studies have identified antibodies and proteins with broad binding to the three-finger neurotoxins (3FTXs), almost entirely the subclass of long-chain neurotoxins (LNXs). One anti-LNX antibody showed cross-genus binding but provided only partial protection to a single cobra species when administered 10 min after venom injection.<sup>20</sup> Another study used a synthetic yeast library to discover an anti-LNX antibody with broad binding to LNXs from multiple genera, which demonstrated *in vivo* protection against some purified toxins and whole venoms, but with escape variants and insufficient *in vivo* potency against the king cobra (*Ophiophagus hannah*).<sup>21</sup> Additionally, computationally designed proteins have been shown to bind and neutralize LNXs,<sup>22</sup> and a broadly reactive anti-short-chain neurotoxin (anti-SNX) monoclonal antibody was isolated from hybridomas of mice immunized with an SNX, but its *in vivo* efficacy was not evaluated.<sup>23</sup> These examples demonstrate that toxin-reactive antibodies and proteins with broad neutralizing activity can be identified; however, since snake venoms generally have multiple toxins, targeting only a single-component toxin with a monoclonal therapy appears to be insufficient for an effective antivenom in most snake species.

In this study, we aimed to determine whether a cocktail of multiple broadly neutralizing agents could protect mice against entire classes of snake toxins and whole venom from diverse snake genera. We applied an “iterative-addition” approach to construct a broad-spectrum antivenom, starting with the *Elapidae* family of neurotoxic snakes. The *Elapidae* family comprises nearly half of venomous snake species, including over 50 genera and 300 species.<sup>24</sup> Over 80% of *Elapidae* venom by mass consists of 3FTXs and phospholipase A2s (PLA2s).<sup>25–27</sup> The 3FTX family includes LNXs and SNXs, which are among the deadliest snake venom toxins.<sup>28</sup> Notably, no small-molecule inhibitors have been identified for LNX or SNX, unlike for enzymatic toxins such as PLA2.<sup>17</sup> LNX and SNX orthologs are abundant in nearly all elapid venoms, and despite high diversity (Figure S1), they maintain conserved high-affinity binding to nicotinic acetylcholine receptors (nAChRs), impairing neuromuscular and neuronal transmission.<sup>29</sup> These toxins paralyze neurons from mammals, birds, reptiles, amphibians, and fish, an evolutionary constraint that requires LNXs and SNXs from all snake species to maintain conserved interfaces with nAChRs,<sup>30</sup> thereby presenting a plausible target for broadly

neutralizing anti-3FTX antibodies. Here, we report the iterative isolation and characterization of two broadly neutralizing antibodies, one against LNX and one against SNX, from the antibody memory of a human with a unique history of snake venom exposure; further, through iterative neutralization of major toxin classes by broadly neutralizing antivenom antibodies and a small-molecule PLA2 inhibitor,<sup>31</sup> we deconstruct the toxicity of elapid snake venom and demonstrate that a minimal cocktail of three components provides *in vivo* protection against a diverse panel of medically relevant elapid venoms.

## RESULTS

### Toxin probes from four genera for antibody isolation

To aid in the isolation and screening of broadly reactive antibodies (Figure 1A), recombinant toxins from diverse clinically significant *Elapidae* were generated. For LNX, the four orthologs chosen were alpha-elapitotoxin-Dpp2a from the black mamba (*Dendroaspis polylepis*) of Sub-Saharan Africa, alpha-cobratoxin/long neurotoxin 1 from the Cape cobra (*Naja nivea*) of Southern Africa, long neurotoxin 1 from the coastal taipan (*Oxyuranus scutellatus scutellatus*) of Australia, and alpha-delta bungarotoxin from the common krait (*Bungarus caeruleus*) of Asia. This panel spans 40 million years since their most recent common ancestor, comprising highly diverse LNX orthologs that share only 48%–64% identity at the amino acid level (Figure S1). As additional toxin classes were evaluated, this process of diverse recombinant toxin probe generation was repeated.

### Iterative deconstruction of elapid venom toxicity from 19 WHO Category 1 and Category 2 species

Whole snake venom contains multiple toxic proteins, each of which could contribute to lethality. To define the minimum but sufficient set of homologous toxins that must be neutralized to achieve broad-spectrum antivenom protection, we first obtained venom from a representative panel of 19 WHO Category 1 and Category 2 genetically varied, geographically diverse, and medically important elapid species, representing the highest potency venoms with the greatest medical risk to human health. All venoms were confirmed to be rapidly lethal in untreated mice. We then used these venoms to iteratively construct an increasingly broad antivenom cocktail by evaluating protection of the antivenom cocktail against the 19-member venom panel as we explored the addition of broadly neutralizing antivenom components against common toxin classes (Figure 1B).

**Figure 1. *In vivo* and *in vitro* selection for broadly neutralizing antitoxin antibodies**

- (A) Broadly neutralizing antibodies were recovered from a donor with an extensive venom exposure history.
- (B) A broad-spectrum antivenom cocktail was developed through iterative addition of components that expanded protection against venom from a 19-species WHO Category 1 and Category 2 diversity set.
- (C) Hyperimmune donor immunization record from years 2001 to 2018.
- (D) Serum reactivity to recombinant LNXs, hyperimmune donor (immune) versus venom-naïve donors (control).
- (E) Antibody repertoire SHM rate of healthy controls (blue); the hyperimmune donor's total antibody repertoire (wine); the hyperimmune donor's antivenom-specific antibody repertoire (orange); and broadly neutralizing antibodies against three-finger toxins (red).
- (F) Mutational variants of the broadly reactive LNX-D09 antibody lineage, with highlighted germline mutations (purple), NP non-templated variation (salmon), CDR boundaries (red dashed lines). Kabat numbering.

See also Figure S1 and Table S2.

## Snake-venom-exposed hyperimmune donor as a source of broadly neutralizing antibodies

A hyperimmune human adult male donor was identified with a documented 18-year history of 856 self-immunizations to venoms, spanning 2001–2018 (Figure 1C). Documented self-immunizations included mambas (*D. polylepis*, *D. viridis*, *D. angusticeps*, *D. jamesoni*), cobras (*N. kaouthia*, *N. haje*, *N. melanoleuca*, *N. nivea*), rattlesnakes (*C. atrox*, *C. scutulatus*), water cobras (*N. annulata*, *N. cristi*), and taipans (*O. scutellatus*, *O. scutellatus canni*), as well as the Eastern coral snake (*Micrurus fulvius*), common krait (*Bungarus caeruleus*), banded krait (*Bungarus multicinctus*), tiger snake (*Notechis scutatus*), and Eastern brown snake (*Pseudonaja textilis*). Hypothesizing that this repeated exposure to diverse venoms may have selected for broadly reactive antivenom antibodies that recognize conserved epitopes shared across the venom toxins of multiple snake species, we sought to isolate such broadly neutralizing antibodies from the immune memory of this donor. In a non-interventional study design, 40 mL of blood was collected from the donor, after obtaining informed consent. Collection was conducted in accordance with Western Institutional Review Board (WIRB) Exemption Work Order #1-1209200-1 (ethics statement). Blood samples were separated into plasma and peripheral blood mononuclear cells (PBMCs).

## Hyperimmune serum samples exhibit broad reactivity to diverse LNXs

We first sought to verify that the collected blood sample showed molecular evidence of robust and broad immune responses to snake venom. Relative to snake venom-naïve healthy control plasma, significantly elevated antivenom antibodies were detected in hyperimmune donor plasma against a panel of recombinant LNXs from the black mamba, Cape cobra, coastal taipan, and common krait, to a level of 1:12,500 dilution in a 1:5 dilution series beginning at 1:100 serum dilution ( $p = 1.0e-5$ ,  $5.9e-8$ ,  $1.4e-4$ , and  $8.3e-8$ ; two-sample equal variance t test with Bonferroni correction to  $p < 0.0025$ ) (Figure 1D).

## Hyperimmune antivenom antibody repertoire exhibits elevated SHM

The adaptive immune system progressively mutates antibodies to optimize their binding to targets—a process known as affinity maturation, which involves somatic hypermutation (SHM). From donor PBMCs, B cell receptor repertoire DNA was isolated, and the isolated variable heavy chain (VH) repertoire underwent high-throughput sequencing (Table S1).<sup>40</sup> Compared with healthy adult controls ( $5.66 \pm 2.52$ ), the hyperimmune donor exhibited an elevated total SHM rate ( $7.32 \pm 2.69$ ) (Figure 1E; see STAR Methods). This rate was significantly higher in the donor's venom-specific antibody repertoire ( $8.61 \pm 2.23$ ), obtained by enrichment panning against biotinylated whole venom from four snake species. The highest SHM rate was observed in the 64 broadly cross-reactive antivenom antibodies isolated against LNX homologs ( $12.06 \pm 1.62$ ). Thus, the hyperimmune sample demonstrated an elevated SHM profile, enriched in the antivenom-specific repertoire and most enriched in the isolated broadly neutralizing antibodies.

## Broadly reactive anti-LNX antibodies isolated from a hyperimmune library

Broadly neutralizing antibodies were isolated from the hyperimmune blood sample, using phage display (Table S1; see STAR Methods). The sample was converted into a hyperimmune antibody library, and this library was then sequentially panned against recombinant LNX from the black mamba, Cape cobra, coastal taipan, and common krait. Recovered clones were screened for reactivity to LNX from the same four species (Table S2; see STAR Methods). Also, 64 broadly reactive neurotoxin-specific clones were identified, and upon sequencing, 61 of the 64 (95%) were found to be from a single dominant antibody lineage, D09, which utilized the same VDJ rearrangement and contained clone LNX-D09 as a member (Figure 1F).

## Broadly reactive anti-LNX antibody LNX-D09 exhibits a long CDR-H3, extensive SHM, and high thermostability

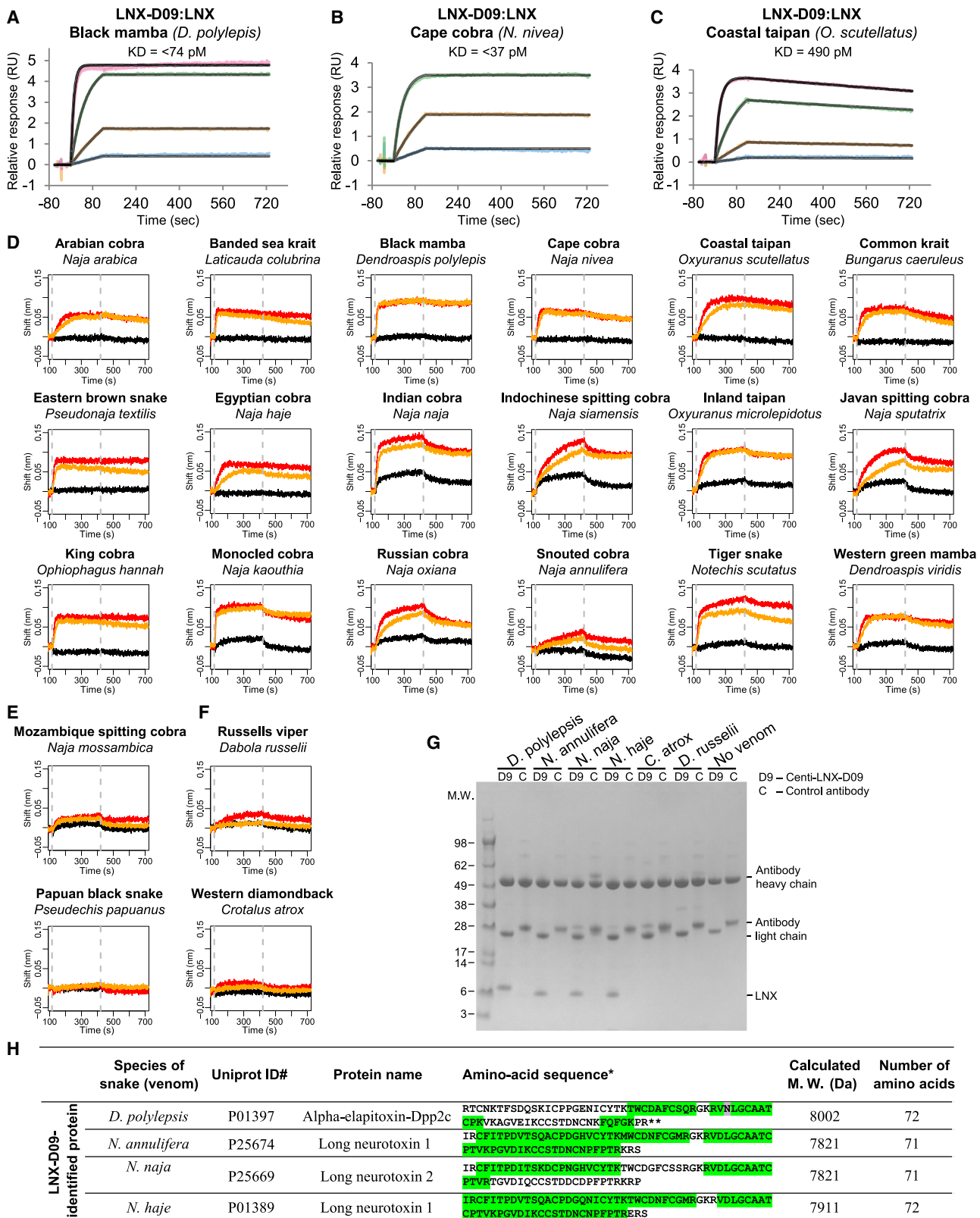
LNX-D09 utilized the IGHV3-13 V-gene segment, a long (18 amino acids) third heavy chain complementarity determining region (CDR-H3) loop with a 7 amino acid non-templated variable-diversity (V-D) junctional region and significant restriction to IGKV1-39 (85%). LNX-D09 had undergone extensive SHM (77.4% ID to VH germ line), heavily concentrated in its paratope, the area of its surface that makes contact with LNX: 27 of 39 non-germline residues were found in the CDRs, including 19 SHM mutations and 8 non-germline CDR-H3 residues not defined by any VDJ segment templates (Figure 1F). SHM this extensive indicates that this antibody is the product of multiple rounds of *in vivo* modification and selection to optimize its binding to the toxin. Despite this degree of SHM, LNX-D09 exhibited high thermostability and aggregation resistance (75°C Tm1, 75°C Tagg 266).

## LNX-D09 exhibits sequence convergence with antibody 95Mat5

Comparing LNX-D09 to other anti-LNX antibodies revealed remarkable sequence convergence with 95Mat5, a broadly reactive antibody recently discovered from a synthetic yeast library.<sup>21</sup> Both LNX-D09 and 95Mat5 share an identical and unusually long CDR-H3 length (95.4th percentile), three identical residues in a critical LNX-binding motif, and nearly identical light-chain sequences. Khalek et al. also noted a dominant bias toward this specific CDR-H3 length and binding motif.<sup>21</sup> LNX-D09 exhibited significantly greater SHM than 95Mat5, likely due to continuous *in vivo* affinity maturation over 18 years of self-immunization. This higher SHM may explain LNX-D09's greater breadth and reactivity to whole venom, noted against species like Eastern brown, tiger snake, *king cobra*, banded sea krait (*Laticauda colubrina*), many-banded krait (*Bungarus multicinctus*), and mulga snake (*Pseudechis australis*) (Figure S3). Since 95Mat5 was independently derived from a synthetic library without influence from LNX-D09, the LNX-D09/95Mat5 class of neutralizing antibodies likely represents a global optimum in the human antibody repertoire for broadly neutralizing LNXs.

## LNX-D09 binds selectively and with high affinity to diverse LNX homologs

Initial ELISA screening indicated broad reactivity of lineage D09 to the representative recombinant LNXs from the black mamba,



(legend on next page)

Cape cobra, coastal taipan, and common krait (Table S2). Kinetics assays, using surface plasmon resonance (SPR), demonstrated picomolar affinity monovalent interactions between lineage member LNX-D09 and LNXs from diverse species: <74 pM to black mamba, <37 pM to Cape cobra, and 490 pM to coastal taipan, as well as high-affinity interactions to these toxins by LNX-B11, another member of the lineage (Figures 2A–2C and S2; see STAR Methods).

To further characterize the breadth of LNX-D09, we used biolayer interferometry to assess the reactivity of LNX-D09 to whole venom from 24 elapid species. In 22 species, we observed clear reactivity (Figures 2D and S3), and in 2, the Mozambique spitting cobra (*Naja mossambica*) and Papuan black snake (*Pseudechis papuanus*), we observed no or marginal reactivity (Figure 2E). Consistent with this observation, Papuan black snake venom has been reported to contain no LNX,<sup>32</sup> and an analysis of a published top-down mass spectrometry analysis of Mozambique spitting cobra venom identified no LNX.<sup>33</sup> As negative controls, we also tested two viperid venoms not expected to contain LNX, Russell's viper (*Daboia russelii*) and Western diamondback rattlesnake (*Crotalus atrox*), and observed no/marginal reactivity (Figure 2F).

To confirm that the reactivity to venoms corresponded to selective recognition by LNX-D09 of LNX, we performed immunoprecipitation pull-down and mass spectrometry peptide sequencing experiments with LNX-D09 and whole venom and observed clear evidence for LNX binding with bands of the expected size for LNXs for the black mamba, Indian cobra (*Naja naja*), snouted cobra (*Naja annulifera*), and Egyptian cobra (*Naja haje*) but not with negative control Russell's viper or Western diamondback (Figure 2G). Mass spectrometry confirmed the specific molecular identity of the pulled-down peptides to be LNX in every instance where a band was observed (Figure 2H; full data in Table S3).

Overall, these binding experiments demonstrate that LNX-D09 binds specifically to LNX homologs, with breadth extending to all 22 diverse LNX+ elapids tested, and that the antibody binds with high affinity in all genera where affinity was directly evaluated.

### Crystal structures of LNX-D09 with LNXs reveal a conserved epitope competitive with nAChR:LNX interface

To elucidate the atomic-level basis for LNX-D09's broad reactivity with LNXs, we determined crystal structures of the LNX-D09 Fab complexed with LNXs from the black mamba, Cape cobra, coastal taipan, and common krait (Figure 3A; Table S4; Data S1). The antibody interface was similar across all four LNXs, characterized by a combined buried surface area (BSA) of approximately 1,500–1,700 Å<sup>2</sup> shared between Fab and toxin.

The interactive surface was primarily contributed by CDR-H3, with additional hydrophobic interactions and hydrogen bonds (H-bonds) from CDR-H1, CDR-L1, and CDR-L2.

Comparing these structures with a previously determined structure of krait LNX bound to nAChR (PDB: 6UWZ)<sup>34</sup> revealed that the LNX-D09 epitope overlapped with the interface LNXs use to bind nAChR (Figures 3B and 3C). Superimposing LNX-D09 and nAChR bound to krait LNX revealed that the antibody's CDR-H3 approximated the position of nAChR's "loop C" in the α chain interface (Figure 3D; Table S5; Data S1). Residues Y100<sub>HC</sub>, T100A<sub>HC</sub>, and Y100E<sub>HC</sub> of LNX-D09 mimicked the contact residues Y190<sub>nAChRα</sub>, T191<sub>nAChRα</sub>, and Y198<sub>nAChRα</sub> of nAChR (for clarity, we add as a subscript, the parent molecule of each named residue). In the toxin, the key R36<sub>Toxin</sub> extended between F32<sub>Toxin</sub> and Y198<sub>nAChRα</sub> to form a critical stacking interaction with the receptor<sup>34</sup>; similarly, in LNX-D09, the aliphatic portion of R36<sub>Toxin</sub> was sandwiched between F32<sub>Toxin</sub> and Y100E<sub>HC</sub> and flanked by Y100<sub>HC</sub>. Residues H99<sub>HC</sub> and L97<sub>HC</sub> occupied the pocket formed by residues 6–11 of the toxin, replacing Y189<sub>nAChRα</sub> and W187<sub>nAChRα</sub>. Additionally, the R36<sub>Toxin</sub> guanidinium group formed two H-bonds with D100H<sub>HC</sub>, which are absent in nAChR (Figure 3D).

The LNX interaction with the nAChR δ chain was partially mimicked by the antibody's light chain (Figures 3B and 3D; Tables S4 and S5; Data S1). While the receptor's δ subunit interface with the toxin was mainly stabilized by hydrophobic interactions, LNX-D09's light-chain-toxin interface involved both hydrophobic interactions and H-bonds. Y32<sub>LC</sub> on the light chain was positioned similarly to W57<sub>nAChRδ</sub>, helping to cradle F32<sub>Toxin</sub> and R36<sub>Toxin</sub>.

Superimposing all four LNX-D09 complexes (Figure 3E) revealed that the LNX interface is highly conserved across the homologs, with interface side chains adopting nearly identical orientations and contact residues being highly conserved.

On the antibody side, the paratope interface was extensively modified from the germ line (Figure 3F). We observed that 8 of the 19 (42.1%) direct LNX contact positions were mutated by SHM or non-templated additions during VDJ recombination, with an additional 10 non-germline mutations within 5.0 Å of the direct contact positions. The substantial resurfacing during affinity maturation may explain LNX-D09's extreme affinity and greater breadth, compared with 95Mat5.

On the LNX side, the LNX-D09 epitope was extremely conserved (Figure 3G; see STAR Methods). Conservation analysis showed that the antibody bound to the most highly conserved surface patch across LNX homologs, which is also the interface LNXs use to bind nAChR and exert their toxic function. Analysis of per-position BSA revealed that LNX-D09 contacts the same amino acids as nAChR, with both interfaces

**Figure 2. Kinetics and whole-venom binding studies reveal breadth and affinity of LNX-D09 for LNXs**

(A–C) Surface plasmon resonance monovalent affinity of LNX-D09 versus recombinant LNX for (A) black mamba, (B) Cape cobra, and (C) coastal taipan. Curve fit in black.

(D–F) Biolayer interferometry reactivity of LNX-D09 versus whole venom at 500 nM (red), 250 nM (orange), negative control mAb (black). (D) Eighteen elapid venoms with confirmed reactivity; (E) two elapid venoms with no LNX; and (F) two negative control viperid venoms with no LNX.

(G and H) (G) Immunoprecipitation by LNX-D09 from whole venom of four snakes with venom containing an LNX (left lanes) and three samples without (right lanes), confirmed by (H) mass spectrometry.

See also Figures S2 and S3 and Table S3.

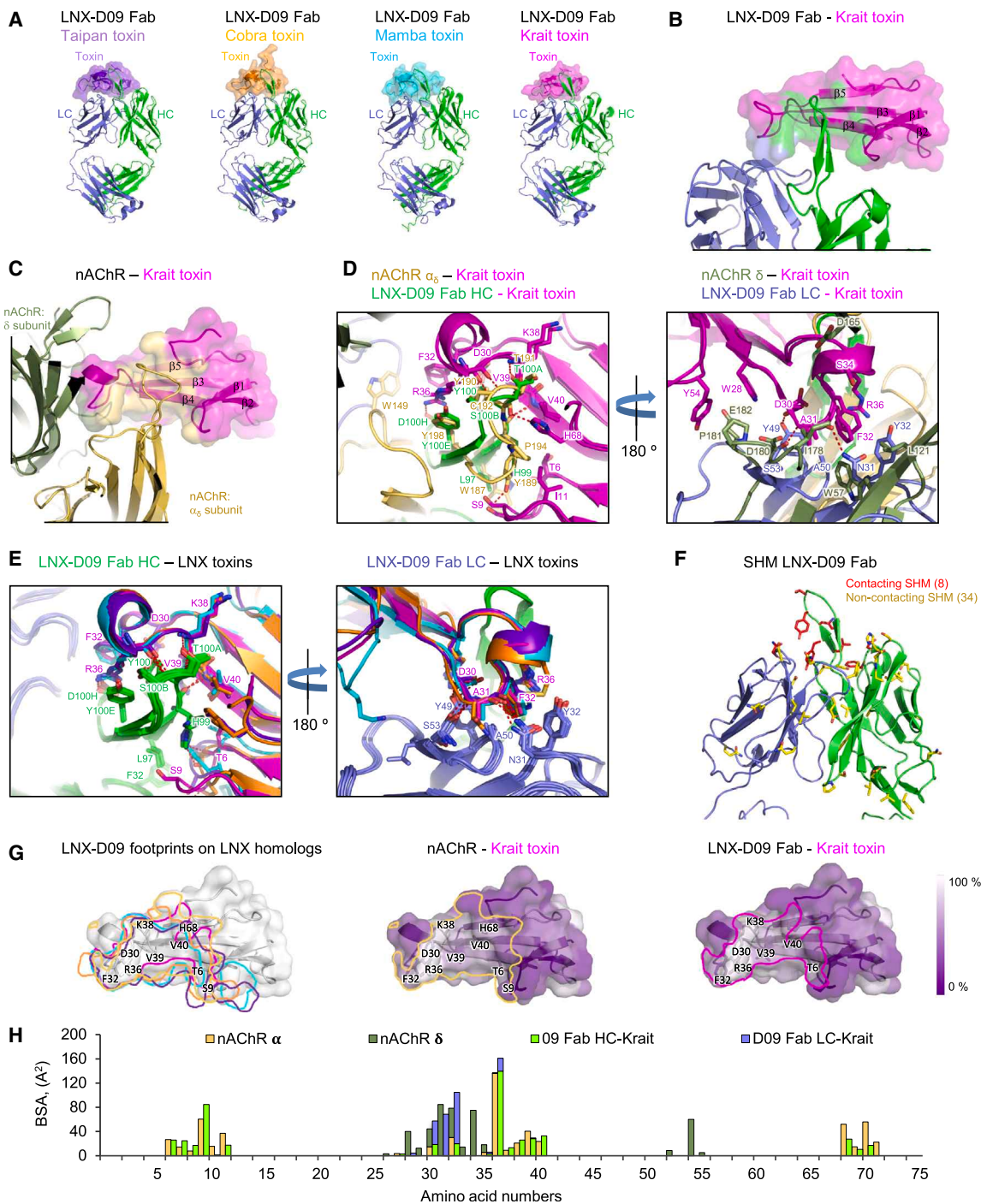


**Figure 3. Crystal structures of complexes reveal similarity in long neurotoxin recognition between LNX-D09 and nAChR**

- (A) Crystal structures of LNX-D09 in complex with long-chain neurotoxins (LNXs) from taipan (PDB: 8D9Y, purple), cobra (PDB: 8D9Z, orange), mamba (PDB: 8DA0, cyan), and krait (PDB: 8DA1, magenta).
- (B-D) Comparison of recognition of LNX (magenta) by nAChR (subunits  $\alpha_\delta$  gold and  $\delta$  dark green) or LNX-D09 (heavy chain green and light chain blue).
- (B) Krait toxin recognition by LNX-D09. LNX surface contacts highlighted for heavy chain (green) and light chain (blue).
- (C) Krait LNX-binding nAChR. LNX surface contacts highlighted for  $\alpha_\delta$  (gold) and  $\delta$  (green) (PDB: 6UWZ).
- (D) Complex superpositions of LNX-D09 and nAChR  $\alpha_\delta$  with krait LNX. Interacting residue side chains shown with numbering indicated (Kabat numbering for LNX-D09). Left panel demonstrates similarity of nAChR  $\alpha_\delta$  loop C interface side-chain placement to LNX-D09 CDR-H3 residues Y100, T100A, and Y100E. Right panel rotated 180°.

(legend continued on next page)

exhibiting similar BSA emphasis on each contacted residue (Figure 3H).

These results indicate that LNX-D09 achieves broad recognition by directly binding the conserved interface through which these toxins bind their host target, nAChR, suggesting that LNX-D09 would exhibit broad neutralization of LNXs.

### In vivo protection from recombinant LNX and whole venom by LNX-D09

To assess whether the broad *in vitro* reactivity of LNX-D09 translates to protective *in vivo* neutralization, we conducted recombinant LNX neurotoxin and whole-venom challenge experiments in C57BL/6 mice under approved IACUC protocol CR-0119.

We first evaluated whether LNX-D09 could provide *in vivo* protection against recombinant LNX from the Cape cobra, common krait, coastal taipan, and black mamba. Recombinant LNX at LD<sub>100</sub> doses (0.5 mg/kg for *common krait*, 1.0 mg/kg for the others) caused 100% lethality within 60 min to 2 h, except one mouse with *Cape cobra*. Pre-mixed injections of recombinant LNX with 30 mg/kg LNX-D09 provided complete protection beyond 24 h (Figure 4A). Thus, LNX-D09 offered broad neutralizing protection against LNXs from diverse elapids.

Next, we performed whole-venom challenge studies with LNX-D09 on snakes where 3FTX constituted 63%–88% of venom.<sup>13</sup> LNX-D09 provided robust protection against lethal whole-venom challenges for multiple cobra species (Figures 4B–4E). Complete protection was observed for the Cape cobra, Indian cobra, Egyptian cobra, and monocled cobra (*Naja kaouthia*), where 9 out of 10 mice were protected. LNX-D09 also fully protected against the non-cobra genera black mamba and king cobra (*Ophiophagus hannah*) (Figures 4F and 4G). These results indicate that 3FTX, specifically LNX, is the main determinant of lethality in these species, and they demonstrate full protection against king cobra by a broadly neutralizing anti-LNX antibody.

In the studies above, we used an intraperitoneal (i.p.) injection model with venom pre-mixed with LNX-D09, which differs from natural snake bites where venom is injected first (typically subcutaneously or intramuscularly [IM]), and antivenom is administered later intravenously (i.v.). Given the high affinity between LNX neurotoxins and their nAChR target, we needed to confirm whether LNX-D09 could protect when administered after envenomation. We repeated the protection studies with the black mamba, king cobra, and several cobra species in a rescue model: venom was injected IM, followed by i.v. injection of LNX-D09 after a 10-min delay (Figure 4H). Despite IM being a relatively rapid model (as elapid fang lengths are typically too short for IM), LNX-D09 still provided complete protection, con-

firmed its sufficient affinity to outcompete nAChR for LNX binding. This aligns with clinical reports where antivenom administered after neurotoxic symptoms can stabilize patients.<sup>35,36</sup>

### In vivo protection from whole venom by a cocktail of LNX-D09 and varespladib

PLA2 is the second most abundant toxin in most elapid venoms after 3FTX. To assess its contribution to venom lethality, we conducted whole-venom challenge studies using varespladib—a broad-spectrum PLA2 inhibitor—both alone and in combination with LNX-D09 on tiger snake, coastal taipan, and inland taipan (*Oxyuranus microlepidotus*) (Figures 4I–4K).

For tiger snake venom, which comprises 74.5% PLA2 and 5.6% 3FTX,<sup>13</sup> we observed 100% lethality in mice within 2 h after injection of venom (Figure 4I). Addition of LNX-D09 resulted in one out of five mice surviving up to 10 h, while the others showed a 30-min extension in survival, compared with venom alone. Varespladib, included either alone or combined with LNX-D09, provided protection against lethality for 24 h. Complete protection was achieved when both LNX-D09 and varespladib were included, with varespladib redosed every 8 h to compensate for its short pharmacokinetics.

A similar pattern emerged with taipan venoms. Inland taipan venom, containing 38% PLA2 and 12.2% 3FTX,<sup>13</sup> was 100% lethal within 2 h (Figure 4J). Coastal taipan venom resulted in 100% lethality within 24 h. Including LNX-D09, the time to death was marginally extended by a few minutes for both species. However, the inclusion of varespladib, either alone or in combination with LNX-D09, completely protected mice against lethal doses of both inland and coastal taipan venoms (Figure 4K).

These results confirm that PLA2 is the predominant toxin contributing to lethality in these three species.

### Broadly reactive anti-SNX antibodies were isolated from a hyperimmune library

Although LNX and PLA2 blockade protected nine elapid WHO Category 1 and Category 2 species across five genera, venoms from common krait, Eastern brown, Javan spitting cobra (*Naja sputatrix*), and Western green mamba (*Dendroaspis viridis*) remained lethal when treated with the two-component cocktail.

Suspecting that short neurotoxins (SNXs)—the third most abundant toxins in elapid venom—were responsible, we sought a broadly neutralizing antibody against them. Our LNX-D09 immunoprecipitation and mass spectrometry studies did not detect SNX sequences, indicating that LNX-D09 did not cross-react with SNXs (Figures 2G and 2H). While LNXs and SNXs are homologous and both targeting nAChR, SNXs bind a different receptor region via a distinct conserved interaction

(E) Superposition of LNX-D09 in complex with taipan, cobra, mamba, and krait LNX. Numbering indicated for interacting side chains. LNXs colored as in (A). LNX-D09 heavy- and light-chain toxin interactions in left and right panels, respectively.

(F) SHMs of LNX-D09: 8 mutated antigen contacts (red) and 34 mutated non-contacting residues (yellow).

(G) LNX:LNX-D09 interaction footprints of krait, cobra, mamba, taipan (colored as in A) and LNX:nAChR (yellow) superposed on the surface of krait. Middle and right panels show individual nAChR and LNX-D09 footprints on krait LNX in context of LNX sequence conservation, with white indicating 100% conservation and purple indicating variability.

(H) Per-position buried surface area (BSA) of krait toxin residues involved in binding of LNX-D09 and nAChR receptor: antibody and receptor bind and bury the same LNX residues to a similar degree.

See also Tables S3 and S4 and Data S1.

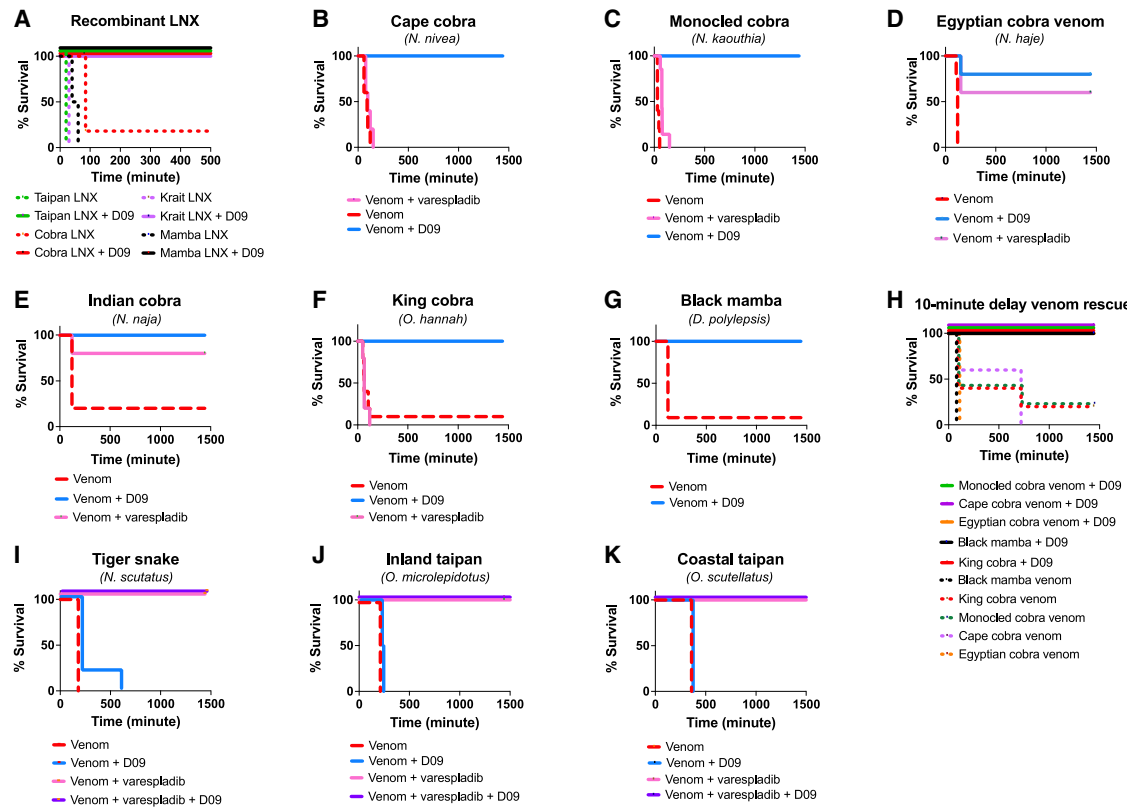


**Figure 4. *In vivo* protection from recombinant LNX neurotoxin and whole venom with LNX-D09 and varespladib**

Kaplan-Meier survival curves for C57BL/6 mice injected intraperitoneally with (A) recombinant LNX/antibody premix, (B–G and I–K) whole venom/antibody premix, or (H) IM by venom followed by 10-min delay before receiving antibody i.v. LNX-D09 provided full *in vivo* protection against (A) recombinant LNX from four elapid species ( $n = 10$ ) and whole-venom challenge ( $n = 5$ ), including (B–E) four species of cobra and (F and G) whole venom from two non-cobra elapids. Full protection was extended to whole venom from (J) tiger snake and (K and L) inland and coastal taipans with the addition of PLA<sub>2</sub> inhibitor varespladib.

interface. No conserved surface patch exists between LNXs and SNXs, which we believe is essential for antibody cross-reactivity.

The hyperimmune donor's serum reacted with SNXs from diverse species, suggesting that anti-SNX antibodies were present in the antibody repertoire (Figure 5A). Using the same discovery approach as for LNX, we isolated clone SNX-B03, which exhibited broad reactivity to SNXs at 15–30 nM for the black mamba, Cape cobra, tiger snake, and rough-scaled snake (*Trachylepis carinatus*) (Figure 5B).

#### SHM of broadly reactive anti-SNX lineage, SNX-B03

Sequencing of SNX-B03 antibody variable domains revealed it to be a distinct lineage from LNX-D09, with different segment usage and CDR-H3 length. Like LNX-D09, SNX-B03 showed evidence of SHM (Figure 5C), although with fewer mutations overall.

#### SNX-B03 binds selectively and broadly to diverse SNX homologs

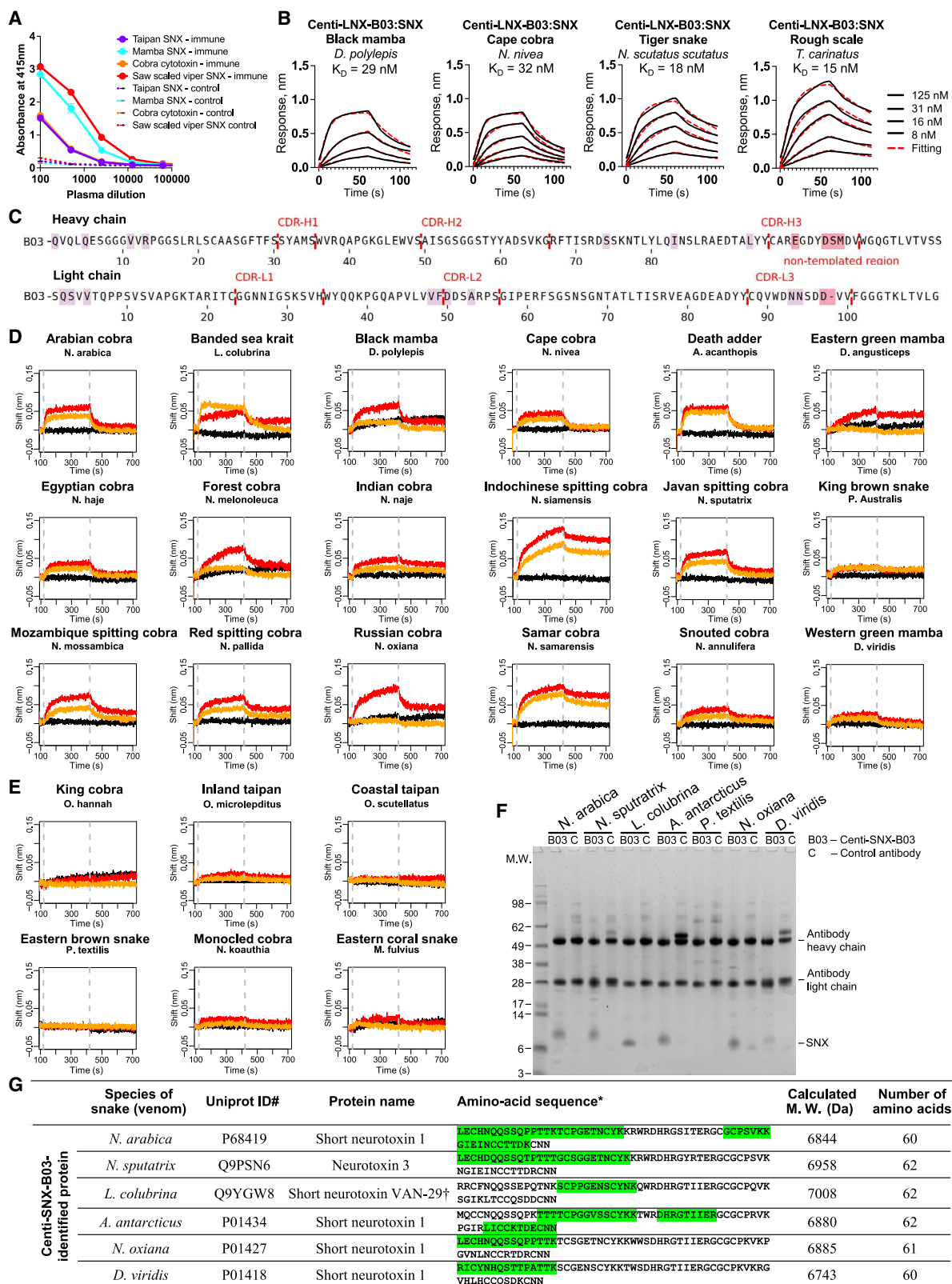
Biolarayer interferometry (BLI) reactivity screening of SNX-B03 against whole venom from a panel of diverse elapid species showed broad reactivity to most (Figure 5D), although six species showed no or undetectable reactivity (Figure 5E). Interest-

ingly, marginal reactivity was detected for the Western green mamba, mulga snake, common krait, and banded krait, although subsequent *in vivo* studies established protective *in vivo* benefits of SNX-B03 against these venoms, suggesting that its relatively low 15- to 30-nM affinity may result in a higher limit of detection in the whole-venom BLI assay, compared with LNX-D09.

To confirm that SNX-B03's reactivity corresponded to selective recognition of SNX, we performed immunoprecipitation and mass spectrometry peptide sequencing with SNX-B03 and whole venom. We observed clear evidence of SNX binding, with bands in the 6- to 7-kDa range for Javan spitting cobra, banded sea krait, Western green mamba, Arabian cobra (*Naja arabica*), common death adder (*Acanthophis antarcticus*), and Russian cobra (*Naja oxiana*) but not for the Eastern brown snake (Figure 5F). Mass spectrometry confirmed that the pull-down peptides were SNX in every instance where a band was observed (Figure 5F; see Table S3).

#### Crystal structures of SNX-B03 with SNX reveal epitope mimicry of the nAChR:SNX interface

To provide an atomic-level understanding for the broad reactivity of SNX-B03 with SNXs, we determined crystal structures



(legend on next page)

of SNX-B03 Fab in complex with SNX from the black mamba (**Figure 6A**; **Table S6**; **Data S1**). Analysis of the interfaces between the two proteins revealed BSAs of  $\sim 1,450 \text{ \AA}^2$ , shared between Fab and toxin (**Data S1**). The interactive surface area was primarily contributed by CDR-H3 and L3, although other CDRs contributed a mixture of hydrophobic interactions and H-bonds.

Comparison with the previously determined structure of nAChR in complex with recombinant short-chain  $\alpha$ -neurotoxin<sup>37</sup> revealed that both the receptor and the antibody bound toxin finger II (**Figures 6B** and **6C**; **Table S7**; **Data S1**). In the receptor-toxin complex, the highly conserved H30<sub>Toxin</sub> interacted with W57<sub>nAChR $\delta$</sub> , L121<sub>nAChR $\delta$</sub> , and Y93<sub>nAChR $\alpha$</sub> . Conserved R31<sub>Toxin</sub> interacted with Y93<sub>nAChR $\alpha$</sub> , Y190<sub>nAChR $\alpha$</sub> , and Y198<sub>nAChR $\alpha$</sub> . In the antibody-toxin complex, H30<sub>Toxin</sub> was trapped in the deep pocket formed by A33<sub>HC</sub>, W47<sub>HC</sub>, Y58<sub>HC</sub>, D99<sub>HC</sub>, and D95A<sub>LC</sub>. It was sandwiched between Y58<sub>HC</sub> and D99<sub>HC</sub>, and formed H-bonds with D99<sub>HC</sub> and D95A<sub>LC</sub>. R31<sub>Toxin</sub> formed a salt bridge with D97<sub>HC</sub>. Conserved W27<sub>Toxin</sub> was involved in hydrophobic interactions with Y98<sub>HC</sub> and W91<sub>LC</sub>.

Analysis of conservation in the nAChR and the toxin revealed the interface to be relatively conserved across SNXs relative to some other sites on the toxin, although not as conserved as the LNX D09 epitope, consistent with our binding study observations (**Figures 6G** and **S1**; see **STAR Methods**). In general, antibody and receptor interacted with similar toxin residues (**Figures 6F**, **6G**, and **6I**), with the heavy chain in the position of the nAChR  $\alpha$  chain and the light chain in the position of the nAChR  $\delta$  chain (**Figure 6F**). Conservation did appear to relate to interfacial surface area (**Figure 6H**), and buried interfacial surface areas of toxin with nAChR were substantially larger (15%–35%) than the surfaces areas with antibody, although the affinity of antibody and toxin to nAChR was comparable<sup>37</sup> (**Figure 6H**). Overall, SNX-B03 exhibits broad neutralization of SNX neurotoxicity by directly binding to conserved residues of the toxin:nAChR interface and therefore blocking the toxin from acting on the neuronal receptor.

Collectively, these results reveal the second instance of the mechanism of broad neutralization to be due to direct recognition of the conserved interface that these toxins make with their host target, nAChR. It is notable that while LNX and SNX do not share a homologous interface with nAChR, in both cases, our antibodies bind directly to the surface of the toxin that participates in the interaction (**Figures 3D**, **3H**, **6E**, **6F**, and **6I**). The evolutionary selection pressure across 300 species of *Elapidae* to maintain a conserved interface with nAChR on their neurotoxins has created a vulnerability that these antibodies are able to exploit.

### In vivo protection from recombinant SNX and whole venom by a cocktail of LNX-D09, varespladib, and SNX-B03

We began by evaluating whether SNX-B03 could provide *in vivo* protection against recombinant SNX of the black mamba and rough-scaled snake. Recombinant SNX from these snakes, injected at the pre-determined LD<sub>100</sub> of 1.0 mg/kg, caused 100% lethality within 30–60 min. Treatment with 30 mg/kg of SNX-B03 provided full protection throughout the 500-min evaluation (**Figure 7A**).

Next, we assessed whether SNX-B03 could protect against whole venom from species where LNX-D09 and varespladib were ineffective. Western green mamba venom was lethal at 1.0 mg/kg within 20 min, with no protective benefit from LNX-D09 or varespladib (**Figure 7B**). However, including 30 mg/kg SNX-B03 in the venom resulted in a 9.3-fold extension in survival time, including complete protection in 40% of mice.

Finally, we evaluated whether adding SNX-B03 to a cocktail containing LNX-D09 and varespladib could enhance protection against venoms inadequately addressed by LNX and PLA2 blockade alone. Common krait venom, consisting of 64.5% PLA2 and 19% 3FTX,<sup>13</sup> caused 100% lethality after 3 h. LNX-D09 or varespladib alone doubled survival time to 6 and 7 h, respectively. The combination of LNX-D09 and varespladib showed enhanced effects, with four out of five mice surviving 12 h and one recovering completely. Redosing varespladib every 8 h did not improve protection. However, including SNX-B03 along with LNX-D09 and varespladib resulted in full protection (**Figure 7C**). Thus, with common krait venom, all three components provided partial protection individually, and their combination achieved synergistic full protection.

Similarly, Eastern brown snake venom was 100% lethal after 2 h. LNX-D09 extended survival of two out of five mice to 6 h. Varespladib alone or with LNX-D09 extended survival of all mice to 6 h. With repeated varespladib dosing every 8 h, two mice survived to 24 h but then died. A three-component mixture including SNX-B03, however, resulted ( $n = 10$ ) in a 7.6-fold survival extension, with four out of 10 mice surviving over 20 h (**Figure 7D**).

Given the demonstrated protection by SNX-B03 against lethal recombinant SNXs and its enhancement of partial protection where other cocktails had limited benefit, we added SNX-B03 as the third component of the cocktail. We tested the final panel of 7 elapid venoms from our 19-member diversity set in mice, either alone or with the cocktail. We observed complete protection for banded krait, Eastern coral snake, and mulga snake and significant survival extensions in Javan spitting cobra (7.6-fold), Arabian cobra (4.1-fold), Russian cobra (3.7-fold), and common death adder (10.5-fold) (**Figures 7E–7K**).

### Figure 5. Kinetics and whole-venom binding studies reveal breadth and affinity of SNX-B03

- (A) Hyperimmune serum (immune) reacted strongly to four diverse SNXs from four genera, compared with venom-naive donor serum (control).
- (B) Biolayer interferometry monovalent affinity of SNX-B03 to SNX from black mamba, Cape cobra, tiger snake, and rough-scaled snake.
- (C) Sequence of SNX-B03, non-germline positions indicated in light purple, and non-templated CDR-H3 positions indicated in salmon.
- (D and E) Biolayer interferometry reactivity of SNX-B03 versus whole venom at 500 nM (red) and 250 nM (orange), with negative control mAb (black).
- (D) Eighteen elapid species with confirmed reactivity.
- (E) Six elapid species with no/marginal reactivity.
- (F and G) Immunoprecipitation of SNX by SNX-B03 from whole venom, confirmed by (G) mass spectrometry.
- See also **Table S3**.

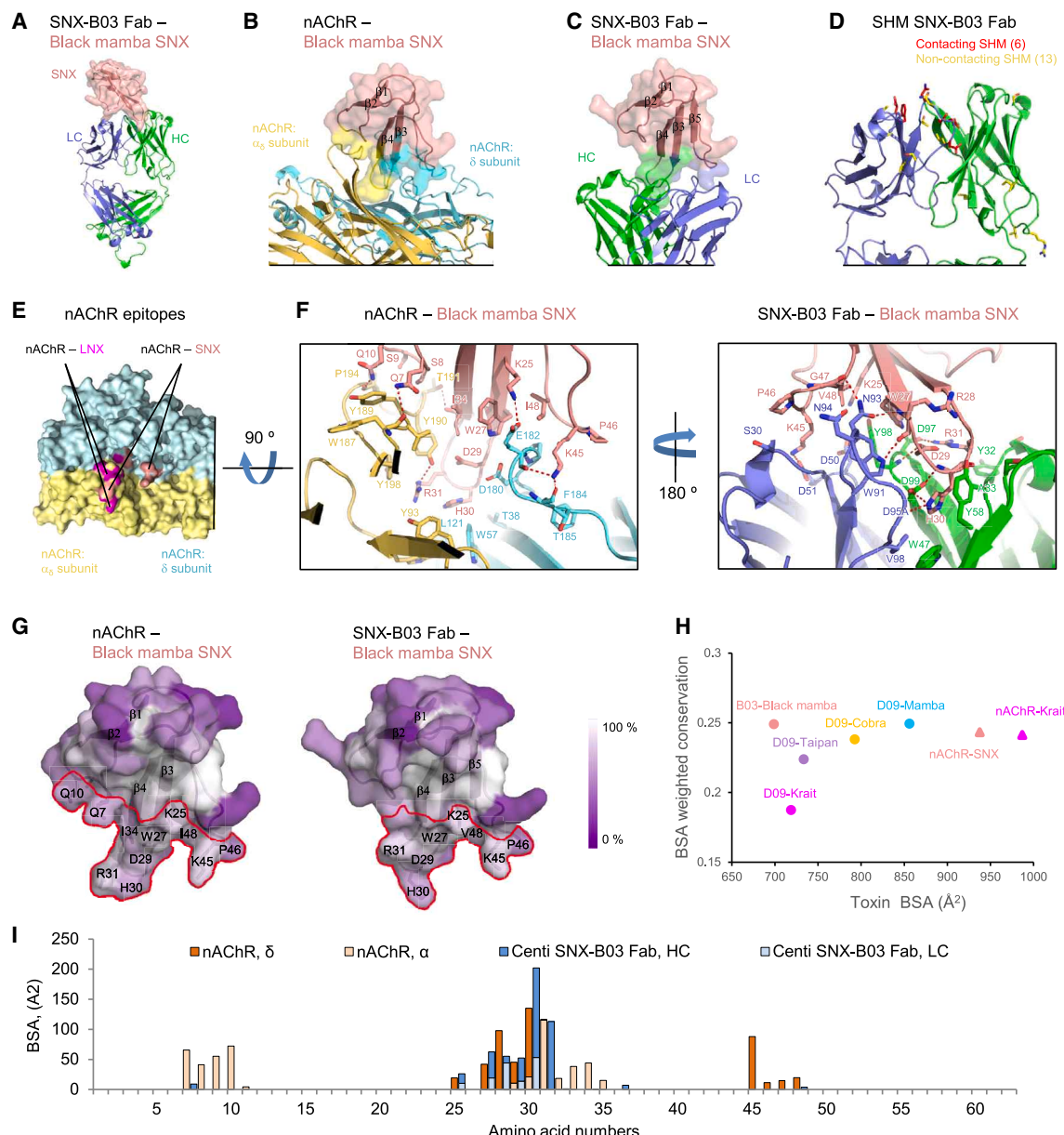
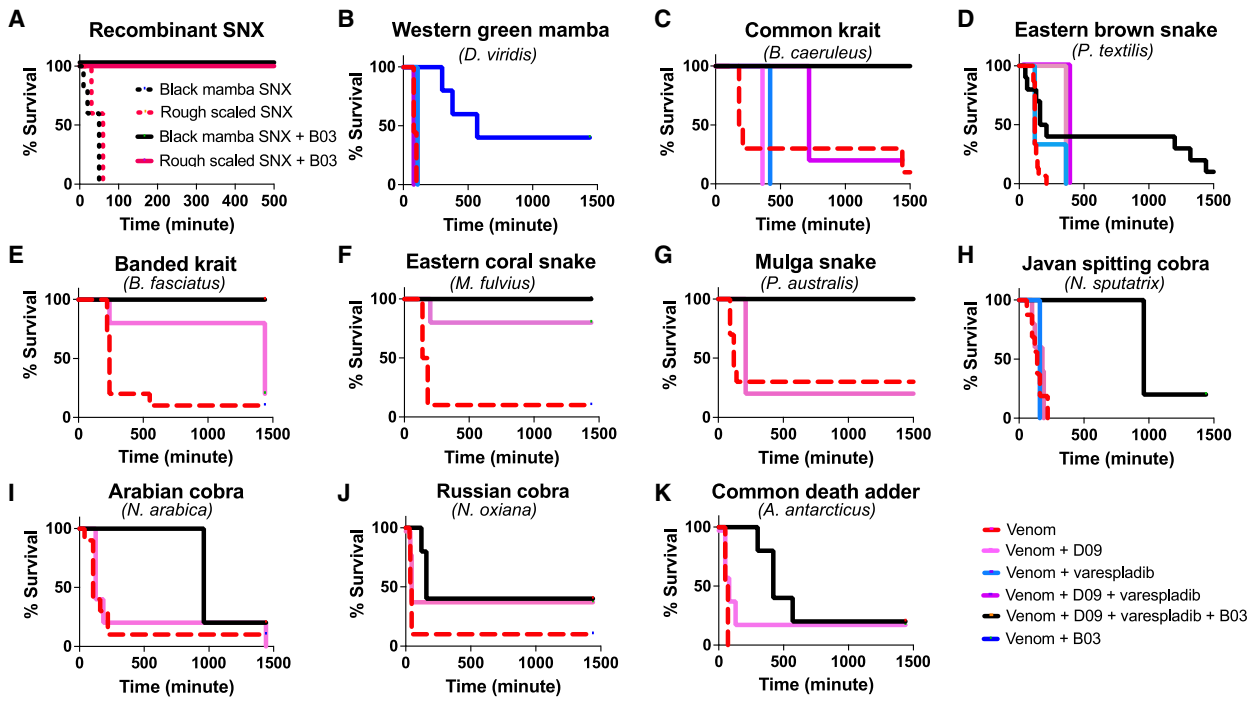


**Figure 6. Crystal structure reveals basis of broad neutralization of SNXs by SNX-B03**

- (A) Crystal structure of SNX-B03 (heavy chain green and light chain blue) in complex with black mamba SNX (brown, PDB: 8V13).
  - (B) Recognition of nAChR (subunits  $\alpha_8$  gold and  $\delta$  light blue) by SNX (PDB: 7Z14). SNX surface contacts highlighted for  $\alpha_8$  (yellow) and  $\delta$  (light blue).
  - (C) Recognition of SNX by SNX-B03. SNX surface contacts highlighted for heavy chain (green) and light chain (blue).
  - (D) SHMs of SNX-B03: six mutated antigen contacts (red) and 13 mutated non-contacting residues (yellow).
  - (E–G) (E) Partial overlap of distinctive LNX (magenta) and SNX (brown) epitopes on surface of nAChR. Complex interface side chains and position numbering highlighted for complexes between (F) SNX and nAChR and (G) SNX and SNX-B03 (Kabat numbering for antibody). (G) Left and right panels show footprints of nAChR and SNX-B03, respectively, on SNX in the context of SNX sequence conservation, with white indicating 100% conservation and purple indicating variability.
  - (H) Weighted conservation versus BSA plot for the receptor-toxin and antibody-toxin complexes: LNX-D09 and SNX-B03 have equally conserved but smaller epitopes than nAChR.
  - (I) Per-position BSA of krait toxin residues involved in binding of SNX-B03 and nAChR receptor: SNX-B03 binds a subset of residues bound by nAChR.
- See also Tables S3 and S5 and Data S1.



† Partial protection with significant time delay to death observed relative to venom-only.

\* WHO Cat 1: Medically important venomous snake, highest medical importance. Definition: highly venomous snakes which are common or widespread and cause numerous snake-bites, resulting in high levels of morbidity, disability or mortality.

\*\* WHO Cat 2: Medically important venomous snake, secondary medical importance. highly venomous snakes capable of causing morbidity, disability or death, but: (a) for which exact epidemiological or clinical data may be lacking; and/or (b) are less frequently implicated (owing to their activity cycles, behavior, habitat preferences or occurrence in areas remote from large human populations).

(legend on next page)

### Geographic, phylogenetic, and clinically relevant coverage of the final 3-member cocktail

A cocktail of three agents (LNX-D09, SNX-B03, and varespladib) provided complete *in vivo* protection against ten WHO Category 1 snakes, complete protection for three WHO Category 2 snakes, and partial protection for five WHO Category 1 snakes and one WHO Category 2 snake (Figure 7L). Protection by this cocktail of three agents spanned North America, Africa (including North Africa/Middle East, Sub-Saharan Africa, and South Africa), Asia (including West Asia/Middle East, the Arabian Peninsula, Central Asia, Southeast Asia, and the Indian subcontinent), Australia, and Oceania. Protection was 100% in 13 species; in the remaining 6, there was protection of some mice; and there was a cocktail-dependent survival extension of  $3.7\times$ – $10.5\times$ , depending on species. The phylogenetic diversity of these 19 species spans *Elapidae*, such that the phylogenetic distance of all 300 members of *Elapidae* to a species demonstrated protected in this study is less than the phylogenetic distance between the two most distant members, for which we have already confirmed protection.

### DISCUSSION

We demonstrate the successful combination of a minimal cocktail of broadly neutralizing antibodies and a small-molecule inhibitor as a proof of principle for a universal antivenom. We present a method for the systematic assembly of a broadly neutralizing antivenom cocktail, as well as the results of that method: a cocktail of two broadly neutralizing antibodies and a broad small-molecule inhibitor, which provides protection against a 19-member elapid diversity set of the WHO's list of snakes of greatest medical concern. We report the discovery of LNX-D09 and SNX-B03, two broadly neutralizing antibodies capable of binding and neutralizing diverse LNX and SNX neurotoxins. These antibodies are significant because no small-molecule inhibitors have been identified for venom neurotoxins, unlike those reported for enzymatic toxins.<sup>17</sup>

By using an iterative discovery approach, we first identified LNX-D09 as an effective single agent that protected against venoms from six species, indicating that their toxicity was mainly due to LNX. We then added the PLA2 inhibitor varespladib, which extended protection to three additional species whose venom toxicity was mainly due to PLA2, and provided synergistic benefits against common krait venom when both LNX and PLA2 were blocked. For venoms where lethality persisted, we included SNX blockade alongside LNX and PLA2 inhibitors, expanding protection to all 19 members of the diversity panel and achieving total protection for most venoms. In this way, we established a minimally defined cocktail with broad action across the entire *Elapidae* family.

LNX-D09 alone fully protected against lethal venom challenges from four cobra species, black mamba, and king cobra, even with

a 10-min treatment delay. When combined with the PLA2 inhibitor varespladib, complete protection extended to the tiger snake, inland taipan, and coastal taipan, mainly due to the effects of varespladib. Adding SNX-B03 further extended full protection to the common krait, mulga, Eastern coral snake, and banded krait. The cocktail also provided partial protection against the Russian cobra, Javan spitting cobra, Arabian cobra, Western green mamba, and common death adder, with some mice surviving and others experiencing significantly extended survival times. Overall, the cocktail protected against lethal challenges from all 19 elapid species tested, including 10 genera on the WHO's Category 1 and Category 2 lists, suggesting that LNX, PLA2, and SNX are the dominant toxins in most elapid venoms. We observed synergistic protection in some venoms, and some were protected by LNX-D09, varespladib, or SNX-B03 alone, reaffirming the variation in venom composition across *Elapidae*. Given the recognized diversity of genera, this cocktail could be reasonably anticipated to provide complete protection against venom from additional members of the 300 venomous *Elapidae* species.

In six of the 19 species tested, we observed significant delays in death but only partial protection. This may be due to SNX-B03's lower affinity, compared with that of LNX-D09, or because additional toxins contribute to lethality at the tested doses. Future experiments will focus on enhancing SNX-B03's affinity and identifying additional broadly neutralizing antibodies against other toxins like cardiotoxins, using our established iterative approach. We also noted that some animals died 24 h after a single dose of varespladib. When we administered the cocktail and redosed varespladib every 8 h, full protection was achieved for some venoms. This suggests that the short half-life (5.5 h  $t_{1/2}$ ) of varespladib led to the delayed death.<sup>38</sup> In future studies, replacing varespladib with a molecule with longer half-life may provide protection with a single injection; we note in this context that long-acting small molecules have been identified, which require dosing only every 6 months.<sup>39</sup>

Lastly, the antibodies described in this study were isolated from a hyperimmune individual exposed to a wide variety of venoms, resulting in potent, broadly cross-neutralizing antibodies against homologous snake toxins. Structural analyses reveal that these antibodies target conserved active sites in the toxin families, which have remained unchanged over evolution in order to bind conserved receptor sites across many vertebrates. Consequently, since functional proteins often have conserved active and binding sites, we anticipate that similar broadly neutralizing antibodies could be recovered from this immune library for other snake toxin families.

The global medical impact of a single, universal, human-derived antivenom would be substantial. A universal antivenom would avoid the need for species identification as a pre-requisite for administering antivenom treatment. It would provide coverage

### Figure 7. Extending antivenom cocktail whole-venom *in vivo* protection with addition of SNX-neutralizing SNX-B03

(A–D) Kaplan-Meier survival curves for C57BL/6 mice injected intraperitoneally with venom/antibody premix, for (A) recombinant SNX and SNX-B03 (B03) from two elapid species ( $n = 10$ ); (B) Western green mamba whole venom and each antivenom cocktail component separately; (C and D) common krait and Eastern brown snake whole venom and sequential addition of antivenom components. Dotted red: only venom, black: whole cocktail, blue: SNX-B03, pink: LNX-D09. (E–K) Cocktail protection on six additional species.

(L) Summary of protection and survival extension of iterative antivenom cocktail versus a diversity set of 19 WHO Category 1 and Category 2 snake species. Cocktail survival extension is calculated as average fold change in delay to death.

for many of the 650 species of venomous snakes and diverse geographies for which there is no current adequate antivenom. Furthermore, it would be anticipated to provide more uniform coverage across genetically diverse variants of snakes even within a single species; a significant limitation of current commercial anti-venoms. It would allow stockpiling of a single product to replace many discrete species-specific products and unite a larger market, easing commercialization constraints and therefore potentially aiding in reducing antivenom shortages. Even for species where non-human antivenoms are currently available, a recombinant antivenom composed of defined, reproducibly produced, high-affinity functional human-derived antibodies would be anticipated to have superior potency, safety, and reliability. Fully human IgG antibodies avoid the risk of anaphylaxis and serum sickness that arises from administration of non-human serum antivenoms, while greatly extending the half-life of the product from hours to weeks, enabling an end to the current practice of frequent administration of 8–20 vials over the course of typical antivenom treatment. Being recombinant, the safety and half-life profile could be further extended through the introduction of modern half-life extending and effector-function muting Fc mutations to enhance safety and extend protection. As a defined recombinant product, it would greatly simplify efforts to identify appropriate lyophilization excipient conditions, greatly reducing the cold-chain requirements for distribution and storage. Clinically, human antibodies have evolved to be expressed and tolerated at high doses and with long half-life in human serum, with 175 approved monoclonal therapies and over a 1,000 candidates currently in clinical trials; additionally, human antibodies enjoy an unparalleled derisked toxicological safety profile over small-molecule therapeutics or *de novo* designed proteins, such as those recently designed by AI.<sup>22</sup> In general, the distinct origin of these antibodies, evolved to high potency within a healthy human host, may offer safety and developability advantages when used to protect other humans.

### Limitations of the study

These *in vivo* protection models have limitations. While we observe broad protection across 10 genera at the tested venom doses, actual snake bites may inject higher venom doses, potentially revealing toxic effects of additional components not detected here. These are also mice, not humans. Therefore, we interpret our results as identifying the most dominant lethal venom components and systematically deconstructing their contributions by neutralizing the most toxic toxins. Future studies should increase venom doses in fully protected animals, and use larger model organisms, to uncover if additional key toxins require targeting. Furthermore, for a universal antivenom, *Elapidae* represents only half of venomous snakes; *Viperidae* will require additional broad-spectrum agents. The iterative method outlined here could be repeated to address these limitations.

### RESOURCE AVAILABILITY

#### Lead contact

Further information and requests for resources and reagents should be directed to and will be fulfilled by the lead contact, Jacob Glanville ([jake@centivax.com](mailto:jake@centivax.com)).

### Materials availability

Plasmids generated in this study are available upon request.

### Data and code availability

- Crystal structures have been deposited to PDB with accession codes PDB: 8D9Y, 8D9Z, 8DA0, 8DA1, 8V13.
- This paper does not report original code.
- Any additional information required to reanalyze the data reported in this paper is available from the [lead contact](#) upon request.

### ACKNOWLEDGMENTS

We thank Timothy Friede for blood sample donations and detailed knowledge of herpetology; Kent Matlack for insightful discussion, comments, and detailed editorial review of the manuscript; Jonathan Stuckey for assistance with figures; and members of the Virology Laboratory, Vaccine Research Center, for comments and discussions. Funding was provided in part by the Vaccine Research Center, an intramural Division of the National Institute of Allergy and Infectious Diseases of the National Institutes of Health, and the National Institutes of Health Small Business Innovation Research program. Use of sector 22 (Southeast Region Collaborative Access team) at the Advanced Photon Source was supported by the US Department of Energy, Basic Energy Sciences, Office of Science, under contract number W-31-109-Eng-38.

### AUTHOR CONTRIBUTIONS

Conceptualization and design, J.G. and P.D.K.; methodology, J.G., M.B., S.P., B.Z., J.C.A., Sangil Kim, D.T., R.V., R.B., S.L., R.N., N.L.B., S.Y., E.S.T., T.B., Sujeong Kim, H.H., T.L., and P.D.K.; formal analysis, J.G., S.P., B.Z., R.B., and M.B.; investigation, J.G., M.B., S.P., B.Z., J.C.A., Sangil Kim, D.T., R.V., R.B., S.L., R.N., N.L.B., S.Y., E.S.T., T.B., Sujeong Kim, H.H., and T.L.; funding acquisition, project administration, and supervision, J.G. and P.D.K.; writing – original draft, J.G., S.P., B.Z., and P.D.K.; writing – review and editing, J.G. and P.D.K., with input from all authors.

### DECLARATION OF INTERESTS

J.G., N.L.B., D.T., and S.Y. are co-founders and shareholders of Centivax. J.C.A., M.B., H.H., Sangil Kim, R.B., and Sujeong Kim are employees and shareholders of Centivax.

### STAR METHODS

Detailed methods are provided in the online version of this paper and include the following:

- **KEY RESOURCES TABLE**
- **EXPERIMENTAL MODEL AND SUBJECT DETAILS**
  - Ethics Statement
  - Donor blood samples
  - Plasma & PBMCs
  - In vivo
- **METHOD DETAILS**
  - Venom diversity panel
  - Serum ELISA
  - Amplicons
  - Library
  - Recombinants
  - Panning
  - PPE Screening
  - Informatics
  - Kinetics
  - Antibody immunoprecipitation of 3FTX from venom with mass spectroscopy identification
  - Conservation
  - Purification for crystallography
  - Biolayer interferometry reactivity to whole venom

- Crystallization
- Data collection and processing
- Structure determination and analysis
- In vivo challenge
- QUANTIFICATION AND STATISTICAL ANALYSIS

## SUPPLEMENTAL INFORMATION

Supplemental information can be found online at <https://doi.org/10.1016/j.cell.2025.03.050>.

Received: February 27, 2024

Revised: December 18, 2024

Accepted: March 31, 2025

Published: May 2, 2025

## REFERENCES

1. Chippaux, J.-P. (2017). Snakebite envenomation turns again into a neglected tropical disease!. *J. Venom Anim. Toxins Incl. Trop. Dis.* 23, 38. <https://doi.org/10.1186/s40409-017-0127-6>.
2. Chippaux, J.P. (1998). Snake-bites: appraisal of the global situation. *Bull. World Health Organ.* 76, 515–524.
3. Gutiérrez, J.M., Calvete, J.J., Habib, A.G., Harrison, R.A., Williams, D.J., and Warrell, D.A. (2017). Snakebite envenoming. *Nat. Rev. Dis. Primers* 3, 17063. <https://doi.org/10.1038/nrdp.2017.63>.
4. Gutiérrez, J.M., León, G., Lomonte, B., and Angulo, Y. (2011). Antivenoms for snakebite envenomings. *Inflamm. Allergy Drug Targets* 10, 369–380. <https://doi.org/10.2174/187152811797200669>.
5. Pucca, M.B., Cerni, F.A., Janke, R., Bermúdez-Méndez, E., Ledsgaard, L., Barbosa, J.E., and Laustsen, A.H. (2019). History of Envenomotherapy and Current Perspectives. *Front. Immunol.* 10, 1598. <https://doi.org/10.3389/fimmu.2019.01598>.
6. Ariaratnam, C.A., Sheriff, M.H.R., Arambepola, C., Theakston, R.D.G., and Warrell, D.A. (2009). Syndromic approach to treatment of snake bite in Sri Lanka based on results of a prospective national hospital-based survey of patients envenomed by identified snakes. *Am. J. Trop. Med. Hyg.* 81, 725–731. <https://doi.org/10.4269/ajtmh.2009.09-0225>.
7. León, G., Herrera, M., Segura, Á., Villalta, M., Vargas, M., and Gutiérrez, J.M. (2013). Pathogenic mechanisms underlying adverse reactions induced by intravenous administration of snake antivenoms. *Toxicon* 76, 63–76. <https://doi.org/10.1016/j.toxicon.2013.09.010>.
8. Sousa, L.F., Nicolau, C.A., Peixoto, P.S., Bernardoni, J.L., Oliveira, S.S., Portes-Junior, J.A., Mourão, R.H.V., Lima-dos-Santos, I., Sano-Martins, I.S., Chalkidis, H.M., et al. (2013). Comparison of phylogeny, venom composition and neutralization by antivenom in diverse species of bo-throps complex. *PLoS Negl. Trop. Dis.* 7, e2442. <https://doi.org/10.1371/journal.pntd.0002442>.
9. Patra, A., Banerjee, D., Dasgupta, S., and Mukherjee, A.K. (2021). The in vitro laboratory tests and mass spectrometry-assisted quality assessment of commercial polyvalent antivenom raised against the “Big Four” venomous snakes of India. *Toxicon* 192, 15–31. <https://doi.org/10.1016/j.toxicon.2020.12.015>.
10. Gummin, D.D., Mowry, J.B., Spyker, D.A., Brooks, D.E., Fraser, M.O., and Banner, W. (2017). 2016 Annual Report of the American Association of Poison Control Centers’ National Poison Data System (NPDS): 34th Annual Report. *Clin. Toxicol. (Phila)* 55, 1072–1252. <https://doi.org/10.1080/15563650.2017.1388087>.
11. Jiang, Y., Li, Y., Lee, W., Xu, X., Zhang, Y., Zhao, R., Zhang, Y., and Wang, W. (2011). Venom gland transcriptomes of two elapid snakes (*Bungarus multicinctus* and *Naja atra*) and evolution of toxin genes. *BMC Genomics* 12, 1. <https://doi.org/10.1186/1471-2164-12-1>.
12. WHO Expert Committee on Biological Standardization. (2017). Annex 5 – Guidelines for the production, control and regulation of snake antivenom immunoglobulins. <https://www.who.int/publications/m/item/snake-antivenom-immunoglobulins-annex-5-trs-no-1004>.
13. Tasoulis, T., and Isbister, G.K. (2017). A Review and Database of Snake Venom Proteomes. *Toxins* 9, 290. <https://doi.org/10.3390/toxins9090290>.
14. Gilliam, L.L., Carmichael, R.C., Holbrook, T.C., Taylor, J.M., Ownby, C.L., McFarlane, D., and Payton, M.E. (2013). Antibody Responses to Natural Rattlesnake Envenomation and a Rattlesnake Toxoid Vaccine in Horses. *Clin. Vaccine Immunol.* 20, 732–737. <https://doi.org/10.1128/CVI.00004-13>.
15. Ledsgaard, L., Jenkins, T.P., Davidsen, K., Krause, K.E., Martos-Esteban, A., Engmark, M., Rørdam Andersen, M., Lund, O., and Laustsen, A.H. (2018). Antibody cross-reactivity in antivenom research. *Toxins* 10, 393. <https://doi.org/10.3390/toxins10100393>.
16. Vanuopadath, M., Raveendran, D., Nair, B.G., and Nair, S.S. (2020). Evaluating the Immunological cross-reactivity of Indian polyvalent antivenoms towards the venom of *Hypnale hypnale* (hump-nosed pit viper) from the Western Ghats. Preprint at bioRxiv.
17. Clare, R.H., Hall, S.R., Patel, R.N., and Casewell, N.R. (2021). Small molecule drug discovery for neglected tropical snakebite. *Trends Pharmacol. Sci.* 42, 340–353. <https://doi.org/10.1016/j.tips.2021.02.005>.
18. Bracci, L., Pini, A., Lozzi, L., Lelli, B., Battestin, P., Spreafico, A., Bernini, A., Niccolai, N., and Neri, P. (2001). Mimicking the nicotinic receptor binding site by a single chain Fv selected by competitive panning from a synthetic phage library. *J. Neurochem.* 78, 24–31. <https://doi.org/10.1046/j.1471-4159.2001.00398.x>.
19. Ledsgaard, L., Laustsen, A.H., Pus, U., Wade, J., Villar, P., Boddum, K., Slavny, P., Masters, E.W., Arias, A.S., Oscoz, S., et al. (2022). In vitro discovery of a human monoclonal antibody that neutralizes lethality of cobra snake venom. *mAbs* 14, 2085536. <https://doi.org/10.1080/19420862.2022.2085536>.
20. Ledsgaard, L., Wade, J., Jenkins, T.P., Boddum, K., Oganesyan, I., Harrison, J.A., Villar, P., Leah, R.A., Zenobi, R., Schoffelen, S., et al. (2023). Discovery and optimization of a broadly-neutralizing human monoclonal antibody against long-chain  $\alpha$ -neurotoxins from snakes. *Nat. Commun.* 14, 682. <https://doi.org/10.1038/s41467-023-36393-4>.
21. Khalek, I.S., Senji Laxme, R.R., Nguyen, Y.T.K., Khochare, S., Patel, R.N., Woehl, J., Smith, J.M., Saye-Francisco, K., Kim, Y., Misson Mindrebo, L., et al. (2024). Synthetic development of a broadly neutralizing antibody against snake venom long-chain  $\alpha$ -neurotoxins. *Sci. Transl. Med.* 16, eadk1867. <https://doi.org/10.1126/scitranslmed.adk1867>.
22. Vázquez Torres, S., Benard Valle, M., Mackessy, S.P., Menzies, S.K., Casewell, N.R., Ahmadi, S., Burlet, N.J., Muratspahić, E., Sappington, I., Overath, M.D., et al. (2025). De novo designed proteins neutralize lethal snake venom toxins. *Nature* 639, 225–231. <https://doi.org/10.1038/s41586-024-08393-x>.
23. Tréméau, O., Boulain, J.C., Couderc, J., Fromageot, P., and Ménez, A. (1986). A monoclonal antibody which recognized the functional site of snake neurotoxins and which neutralizes all short-chain variants. *FEBS Lett.* 208, 236–240. [https://doi.org/10.1016/0014-5793\(86\)81024-9](https://doi.org/10.1016/0014-5793(86)81024-9).
24. Kelly, C.M.R., Barker, N.P., Villet, M.H., and Broadley, D.G. (2009). Phylogeny, biogeography and classification of the snake superfamily Elapoidea: a rapid radiation in the late Eocene. *Cladistics* 25, 38–63. <https://doi.org/10.1111/j.1096-0031.2008.00237.x>.
25. Nirthanan, S. (2020). Snake three-finger  $\alpha$ -neurotoxins and nicotinic acetylcholine receptors: molecules, mechanisms and medicine. *Biochem. Pharmacol.* 181, 114168. <https://doi.org/10.1016/j.bcp.2020.114168>.
26. Nirthanan, S., and Gwee, M.C.E. (2004). Three-Finger  $\alpha$ -Neurotoxins and the Nicotinic Acetylcholine Receptor, Forty Years On. *J. Pharmacol. Sci.* 94, 1–17. <https://doi.org/10.1254/jphs.94.1>.
27. Fry, B.G., Wüster, W., Kini, R.M., Brusick, V., Khan, A., Venkataraman, D., and Rooney, A.P. (2003). Molecular evolution and phylogeny of elapid snake venom three-finger toxins. *J. Mol. Evol.* 57, 110–129. <https://doi.org/10.1007/s00239-003-2461-2>.

28. Senji Laxme, R.R., Khochare, S., de Souza, H.F., Ahuja, B., Suranse, V., Martin, G., Whitaker, R., and Sunagar, K. (2019). Beyond the “big four”: Venom profiling of the medically important yet neglected Indian snakes reveals disturbing antivenom deficiencies. *PLoS Negl. Trop. Dis.* 13, e0007899. <https://doi.org/10.1371/journal.pntd.0007899>.
29. Antil-Delbeke, S., Gaillard, C., Tamiai, T., Corringer, P.J., Changeux, J.P., Servent, D., and Ménez, A. (2000). Molecular determinants by which a long chain toxin from snake venom interacts with the neuronal alpha 7-nicotinic acetylcholine receptor. *J. Biol. Chem.* 275, 29594–29601. <https://doi.org/10.1074/jbc.M909746199>.
30. Bossy, B., Ballivet, M., and Spierer, P. (1988). Conservation of neural nicotinic acetylcholine receptors from *Drosophila* to vertebrate central nervous systems. *EMBO J.* 7, 611–618. <https://doi.org/10.1002/j.1460-2075.1988.tb02854.x>.
31. De Luca, D., Minucci, A., Trias, J., Tripodi, D., Conti, G., Zuppi, C., and Capoluongo, E.; Study Group on Secretory Phospholipase in Pediatrics (2012). Varespladib inhibits secretory phospholipase A2 in bronchoalveolar lavage of different types of neonatal lung injury. *J. Clin. Pharmacol.* 52, 729–737. <https://doi.org/10.1177/0091270011405498>.
32. Kuruppu, S., Reeve, S., Smith, A.I., and Hodgson, W.C. (2005). Isolation and pharmacological characterisation of papuantoxin-1, a postsynaptic neurotoxin from the venom of the Papuan black snake (*Pseudechis papuanus*). *Biochem. Pharmacol.* 70, 794–800. <https://doi.org/10.1016/j.bcp.2005.06.003>.
33. Kazandjian, T.D., Petras, D., Robinson, S.D., van Thiel, J., Greene, H.W., Arbuckle, K., Barlow, A., Carter, D.A., Wouters, R.M., Whiteley, G., et al. (2021). Convergent evolution of pain-inducing defensive venom components in spitting cobras. *Science* 371, 386–390. <https://doi.org/10.1126/science.abb9303>.
34. Rahman, M.M., Teng, J., Worrell, B.T., Noviello, C.M., Lee, M., Karlin, A., Stowell, M.H.B., and Hibbs, R.E. (2020). Structure of the native muscle-type nicotinic receptor and inhibition by snake venom toxins. *Neuron* 106, 952–962.e5. <https://doi.org/10.1016/j.neuron.2020.03.012>.
35. Silva, A., Hodgson, W.C., and Ibslister, G.K. (2017). Antivenom for Neuromuscular Paralysis Resulting From Snake Envenoming. *Toxins (Basel)* 9, 143. <https://doi.org/10.3390/toxins9040143>.
36. Alfa-Ibrahim Adio, A., Malami, I., Lawal, N., Jega, A.Y., Abubakar, B., Bello, M.B., Ibrahim, K.G., Abubakar, M.B., Abdussamad, A., and Imam, M.U. (2024). Neurotoxic snakebites in Africa: Clinical implications, therapeutic strategies, and antivenom efficacy. *Toxicon* 247, 107811. <https://doi.org/10.1016/j.toxicon.2024.107811>.
37. Nys, M., Zarkadas, E., Brams, M., Mehregan, A., Kambara, K., Kool, J., Casewell, N.R., Bertrand, D., Baeniger, J.E., Nury, H., et al. (2022). The molecular mechanism of snake short-chain  $\alpha$ -neurotoxin binding to muscle-type nicotinic acetylcholine receptors. *Nat. Commun.* 13, 4543. <https://doi.org/10.1038/s41467-022-32174-7>.
38. Zinenko, O., Tovstukha, I., and Korniyenko, Y. (2020). PLA2 Inhibitor Varespladib as an Alternative to the Antivenom Treatment for Bites from Nikolsky's Viper *Vipera berus nikolskii*. *Toxins (Basel)* 12, 356. <https://doi.org/10.3390/toxins12060356>.
39. Bekker, L.-G., Das, M., Abdool Karim, Q., Ahmed, K., Batting, J., Brumskine, W., Gill, K., Harkoo, I., Jaggernath, M., Kigozi, G., et al. (2024). Twice-Yearly Lenacapavir or Daily F/TAF for HIV Prevention in Cisgender Women. *N. Engl. J. Med.* 391, 1179–1192. <https://doi.org/10.1056/NEJMoa2407001>.
40. Glanville, J., Zhai, W., Berka, J., Telman, D., Huerta, G., Mehta, G.R., Ni, I., Mei, L., Sundar, P.D., Day, G.M.R., et al. (2009). Precise determination of the diversity of a combinatorial antibody library gives insight into the human immunoglobulin repertoire. *Proc. Natl. Acad. Sci. USA* 106, 20216–20221. <https://doi.org/10.1073/pnas.0909775106>.
41. Wu, X., Yang, Z.-Y., Li, Y., Hogerkorp, C.-M., Schief, W.R., Seaman, M.S., Zhou, T., Schmidt, S.D., Wu, L., Xu, L., et al. (2010). Rational Design of Envelope Identifies Broadly Neutralizing Human Monoclonal Antibodies to HIV-1. *Science* 329, 856–861. <https://doi.org/10.1126/science.1187659>.
42. Winn, M.D., Ballard, C.C., Cowtan, K.D., Dodson, E.J., Emsley, P., Evans, P.R., Keegan, R.M., Krissinel, E.B., Leslie, A.G.W., McCoy, A., et al. (2011). Overview of the CCP4 suite and current developments. *Acta Crystallogr. D Biol. Crystallogr.* 67, 235–242. <https://doi.org/10.1107/S0907444910045749>.
43. Pettersen, E.F., Goddard, T.D., Huang, C.C., Couch, G.S., Greenblatt, D.M., Meng, E.C., and Ferrin, T.E. (2004). UCSF Chimera—a visualization system for exploratory research and analysis. *J. Comput. Chem.* 25, 1605–1612. <https://doi.org/10.1002/jcc.20084>.
44. Pettersen, E.F., Goddard, T.D., Huang, C.C., Meng, E.C., Couch, G.S., Croll, T.I., Morris, J.H., and Ferrin, T.E. (2021). UCSF ChimeraX: Structure visualization for researchers, educators, and developers. *Protein Sci.* 30, 70–82. <https://doi.org/10.1002/proc.3943>.
45. Emsley, P., and Cowtan, K. (2004). Coot: model-building tools for molecular graphics. *Acta Crystallogr. D Biol. Crystallogr.* 60, 2126–2132. <https://doi.org/10.1107/S0907444904019158>.
46. Emsley, P., Lohkamp, B., Scott, W.G., and Cowtan, K. (2010). Features and development of Coot. *Acta Crystallogr. D Biol. Crystallogr.* 66, 486–501. <https://doi.org/10.1107/S0907444910007493>.
47. Ye, J., Ma, N., Madden, T.L., and Ostell, J.M. (2013). IgBLAST: an immunoglobulin variable domain sequence analysis tool. *Nucleic Acids Res.* 41, W34–W40. <https://doi.org/10.1093/nar/gkt382>.
48. Barad, B.A., Echols, N., Wang, R.Y.-R., Cheng, Y., DiMaio, F., Adams, P.D., and Fraser, J.S. (2015). EMRinger: side chain-directed model and map validation for 3D cryo-electron microscopy. *Nat. Methods* 12, 943–946. <https://doi.org/10.1038/nmeth.3541>.
49. Williams, C.J., Headd, J.J., Moriarty, N.W., Prisant, M.G., Videau, L.L., Deis, L.N., Verma, V., Keedy, D.A., Hintze, B.J., Chen, V.B., et al. (2018). MolProbity: More and better reference data for improved all-atom structure validation. *Protein Sci.* 27, 293–315. <https://doi.org/10.1002/pro.3330>.
50. Sethna, Z., Elhanati, Y., Callan, C.G., Jr., Walczak, A.M., and Mora, T. (2019). OLGA: fast computation of generation probabilities of B- and T-cell receptor amino acid sequences and motifs. *Bioinformatics* 35, 2974–2981. <https://doi.org/10.1093/bioinformatics/btz035>.
51. Krissinel, E., and Henrick, K. (2007). Inference of macromolecular assemblies from crystalline state. *J. Mol. Biol.* 372, 774–797. <https://doi.org/10.1016/j.jmb.2007.05.022>.
52. Liebschner, D., Afonine, P.V., Baker, M.L., Bunkóczki, G., Chen, V.B., Croll, T.I., Hintze, B., Hung, L.W., Jain, S., McCoy, A.J., et al. (2019). Macromolecular structure determination using X-rays, neutrons and electrons: recent developments in Phenix. *Acta Crystallogr. D Struct. Biol.* 75, 861–877. <https://doi.org/10.1107/S2059798319011471>.
53. Afonine, P.V., Grosse-Kunstleve, R.W., Echols, N., Headd, J.J., Moriarty, N.W., Mustyakimov, M., Terwilliger, T.C., Urzhumtsev, A., Zwart, P.H., and Adams, P.D. (2012). Towards automated crystallographic structure refinement with phenix.refine. *Acta Crystallogr. D Biol. Crystallogr.* 68, 352–367. <https://doi.org/10.1107/S0907444912001308>.
54. Adams, P.D., Afonine, P.V., Bunkóczki, G., Chen, V.B., Davis, I.W., Echols, N., Headd, J.J., Hung, L.-W., Kapral, G.J., Grosse-Kunstleve, R.W., et al. (2010). PHENIX: a comprehensive Python-based system for macromolecular structure solution. *Acta Crystallogr. D Biol. Crystallogr.* 66, 213–221. <https://doi.org/10.1107/S0907444909052925>.
55. Cates, C.C., Valore, E.V., Couto, M.A., Lawson, G.W., and McCabe, J.G. (2015). Comparison of the protective effect of a commercially available western diamondback rattlesnake toxoid vaccine for dogs against envenomation of mice with western diamondback rattlesnake (*Crotalus atrox*), northern Pacific rattlesnake (*Crotalus oreganus oreganus*), and southern Pacific rattlesnake (*Crotalus oreganus helleri*) venom. *Am. J. Vet. Res.* 76, 272–279. <https://doi.org/10.2460/ajvr.76.3.272>.
56. Hastie, K.M., Li, H., Bedinger, D., Schendel, S.L., Dennison, S.M., Li, K., Rayaprolu, V., Yu, X., Mann, C., Zandonatti, M., et al. (2021). Defining variant-resistant epitopes targeted by SARS-CoV-2 antibodies: A global

- consortium study. *Science* 374, 472–478. <https://doi.org/10.1126/science.abh2315>.
57. Rujas, E., Kucharska, I., Tan, Y.Z., Benlekbir, S., Cui, H., Zhao, T., Wasney, G.A., Budylowski, P., Guvenc, F., Newton, J.C., et al. (2021). Multivalency transforms SARS-CoV-2 antibodies into ultrapotent neutralizers. *Nat. Commun.* 12, 3661. <https://doi.org/10.1038/s41467-021-23825-2>.
58. UniProt Consortium (2021). UniProt: the universal protein knowledgebase in 2021. *Nucleic Acids Res.* 49, D480–D489. <https://doi.org/10.1093/nar/gkaa1100>.
59. Glanville, J., Kuo, T.C., Von Büdingen, H.-C., Guey, L., Berka, J., Sundar, P.D., Huerta, G., Mehta, G.R., Oksenberg, J.R., Hauser, S.L., et al. (2011). Naive antibody gene-segment frequencies are heritable and unaltered by chronic lymphocyte ablation. *Proc. Natl. Acad. Sci. USA* 108, 20066–20071. <https://doi.org/10.1073/pnas.1107498108>.
60. Sayers, E.W., Bolton, E.E., Brister, J.R., Canese, K., Chan, J., Comeau, D.C., Connor, R., Funk, K., Kelly, C., Kim, S., et al. (2022). Database resources of the national center for biotechnology information. *Nucleic Acids Res.* 50, D20–D26. <https://doi.org/10.1093/nar/gkab1112>.
61. Potter, S.C., Luciani, A., Eddy, S.R., Park, Y., Lopez, R., and Finn, R.D. (2018). HMMER web server: 2018 update. *Nucleic Acids Res.* 46, W200–W204. <https://doi.org/10.1093/nar/gky448>.
62. Otwinowski, Z., and Minor, W. (1997). Processing of X-ray diffraction data collected in oscillation mode. *Methods Enzymol.* 276, 307–326. [https://doi.org/10.1016/S0076-6879\(97\)76066-X](https://doi.org/10.1016/S0076-6879(97)76066-X).
63. Long, F., Vagin, A.A., Young, P., and Murshudov, G.N. (2008). BALBES: a molecular-replacement pipeline. *Acta Crystallogr. D Biol. Crystallogr.* 64, 125–132. <https://doi.org/10.1107/S0907444907050172>.
64. Murshudov, G.N., Skubák, P., Lebedev, A.A., Pannu, N.S., Steiner, R.A., Nicholls, R.A., Winn, M.D., Long, F., and Vagin, A.A. (2011). REFMAC5 for the refinement of macromolecular crystal structures. *Acta Crystallogr. D Biol. Crystallogr.* 67, 355–367. <https://doi.org/10.1107/S0907444911001314>.
65. Schrödinger, LLC. The PyMOL Molecular Graphics System Version 1.2r3pre. <https://www.pymol.org/>.

## STAR★METHODS

### KEY RESOURCES TABLE

REAGENT or RESOURCE	SOURCE	IDENTIFIER
<b>Antibodies</b>		
LNX-D09	This study	N/A
SNX-B03	This study	N/A
VRC01	Wu et al. <sup>41</sup>	N/A
<b>Chemicals, Peptides, Recombinant Proteins and Biosensors</b>		
Pierce Protein A Agarose	ThermoFisher Scientific	20334
Turbo293 transfection reagent	SPEED BioSystem	PXX1002
AbBooster medium	ABI Scientific	PB2668
<b>Biological Samples</b>		
Arabian Cobra ( <i>Naja arabica</i> )	Mtoxins	<a href="https://medtoxin.com/">https://medtoxin.com/</a>
Banded Sea Krait ( <i>Laticauda colubrina</i> )	Mtoxins	<a href="https://medtoxin.com/">https://medtoxin.com/</a>
Black Mamba ( <i>Dendroaspis polylepis</i> )	Mtoxins	<a href="https://medtoxin.com/">https://medtoxin.com/</a>
Cape Cobra ( <i>Naja nivea</i> )	Mtoxins	<a href="https://medtoxin.com/">https://medtoxin.com/</a>
Coastal Taipan ( <i>Oxyuranus scutellatus</i> )	Mtoxins	<a href="https://medtoxin.com/">https://medtoxin.com/</a>
Common Krait ( <i>Bungarus caeruleus</i> )	Miami Serpentarium Laboratories	<a href="https://www.miamiserpentarium.com/">https://www.miamiserpentarium.com/</a>
Death Adder ( <i>Acanthopis antarcticus</i> )	Venom Supplies	<a href="http://www.venomsupplies.com/">http://www.venomsupplies.com/</a>
Eastern Brown Snake ( <i>Pseudonaja textilis</i> )	Venom Supplies	<a href="http://www.venomsupplies.com/">http://www.venomsupplies.com/</a>
Eastern Coral Snake ( <i>Micruurus fulvius</i> )	Mtoxins	<a href="https://medtoxin.com/">https://medtoxin.com/</a>
Eastern Green Mamba ( <i>Dendroaspis angusticeps</i> )	Latoxan	<a href="https://www.latoxan.com/">https://www.latoxan.com/</a>
Egyptian Cobra ( <i>Naja haje</i> )	Mtoxins	<a href="https://medtoxin.com/">https://medtoxin.com/</a>
Forest Cobra ( <i>Naja melanoleuca</i> )	Latoxan	<a href="https://www.latoxan.com/">https://www.latoxan.com/</a>
Indian Cobra ( <i>Naja naja</i> )	Mtoxins	<a href="https://medtoxin.com/">https://medtoxin.com/</a>
Indochinese Spitting Cobra ( <i>Naja siamensis</i> )	Mtoxins	<a href="https://medtoxin.com/">https://medtoxin.com/</a>
Inland Taipan ( <i>Oxyuranus microlepidotus</i> )	Mtoxins	<a href="https://medtoxin.com/">https://medtoxin.com/</a>
Javan Spitting Cobra ( <i>Naja sputatrix</i> )	Mtoxins	<a href="https://medtoxin.com/">https://medtoxin.com/</a>
King Brown Snake ( <i>Pseudechis australis</i> )	Latoxan	<a href="https://www.latoxan.com/">https://www.latoxan.com/</a>
King Cobra ( <i>Ophiophagus hannah</i> )	Mtoxins	<a href="https://medtoxin.com/">https://medtoxin.com/</a>
Monocled Cobra ( <i>Naja kaouthia</i> )	Mtoxins	<a href="https://medtoxin.com/">https://medtoxin.com/</a>
Mozambique Spitting Cobra ( <i>Naja mossambica</i> )	Mtoxins	<a href="https://medtoxin.com/">https://medtoxin.com/</a>
Papuan Black Snake ( <i>Pseudechis papuanus</i> )	Venom Supplies	<a href="http://www.venomsupplies.com/">http://www.venomsupplies.com/</a>
Red Spitting Cobra ( <i>Naja pallida</i> )	Latoxan	<a href="https://www.latoxan.com/">https://www.latoxan.com/</a>
Russell's Viper ( <i>Daboia russelii</i> )	Mtoxins	<a href="https://medtoxin.com/">https://medtoxin.com/</a>
Russian Cobra ( <i>Naja oxiana</i> )	Mtoxins	<a href="https://medtoxin.com/">https://medtoxin.com/</a>
Samar Cobra ( <i>Naja samarensis</i> )	Mtoxins	<a href="https://medtoxin.com/">https://medtoxin.com/</a>
Snouted Cobra ( <i>Naja annulifera</i> )	Mtoxins	<a href="https://medtoxin.com/">https://medtoxin.com/</a>
Tiger Snake ( <i>Notechis scutatus</i> )	Miami Serpentarium Laboratories	<a href="https://www.miamiserpentarium.com/">https://www.miamiserpentarium.com/</a>
Western Diamondback ( <i>Crotalus atrox</i> )	Mtoxins	<a href="https://medtoxin.com/">https://medtoxin.com/</a>
Western Green Mamba ( <i>Dendroaspis viridis</i> )	Latoxan	<a href="https://www.latoxan.com/">https://www.latoxan.com/</a>
<b>Deposited Data</b>		
Taipan-D09 structure	This study	PDB: 8D9Y
Cobra-D09 structure	This study	PDB: 8D9Z
Mamba-D09 structure	This study	PDB: 8DA0

(Continued on next page)

**Continued**

REAGENT or RESOURCE	SOURCE	IDENTIFIER
Krait-D09 structure	This study	PDB: 8DA1
Black mamba-B03 structure	This study	PDB: 8V13
<b>Experimental Models: Cell Lines</b>		
Expi293F cells	Thermo Fisher	A14527
<b>Recombinant DNA</b>		
pVRC8400-D09 plasmids	This study	N/A
pVRC8400-B03 plasmids	This study	N/A
<b>Software and Algorithms</b>		
CCP4i v7.1	Winn et al. <sup>42</sup>	<a href="https://www CCP4.ac.uk/">https://www CCP4.ac.uk/</a>
UCSF Chimera	Pettersen et al. <sup>43</sup>	<a href="https://www.cgl.ucsf.edu/chimera/">https://www.cgl.ucsf.edu/chimera/</a>
UCSF ChimeraX	Pettersen et al. <sup>44</sup>	<a href="https://www.cgl.ucsf.edu/chimerax/">https://www.cgl.ucsf.edu/chimerax/</a>
Coot v0.9.7	Emsley and Cowtan <sup>45</sup> and Emsley et al. <sup>46</sup>	<a href="https://www2.mrc-lmb.cam.ac.uk/personal/pemsley/coot/">https://www2.mrc-lmb.cam.ac.uk/personal/pemsley/coot/</a>
IgBlast	Ye et al. <sup>47</sup>	<a href="https://www.ncbi.nlm.nih.gov/igblast/">https://www.ncbi.nlm.nih.gov/igblast/</a>
MolProbity	Barad et al. <sup>48</sup> and Williams et al. <sup>49</sup>	<a href="http://molprobity.biochem.duke.edu">http://molprobity.biochem.duke.edu</a>
OLGA	Sethna et al. <sup>50</sup>	<a href="https://github.com/statbiophys/OLGA">https://github.com/statbiophys/OLGA</a>
PDBePISA	Krissinel and Henrick <sup>51</sup>	<a href="https://www.ebi.ac.uk/pdbe/pisa/">https://www.ebi.ac.uk/pdbe/pisa/</a>
Phenix v1.21	Liebschner et al., <sup>52</sup> Afonine et al., <sup>53</sup> and Adams et al. <sup>54</sup>	<a href="https://phenix-online.org">https://phenix-online.org</a>
PRISM	GraphPad Software	<a href="https://www.graphpad.com/scientific-software/prism/">https://www.graphpad.com/scientific-software/prism/</a>
Pymol v1.8.6	Schrödinger LLC	<a href="https://pymol.org/2/">https://pymol.org/2/</a>

## EXPERIMENTAL MODEL AND SUBJECT DETAILS

### Ethics Statement

The study of human samples was strictly non-interventional: the donor was neither directed to expose himself to venom nor provided any guidance on venom self-exposure. Over an 18-year period prior to being contacted by researchers, the donor had independently chosen to self-immunize with snake venom, and had independently developed a standard protocol for periodic venom self-immunizations. The donor notified researchers of his self-immunization schedule, and researchers arranged for a commercial phlebotomy service to obtain 20ml blood samples before and 7 days following the donor's next self-scheduled self-immunization. Informed consent was obtained for the two 20ml blood samples collected. Collection was conducted in accordance with Western Institutional Review Board IRB Exemption Work Order #1-1209200-1. No further samples were taken. Researchers provided materials to donor on the risks of the self-envenomation. In 2018, the donor retired from self-envenoming.

All animal husbandry and experimental protocols were conducted under the guidance of approved IACUC animal use protocol CR-0119, reviewed, approved and assigned by Charles River D Laboratory (CRADL, South San Francisco, CA) IACUC administrator. To minimize the number of animals used, an animal-sparing “up-and-down” methodology of estimating the LD<sub>50</sub> that involved serial intradermal injection of predetermined mg/kg dosages of venom<sup>55</sup> was adopted. In accordance with the IACUC protocol, animals were monitored and mice euthanized if distress signs appeared, including body temperature reduction greater than 4°C, bodyweight loss more than 20% in 24 hours, and hunched posture, ruffled fur, prolonged lack of movement, moribundity, bleeding, or no signs of reversibility. Euthanization was by CO<sub>2</sub> followed by cervical dislocation.

### Donor blood samples

The blood donor participant requested and agreed to divulge his identity and be publicly identified in the Acknowledgements of this publication, and provided authors with written informed consent to this end.

### Plasma & PBMCs

Blood was obtained by ExamOne (<https://www.examone.com/>) in four 10ml purple top EDTA anti-coagulant vials. Plasma and cells from each blood draw were isolated by centrifugation at 25°C for 10 minutes at 300xg. Informed consent was obtained from the

donor. Western Institutional Review Board (WIRB, now wcgIRB) provided IRB exemption determination #1-1209200-1 for the study of the samples of a single donor (1019 39<sup>th</sup> Avenue SE Suite 120, Puyallup, WA98374).

### In vivo

All animal husbandry and experimental protocols were conducted under the guidance of approved IACUC animal use protocol CR-0119 reviewed, approved and assigned by Charles River D Laboratory (CRADL, South San Francisco, CA) IACUC administrator.

The studies used 8 week-old female C57BL/6 mice with body weights ranging between 18–22 g. Mice were maintained in plastic boxes with water and food and libitum, with 12 hour dark/light cycles.

## METHOD DETAILS

### Venom diversity panel

Venoms were sourced from Latoxan, Mtoxins, Venomsupplies, and Medtoxins.

### Serum ELISA

One hundred nanograms of each recombinant, C-terminal his-avi tagged long-neurotoxin protein from Alpha-elapitotoxin-Dpp2a (3L24\_DENPO) from *Dendroaspis polylepis* (black mamba), alpha-cobratoxin/long neurotoxin 1 (3L21\_NAJNI) from *Naja nivea* (Cape cobra), Long neurotoxin 1 (3L21\_OXYSC) from *Oxyuranus scutellatus scutellatus* (coastal taipan), and Alpha-delta bungarotoxin (3L2A\_BUNCE) from *Bungarus caeruleus* (common krait) were added to microtiter plates (Corning), in phosphate-buffered saline (PBS). After incubation at 4°C overnight and blocking with 3% bovine serum albumin (BSA) (Sigma-Aldrich) in PBS for 1 hour at 37°C, serially diluted plasma (fivefold, six dilutions, starting from 1:100) in blocking buffer was added to wells and incubated for 1 hour at 37°C. Then, plates were washed three times with 0.05% (v/v) Tween 20 (Sigma-Aldrich) in PBS (PBST). Horseradish peroxidase (HRP)-conjugated donkey anti-human IgG Ab (Jackson Immuno Research Labs) was added to wells and incubated for 1 hour at 37°C. After washing three times with PBST, 2,2'-azino-bis-3-ethylbenzothiazoline-6-sulfonic acid (Thermo Fisher) was added to the wells. Absorbance was measured at 415 nm using a microplate spectrophotometer (Multiskan Skyhigh, Thermo Fisher). All experiments were performed in triplicate, and data are presented as the mean ± SD.

### Amplicons

PBMC RNA was extracted from cells by RBC lysis followed by RNeasy Mini Kit according to the manufacturer's protocol (QIAgen). PBMC lysate was homogenized via QIAshredder spin columns (QIAgen) prior to use of RNeasy Mini Spin columns. Following RNA isolation, cDNA was generated using a High Capacity cDNA Reverse Transcription Kit (ThermoFisher) following the manufacturer's protocol. Antibody V-genes (VH, VK, VL) were then amplified from cDNA using custom designed HTS+Display primers to add multiplexed dephasing adapted ends for Illumina MiSeq loading as well as Fv-boundary restriction sites to enable direct digestion and library construction (Table S1).

PCR amplification reactions were run with adapted primers at 10 µM using OneTaq Polymerase in GC Buffer (New England Biolabs) at the following cycling conditions: initial denaturation of 2 minutes at 94°C, thirty cycles of 94°C denaturation for 30 seconds, 53°C annealing for 30 seconds, 68°C extension for 45 seconds, and a final extension of 68°C for 2 minutes. A second Paired End PCR reaction was run to further amplify the resulting MiSeq library as well as add additional bases required for hybridization to the MiSeq flow cell with primers dubbed OptPE1 and OptPE2. This reaction was performed with primers at 10 µM and Phusion Polymerase with GC Buffer (New England Biolabs) at the following cycling conditions: initial denaturation at 98°C for 30 seconds, followed by 12 cycles of 98°C denaturation for 8 seconds, 69°C annealing for 12 seconds, 72°C extension for 10 seconds, and a final extension of 72°C for 5 minutes. Each domain was deep sequenced by MiSeq (2x300 v3 kit).

### Library

From the hyperimmune PBMC sample, broadly neutralizing monoclonal antibodies were isolated by phage display. From 40 ml of blood, containing approximately 16 million B cells, antibody variable heavy (VL) and light (VL) domains were amplified by multiplex phage adaptor PCR. Amplicons were digested and cloned into an M13 pIII fusion phage display scFv vector in the VH-VL-pIII orientation, with a 15-mer (G4S1)3 linker bounded by restriction sites, the method adapted from previously described methods.<sup>56,57</sup> The library was cloned into two sub-libraries: one utilizing the VK amplicon as light chain and one using the VL amplicon. The VH/VK library was electroporated into ER2738 bacterial phage display electrocompetent cells (Lucigen) at 9.24e8 transformants and the VH/VL library at 1.28e9 transformants for a total library size of 2.21e9 transformants. The resulting library was then rescued using M13K07 Helper Phage (New England Biolabs) at a Multiplicity of Infection (MOI) of 20.

Sequencing of 4.3 million amplicons identified at least 45,174 unique third heavy chain complementarity determining regions (CDR-H3) sequences and 36,817 unique third light chain (CDR-L3) sequences, excluding singlettons. These domains were underwent combinatoric assembly into an m13 VH-VL scFv-pIII fusion display vector and transformed to a final library size of 2.21e9, such that every observed VH domain was associated with every VL domain in the library, including every original native VH/VL pair.

### Recombinants

From an analysis of 6706 toxins from 703 snake species in the Uniprot database,<sup>58</sup> Alpha-elapitoxin-Dpp2a (Uniprot: 3L24\_DENPO) from *Dendroaspis polylepis* (black mamba), alpha-cobratoxin/long neurotoxin 1 (Uniprot: 3L21\_NAJNI) from *Naja nivea* (Cape cobra), Long neurotoxin 1 (Uniprot: 3L21\_OXYSC) from *Oxyuranus scutellatus scutellatus* (coastal taipan), Alpha-delta bungarotoxin (Uniprot: 3L2A\_BUNCE) from *Bungarus caeruleus* (common krait), and 21 other toxins were selected for recombinant expression. Toxins were assigned C-terminal tags, including toxin-Fc-avitag fusions and toxin-10his-avitag fusions. Fc-tag and 10his tags were provided to assist in toxin purification, and avitags were provided to enable site-specific biotinylation to magnetic beads for automated soluble phase panning. When induced for expression in HEK293 cells, 21 of the 25 toxins expressed. Toxins were tag-purified (protein G Dynabeads or nickel beads for Fc and 10xhis tag toxins, respectively), and 15 constructs had strong reactivity to hyperimmune donor serum over healthy control serum by Octet QK. Confirmation of neurotoxic functional activity was performed *in vivo* in B6 mouse Maximum Tolerated Dose (MTD) studies, with Alpha-elapitoxin-Dpp2a from *Dendroaspis polylepis* (black mamba), alpha-cobratoxin/long neurotoxin 1 from *Naja naja* (Indian cobra), Long neurotoxin 1 from *Oxyuranus microlepidotus* (inland taipan), and Alpha-delta bungarotoxin from *Bungarus caeruleus* (common krait) confirmed to be lethal (LD<sub>100</sub>) at 0.5–1mg/kg.

### Panning

Toxins were site-specifically biotinylated at C-terminal avitags and quality-controlled for biotinylation.<sup>56,57</sup> The donor-derived immune library ( $2.21 \times 10^9$ ) was heated for 10 min at 72 °C and de-selected against Protein G Dynabeads<sup>TM</sup> (Invitrogen), M-280 Streptavidin Dynabeads<sup>TM</sup> (Invitrogen), histone from calf thymus (Sigma), human IgG (Sigma) and ssDNA-Biotin NNK from Integrated DNA Technologies and DNA-Biotin NNK from Integrated DNA Technologies. Next, the library was panned against the biotinylated toxin, captured by M-280 Streptavidin Dynabeads<sup>TM</sup> using an automated protocol on a Kingfisher FLEX (Thermofisher). Selected phages were acid eluted from the beads and neutralized using Tris-HCl pH 7.9 (Teknova). ER2738 cells were infected with the neutralized phage pools at OD<sub>600</sub> 0.001s at OD<sub>11</sub>s were infected with min incubation at 37 °C and 100 rpm, the phage pools were centrifuged and incubated on agar with antibiotic selection overnight at 30 °C. The rescued phages were precipitated by PEG and subjected to three additional rounds of soluble phase automated panning. PBST/1% BSA buffer and/or PBS/1% BSA was used in the de-selection, washes and selection rounds. Four rounds of panning were performed on each of the libraries using site-specific avitag biotinylated recombinant long 3FTX as the antigen with reduced concentration in each round (100nM, 20nM, 4nM and, 1nM, respectively) to ensure high selectivity. A different ortholog of long 3FTX was used in each subsequent round to select for breadth: Alpha-elapitoxin-Dpp2a (3L24\_DENPO) from *Dendroaspis polylepis* (black mamba) in round 1, Long neurotoxin 1 (3L21\_OXYSC) from *Oxyuranus scutellatus scutellatus* (coastal taipan) in round 2, alpha-cobratoxin/long neurotoxin 1 (3L21\_NAJNI) from *Naja nivea* (Cape cobra) in round 3, and Alpha-delta bungarotoxin (3L2A\_BUNCE) from *Bungarus caeruleus* (common krait) in round 4.

### PPE Screening

Following panning, 184 scFv clones were induced for expression by Isopropyl β-D-1-thiogalactopyranoside (IPTG) via the lac operon incorporated in the M13 pIII library vector from each panning output. Periplasmic extracts from these clones were screened for binding to the recombinant toxins from which they were panned by ELISA using pre-coated and pre-BSA blocked 96-well ELISA plates (Pierce) to capture the toxins at 2 ug/mL.

### Informatics

Sanger and HTS sequences were analyzed by VDJFasta2.0,<sup>59</sup> utilizing HMMER v3.2 Fv Hidden-Markov Models and NCBI Blast.<sup>60,61</sup> Figures were rendered with Prism and in R.

The LNX-D09 heavy chain has a long CDR-H3 and bears evidence of extensive SHM. LNX-D09 utilized the IGHV3-13 \*\*\*V-gene framework, and had recombined with IGHD3-10 to form a long (18 aa) CDR-H3 loop. LNX-D09 had been highly mutated, bearing 77.4% identity to germline with evidence of affinity maturation by SHM, with 21 amino acid mutations relative to germline IGHV3-13\*01 (93 positions observable: as the first five positions and the J-segment are impacted by primers that can alter amino acid content and therefore masked from analysis, and CDR-H3 VDJ recombination results in non-templated sequence that cannot be inferred and is therefore filtered from analysis), as well as one J-segment SHM. The mutations were concentrated in the CDRs and particularly concentrated in CDR-H2, with two mutations in CDR-H1, nine mutations in CDR-H2, and one mutation in CDR-H3 vernier Kabat 93. Three additional affinity maturation variants of LNX-D09 VH were recovered, all showing evidence of extensive SHM. The LNX-B11 affinity maturation variant, also had broadly neutralizing activity against the target, although not as potent as LNX-D09.

The LNX-D09 light chain was subjected to diversification mutagenesis analysis, revealing total restriction to IGKV1, strong specific restriction to IGKV1-39, and a strong consensus with polymorphic positions concentrated in CDRs. During immune library generation, all antibody VK domains in the donor's sampled repertoire were associated with each heavy chain. After selection, 118 positive clones were recovered belonging to the B9 VH CDR-H3 lineage. The clones contained 14 unique light chains. The light chains were entirely restricted to four IGKV1 V-segment family members, with 100 (85%) belonging to IGKV1-39, 13 (11%) to IGKV1-12, three (2.5%) to IGKV1-5, one (0.8%) to IGKV1-6, and one (0.8%) unresolvable beyond IGKV1 due to sequence quality. Across the 14 unique light chain variants, 37 positions were observed to tolerate mutations, with only nine positions with Simpson's index greater than 0.5: four in CDR-L1, one in CDR-L2, and four in CDR-L3. In the LNX-D09 clone, there were eight positions altered relative to germline (three L1, one L2, one FW3, and three putative L3 positions: the first four positions of FW1 were excluded from analysis

due to library degenerate assembly primers often introducing spurious mutations at this amplification site), although entirely germline IGKV1-39 light chains were also identified to possess broadly reactive binding.

Sequencing of B03 antibody variable domains showed the sequence to be distinct from LNX-D09 and evidence of SHM. The heavy chain contained seven non-synonymous mutations in the V-gene region and four non-templated amino acid positions in a relatively short 9 CDR-H3. Notably, in contrast to LNX-D09, SNX-B03 was not altered from germline in the V-gene encoded CDRs. The light chain contained seven non-synonymous mutations in the V-gene, including four mutations clustered within and proximal to CDR-L2, and three non-templated CDR-L3 modifications including two that most likely represent SHM. It bears noting that the framework 1 mutations in positions 16 of the heavy and light chain may be attributable to degenerative V-gene specific primer-induced mutations generated during library creation.

### Kinetics

The kinetics and affinities for the interactions of LNX-D09 with  $\alpha$ -neurotoxins at 25°C and 37°C were determined on a Biacore 8K SPR instrument (Cytiva, Marlborough, MA). An anti-human Fc capture chip was prepared by amine-coupling a goat anti-human IgG Fc antibody (catalog No. 2014-01, Southern Biotech, Birmingham, AL) to a Biacore Series S CM4 sensor chip (catalog No. BR100534, Cytiva, Marlborough, MA). The running buffer for the immobilization procedure at 25°C was HBS supplemented with 0.05% (v/v) Tween-20. The anti-human Fc was diluted to 50  $\mu$ g/mL in 10 mM sodium acetate pH 4.5, and injected in all flow cells at 20  $\mu$ L/min for 7 minutes after activation of the surfaces with a 1:1 (v/v) mixture of 400 mM EDC and 100 mM N-hydroxysuccinimide (NHS) for 7 minutes at 10  $\mu$ L/min. Excess reactive esters on the surface of flow cells 1 and 2 were blocked for 7 minutes at 10  $\mu$ L/min with 100 mM ethylenediamine in 200 mM borate buffer pH 8.5. Kinetic assays were conducted at 25°C and 37°C with HBS supplemented with 0.05% (v/v) Tween-20 and 1 mg/mL BSA as running buffer. The LNX-D09 bnAb was diluted to 10  $\mu$ g/mL with running buffer and captured by its Fc onto the anti-human Fc surface for 2 minutes at 10  $\mu$ L/min. His tagged toxins were injected as analyte for 2 minutes followed by a 15 minute dissociation at a flow rate of 30  $\mu$ L/min. Five analyte concentrations were 1.2, 3.7, 11.1, 33.3 and 100 nM in addition to a buffer analyte cycle. The anti-human Fc surfaces were regenerated using three 60 second injections of 75 mM phosphoric acid at 10  $\mu$ L/min. Kinetic data were double-referenced (Myszka, 1999), and fit globally to a simple 1:1 Langmuir binding model using Biacore Insight Evaluation Software (version 3.0).<sup>62</sup>

### Antibody immunoprecipitation of 3FTX from venom with mass spectroscopy identification

Lyophilized venom was dissolved in PBS at 50mg/ml. 1mg of venom solution was mixed with 150 $\mu$ g (150 $\mu$ l) of IgG. 100 $\mu$ l Protein A resin (50  $\mu$ l settled resin volume, GE Health Sciences) were added to the venom-antibody mixture. The mixture was then incubated on a rotating shaker at room temperature for one hour. After incubation, the mixture was loaded on an empty Polyprep column (BioRad). The resin in the column was washed twice with 3ml PBS using gravity flow. The resin was resuspended in PBS buffer and transferred to a 1.5ml microtube. Resin was collected by centrifugation and the clarified solution removed. Bound IgG and toxin proteins were eluted with 50 $\mu$ l SDS-PAGE gel loading buffer (Thermo Fisher Scientific). Proteins bound to the Protein A resin were then separated by SDS-PAGE. The bands running at approximately 6 kDa were cut from the gel and sent for mass spectrum (LC/MS/MS) analysis at Poochon Scientific (Frederick, MD). Protein gel-band samples were digested using trypsin/lysC. The LC/MS/MS analysis was carried out using a Thermo Scientific Orbitrap Exploris 240 Mass Spectrometer and a Thermo Dionex UltiMate 3000 RSLC nano System. The instrument was operated in the data-dependent mode to automatically switch between full scan MS and MS/MS acquisition. The MS raw files were analyzed using Proteome Discoverer 2.4 against a snake protein sequence database containing 6706 toxin proteins from 774 species downloaded from NCBI and UniProtKB websites.<sup>58,60</sup> The proteins with matched peptide sequences identified from each sample are summarized in Table S3.

### Conservation

3FTX diversity analysis: Sequences for all 3FTX long neurotoxins were obtained from UniProt SWISS-PROT by both sequence homology to representative PDB ID:1ABT (blastp, e-val: 1e-5) and by sequence annotation.<sup>58</sup> Sequences were aligned by the Muscle alignment algorithm to structural reference 1ABT. Partial sequences were removed, and the remaining full-length sequences rendered non-redundant at 99% amino acid identity. Simpson's diversity index D was calculated for each position in the alignment.

nAChR diversity analysis: 250 putative ortholog amino acid sequences of human reference nAChR were obtained from UniProtKB by blastp (e<1-e5) and aligned by the Muscle alignment algorithm to the human nAChR crystallographic reference structure of the ligand-binding domain (PDBID:4UY2).<sup>58,60</sup> Common names for each species were obtained by lookup against UniProtKB-provided species binomial nomenclature in NCBI taxonomy; mammals, avians, amphibians, reptiles, fish and sharks were identified. Sequences were curated to remove duplicates, partial sequence fragments, and potential paralogs on a per-species basis, leaving 246 sequences in the dataset. UniprotKD annotations were reviewed to confirm that sequence selection criteria successfully selected putative orthologs. Sequences were cropped to the boundaries of the 4UY2 structurally determined ligand-binding domain of the receptor. The aligned nAChR putative orthologs possessed a median of 83% amino acid percent identity (PID) among all sequence distances, 71% PID between the most distant two sequences in the set, and a median of 94% PID among all species in set when considering only positions within 8 angstroms of contact with the alpha-neurotoxin binding site. When fish were excluded, the sequences were nearly completely conserved (97% PID) across mammals, avians, amphibians, and reptiles. To calculate conservation at each structural position, the sequences were rendered non-redundant at 99 % ID, leaving 85 unique sequences. A

positional weight matrix of amino acid frequencies at each position was calculated and a Simson's diversity index diversity calculation was performed on each position.

### Purification for crystallography

Alpha-elapitoxin-Dpp2a (3L24\_DENPO) from *Dendroaspis polylepis* (black mamba), alpha-cobratoxin/long neurotoxin 1 (3L21\_NAJNI) from *Naja nivea* (Cape cobra), Long neurotoxin 1 (3L21\_OXYSC) from *Oxyuranus scutellatus scutellatus* (coastal taipan), Alpha-delta bungarotoxin (3L2A\_BUNCE) from *Bungarus caeruleus* (common krait) and antibody LNX-D09 genes were synthesized and subcloned into pVRC8400 vectors, with a HRV3C cleavable His or Fc tag (GenScript, NJ). LNX-D09 IgG plasmids (heavy and light chain) were transfected into Expi293F cells (Thermo Fisher) at 1:1 ratio (0.5mg heavy chain plasmid and 0.5mg of light chain plasmid per liter of cell culture), while long neurotoxins were transfected into 293 Freestyle cells (Thermo Fisher). Turbo293 transfection reagent (Speed BioSystems) was used according to manufacturer's protocol at a ratio of 1mg of plasmid to 3ml of transfection reagent. Cells were cultured at 37°C, 8% CO<sub>2</sub> and 80% humidity for six days. Culture supernatants were harvested by centrifugation, and the resulting supernatants were filtered through 0.2μm membranes. Proteins were affinity purified with protein A resin (GE) for LNX-D09 IgG or cOmplete™ His-Tag Purification Resin (Roche) for long neurotoxin. His-tag and Fc regions were cleaved from the proteins by digestion with HRV3C protease (produced in house) followed by a second step of affinity purification with either protein A resin to remove freed Fc fragment and uncleaved IgG or Ni-resin to remove freed his tag.

Fab fragment for LNX-D09 antibody was further purified by size exclusion chromatography on a Superdex200 column (Cytiva) in PBS buffer. The peak corresponding to Fab fragment was concentrated to 10 mg/ml using a spin concentrator with MWCO of 10kDa and used to form complex with long neurotoxins.

Krait long neurotoxin (alpha-bungarotoxin) was purchased from BioTechne (catalog # 2133) in lyophilized form. Protein was dissolved in PBS and purified by size exclusion chromatography (Superdex 200, Cytiva). Peak fractions corresponding to toxin were pooled and concentrated to 1mg/ml by spin concentration on 3kDa cutoff membranes.

### Biolayer interferometry reactivity to whole venom

Affinity of long neurotoxins to LNX-D09 -Fab was assessed using a fortéBio Octet instrument. His-tagged long neurotoxins were immobilized on Ni-NTA biosensors, then dipped into LNX-D09 -Fab in a 2-fold dilution series. Sensograms of the concentration series were corrected with corresponding blank curves and fitted globally with Octet evaluation software using a 1:1 Langmuir model of binding.

### Crystallization

Each neurotoxin was mixed with LNX-D09 Fab fragment at 3:2 molar ratio (toxin:Fab) and incubated at 4 °C overnight. Excess free toxin was removed by separation on a Superdex 200 column (Cytiva). Peak fractions corresponding to complex were pooled and the pool concentrated to 5 mg/ml using a spin concentrator (MWCO 30kDa). Complex between toxin and Fab was confirmed by SDS-PAGE and used immediately for crystallization trials.

Crystallization conditions were screened using Hampton Research, Wizard, and QIAGEN crystal screening kits. Crystal trays were set up using a Mosquito crystallization robot. Crystals initially observed from the wells were manually reproduced. Crystals suitable for data collection were obtained from the following conditions: taipan-LNX-D09: 100mM sodium acetate pH 5.5, 14% PEG8000, 2.65% PEG 400, 500mM NaCl, 10mM Mg<sup>2+</sup>; mamba-LNX-D09: 0.1M Tris pH 8.5, 10% PEG4000, 50mM proline; cobra-LNX-D09: 200 mM (NH<sub>4</sub>)<sub>2</sub>SO<sub>4</sub>, 100 mM sodium acetate pH 4.6, 19% PEG 4000; krait-LNX-D09: 40% PEG 400, 5% PEG 3350, 0.1M sodium acetate pH 5.5; mamba-SNX-B03: 0.1M Tris pH 8.5, 20% PEG4000, 0.2M sodium acetate.

### Data collection and processing

For data collection the crystals were briefly dipped into reservoir solution supplemented with 30% glycerol and flash-frozen in liquid nitrogen. X-ray diffraction data were collected at SER-CAT station 22-ID (Advanced Photon Source, Argonne National Laboratory, Argonne, IL). Prior to data collection the station was tuned to the wavelength of 1Å, the size of the beam was set to 50 μm and the crystal was equilibrated to 100K with a dry nitrogen stream. The data was collected using a continuous rotation method. To achieve completeness and multiplicity 720 degrees of data were collected. Registered intensities were indexed, scaled, and merged with HKL2000.<sup>62</sup> Data collection statistics are shown in [Data S1](#).

### Structure determination and analysis

The structures were solved by molecular replacement with BALBES.<sup>63</sup> Initial solutions were verified and manually corrected with COOT.<sup>46</sup> The coordinates were refined with REFMAC5<sup>64</sup> (CCP4 suite<sup>42</sup>) and PHENIX.REFINE<sup>53</sup> (PHENIX suite<sup>52</sup>) alternating with manual revision of the model with COOT. Structure validation was performed with the Protein Data Bank validation server. Refinement statistics are provided in [Data S1](#). The coordinates and structure factors for the Taipan-LNX-D09, Mamba-LNX-D09, Cobra-LNX-D09, Krait-LNX-D09, and Black mamba-SNX-B03 complexes were deposited in the Protein Data Bank, and are available under accession codes 8D9Y, 8DAO, 8D9Z, 8DA1, and 8V13, respectively.

Interface analysis for all toxin-Fab complexes, for the nAChR-Krait LNX complex (PDB ID: 6UWZ<sup>34</sup>), and for LNX:nAChR in complex with recombinant short-chain α-neurotoxin (PDB ID: 7Z14<sup>37</sup>) was performed with PISA.<sup>51</sup> The details are presented in [Figures 3 and 6](#),

**Tables S3 and S4**, and **Data S1**. The figures illustrating the structures and the Fab/nAChR-LNX/SNX intermolecular interactions were generated by PYMOL.<sup>65</sup>

Sequence variation was calculated for each residue as normalized Shannon's entropy based on 3FTX diversity analysis alignment. Gaps were penalized with  $p(x_{gap})^*\log(1/n)$ , mapped on the Krait structure and colored purple to white to indicate diversity to conservation among sequences.

#### In vivo challenge

Lyophilized venoms were obtained from multiple sources, rehydrated, aliquoted and frozen for storage, and thawed just prior to use. Median lethal dose ( $LD_{50}$ ) and Maximal lethal dose ( $LD_{100}$ ) of each recombinant  $\alpha$ -neurotoxin and whole venom were determined by an animal-sparing “up-and-down” methodology, with core body temperature as an adjunct to endpoint determination. The animal-sparing “up-and-down” methodology of estimating the  $LD_{50}$  involved serial intradermal injection of predetermined mg/kg dosages of venom.<sup>55</sup>

For all *in-vivo* challenges, venom and/or toxin was injected intraperitoneally and the animals monitored via temperature and body weight every 20 minutes for 2-4 hours initially and then once every 8 hours, for 72 hours total. Treatment (LNX-D09) was mixed with venom and/or toxin 30 minutes prior to injection. Varespladib (small molecule inhibitor of PLA2) was formulated in polyethylene glycol-300 (PEG) and Tween 80, and for its treatment group was injected 20 minutes prior to challenge injection. In accordance with the IACUC protocol, animals were monitored and mice euthanized if distress signs appeared, including body temperature reduction greater than 4C, bodyweight loss more than 20% in 24 hours, and hunched posture, ruffled fur, prolonged lack of movement, moribundity, bleeding, or no signs of reversibility. Euthanization was by CO<sub>2</sub> followed by cervical dislocation.

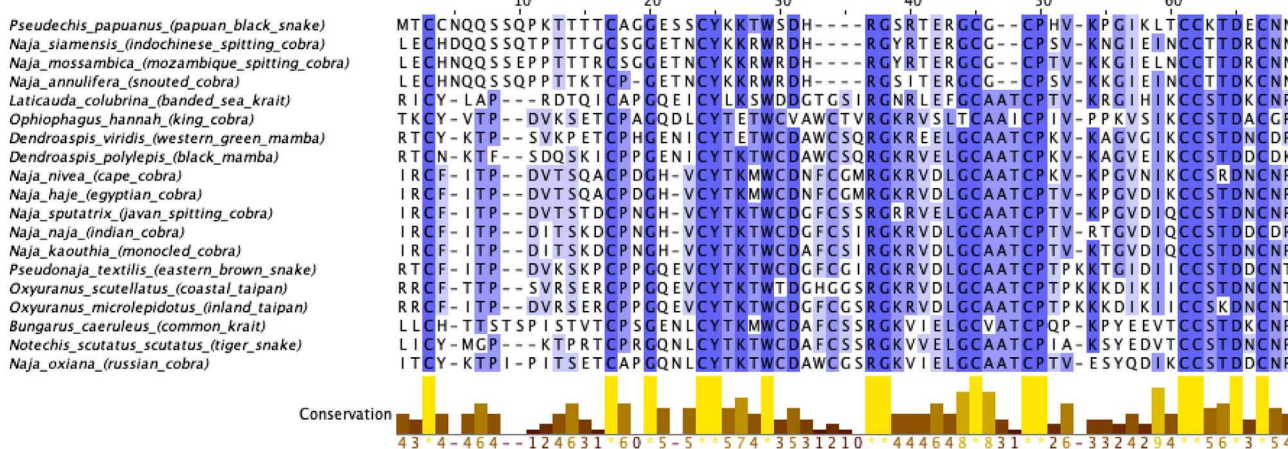
In the *in-vivo* protection assays, a challenge dose of 1x $LD_{0-100}$  of a venom or purified toxin was mixed with 30mg/kg of LNX-D09 (diluted in PBS) and pre-incubated at 25°C for 30 minutes. The mixture containing 1x  $LD_{0-100}$ s of venom was injected intraperitoneally into mice.

#### QUANTIFICATION AND STATISTICAL ANALYSIS

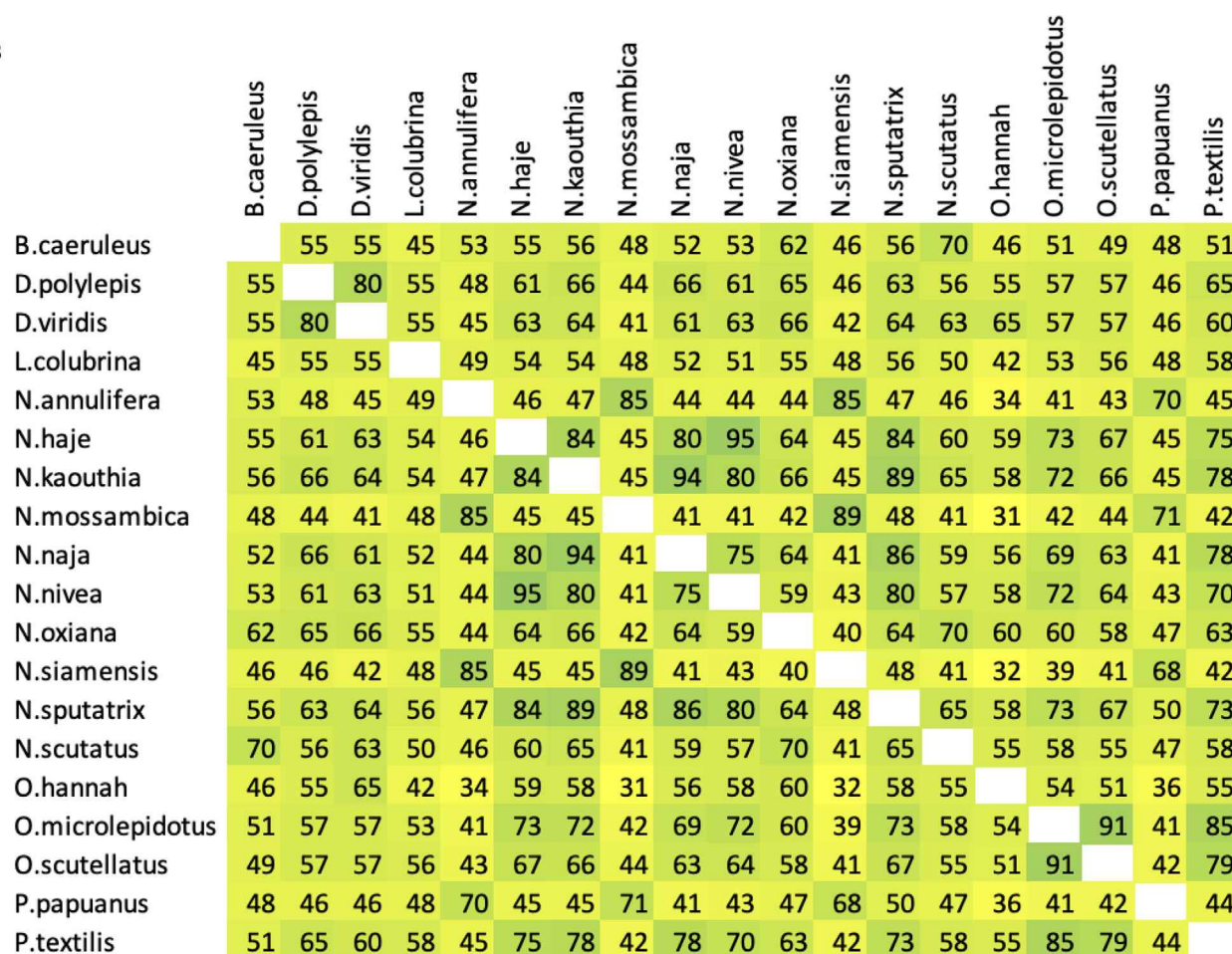
Kaplan-Meier curves were plotted for both *Naja naja* venom  $LD_{50}$  and  $LD_{100}$ . Log-rank test was used to examine the difference of survival curves between control and treatment groups. Survival rate was also compared based on a two-sample proportion test for venom  $LD_{50}$ . Median survival time was calculated for both control and treatment groups in venom  $LD_{50}$ . Analyses were performed using R version 3.3.3.

## Supplemental figures

A



B



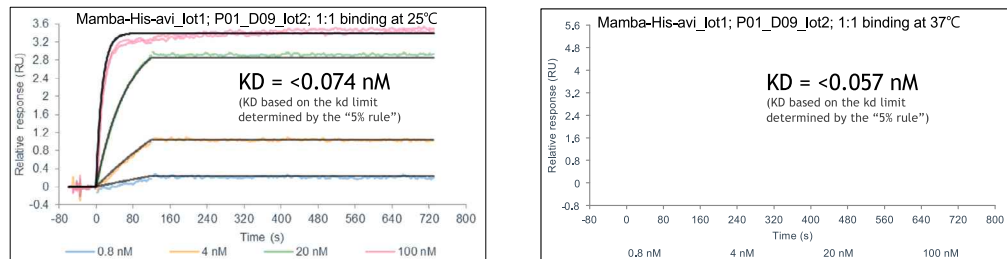
(legend on next page)

**Figure S1. LNX conservation, related to Figure 1**

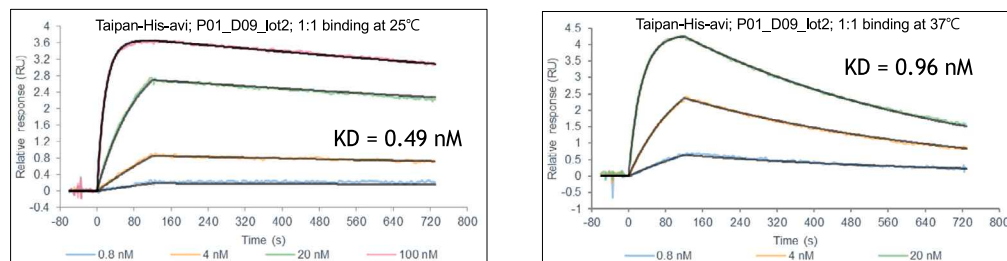
(A) LNX amino acid sequence alignment. A single representative 3FTX sequence was obtained for each species, chosen as the closest sequence to *N. nivea* LNX by amino acid identity. In four cases where no LNX was found in UniProt for the species, a short 3FTX homolog was instead aligned (*P. papuanus*, *N. siamensis*, *N. mossambica*, *N. annulifera*). Conservation indicated in blue.

(B) Pairwise amino acid percentage identity (%ID) between LNXs. Yellow: lower %ID, green: higher %ID.

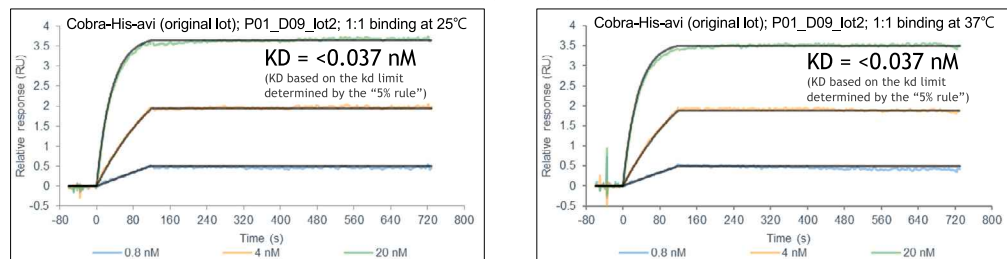
**A** Sensorgrams for Mamba-His-avi lot 1 (at 0.8, 4, 20, 100, and 500 nM nominal concentration) binding to P01\_D09\_lot2 and (-) control hlgG1 at 25°C and 37°C



Sensorgrams for Taipan-His-avi (at 0.8, 4, 20, 100, and 500 nM nominal concentration) binding to P01\_D09\_lot2 and (-) control hlgG1 at 25°C and 37°C



Sensorgrams for Cobra-His-avi (original lot) (at 0.8, 4, 20, 100, and 500 nM nominal concentration) binding to P01\_D09\_lot2 and (-) control hlgG1 at 25°C and 37°C



**B**

Mamba						
Sample ID	T (°C)	Capture level (RU)	ka (1/Ms)	kd (1/s)	KD (nM)	Rmax (RU)
P01_B11_Iot1	25	24	3.6E+05	1.0E-04	0.28	4.0
	37	28	4.2E+05	9.3E-04	4.6	
P01_B11_Iot2	25	42	3.8E+05	1.6E-04	0.41	6.9
	37	51	4.4E+05	9.8E-04	2.2	8.4
P01_D09_Iot2	25	21	7.7E+05	5.7E-05	<0.074	3.4
(-) control hlgG1	25	28	1.0E+06	5.7E-05	<0.057	4.8
	37	99	N/A	N/A	N/A	N/A

Taipan						
Sample ID	T (°C)	Capture level (RU)	ka (1/Ms)	kd (1/s)	KD (nM)	Rmax (RU)
P01_B11_Iot1	25	24	3.1E+05	6.7E-03	21	4.1
	37	28	1.3E+06	3.7E-02	28	3.7
P01_B11_Iot2	25	42	4.2E+05	6.9E-03	17	6.6
	37	51	1.0E+06	3.9E-02	39	6.7
P01_D09_Iot2	25	21	5.6E+05	2.8E-04	0.49	3.7
(-) control hlgG1	25	28	1.8E+06	1.7E-03	0.96	4.5
	37	99	N/A	N/A	N/A	N/A

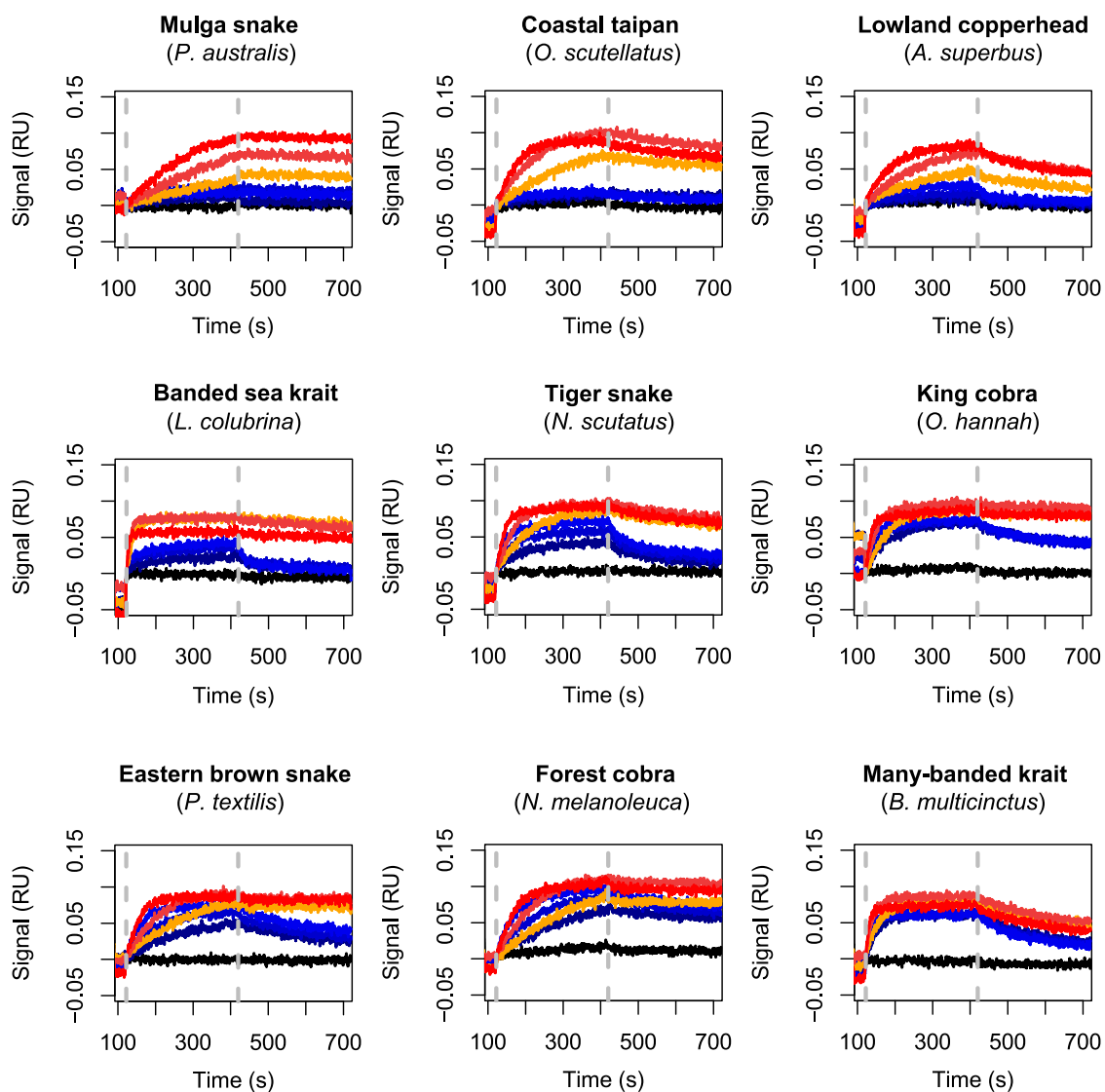
  

Cobra						
Sample ID	T (°C)	Capture level (RU)	ka (1/Ms)	kd (1/s)	KD (nM)	Rmax (RU)
P01_B11_Iot1	25	24	1.1E+06	5.7E-05	<0.053	4.3
	37	28	1.7E+06	7.15E-05	0.043	4.0
P01_B11_Iot2	25	42	1.0E+06	5.7E-05	<0.055	7.5
	37	51	1.5E+06	5.7E-05	<0.039	6.5
P01_D09_Iot2	25	21	1.5E+06	5.7E-05	<0.037	3.7
(-) control hlgG1	25	28	1.6E+06	5.7E-05	<0.037	3.6
	37	99	N/A	N/A	N/A	N/A

**Figure S2. LNX-D09—recombinant monovalent SPR kinetics, related to Figure 2**

(A) SPR sensograms and residuals at 25°C and 37°C for monovalent His-avi-tagged recombinant LNX toxins.

(B) Binding kinetic parameter summary tables, including LNX-D09 and related LNX-B11.



**Figure S3. Comparative breadth of LNX-D09 and 95Mat5 versus whole venom, related to Figure 2**

BLI with antibody (LNX-D09, 95Mat5, or isotype control) captured on probe and whole venom in solution at total protein concentrations of either 500, 250, or 125 nM. LNX-D09 reactivity versus venom at total protein concentrations of 500 (red), 250 (brown), or 125 nM (orange). 95Mat5 reactivity versus venom at total protein concentrations of 500 (dark blue), 250 (medium blue), and 125 nM (light blue). Isotype control antibody versus venom at 500 nM (black).

**Supplemental information**

**Snake venom protection by a cocktail of varespladib  
and broadly neutralizing human antibodies**

**Jacob Glanville, Mark Bellin, Sergei Pletnev, Baoshan Zhang, Joel Christian Andrade, Sangil Kim, David Tsao, Raffaello Verardi, Rishi Bedi, Sindy Liao, Raymond Newland, Nicholas L. Bayless, Sawsan Youssef, Ena S. Tully, Tatsiana Bylund, Sujeong Kim, Hannah Hirou, Tracy Liu, and Peter D. Kwong**

**Table S1. Phage+NGS primers – multiplex display and Illumina sequencing primer set, related to Figure 1**

DB-NGS-VK1-Nsil-R2-md01	GGCATTCTGCTGAACCGCTTCCGATCTNNNNNTCGTAGCatgcattcGACATCCAGATGACCCAGTC
DB-NGS-VK2a-Nsil-R2-md01	GGCATTCTGCTGAACCGCTTCCGATCTNNNNNTCGTAGCatgcattcGATGTTGATGACTCAGTC
DB-NGS-VK2b-Nsil-R2-md01	GGCATTCTGCTGAACCGCTTCCGATCTNNNNNTCGTAGCatgcattcGATATTGTGATGACCCAGATCCC
DB-NGS-VK3-Nsil-R2-md01	GGCATTCTGCTGAACCGCTTCCGATCTNNNNNTCGTAGCatgcattcGAAATTGTTGACGCAGTC
DB-NGS-VK4-Nsil-R2-md01	GGCATTCTGCTGAACCGCTTCCGATCTNNNNNTCGTAGCatgcattcGACATCGTGTGACCCAGTC
DB-NGS-VK5-Nsil-R2-md01	GGCATTCTGCTGAACCGCTTCCGATCTNNNNNTCGTAGCatgcattcGAAACGACACTCACGCAGTC
DB-NGS-VK6-Nsil-R2-md01	GGCATTCTGCTGAACCGCTTCCGATCTNNNNNTCGTAGCatgcattcGAAATTGTCGACTCAGTC
DB-NGS-VI1-Nsil-R2-md01	GGCATTCTGCTGAACCGCTTCCGATCTNNNNNTCGTAGCatgcattcCAGTCTGTSBTGACGCAGCG
DB-NGS-VI3-Nsil-R2-md01	GGCATTCTGCTGAACCGCTTCCGATCTNNNNNTCGTAGCatgcattcTCCTATGWGCTGACWCAGCAC
DB-NGS-VI38-Nsil-R2-md01	GGCATTCTGCTGAACCGCTTCCGATCTNNNNNTCGTAGCatgcattcTCCTATGAGCTGAYRCAGCYACC
DB-NGS-VI4-Nsil-R2-md01	GGCATTCTGCTGAACCGCTTCCGATCTNNNNNTCGTAGCatgcattcCAGCCTGCTGACTCARYC
DB-NGS-VI7.8-Nsil-R2-md01	GGCATTCTGCTGAACCGCTTCCGATCTNNNNNTCGTAGCatgcattcCAGDCTGTTGACYCAGGAGCC
DB-NGS-VI9-Nsil-R2-md01	GGCATTCTGCTGAACCGCTTCCGATCTNNNNNTCGTAGCatgcattcCAGCCWKGKCTGACTCAGCCMCC
DB-NGS-VI11-Nsil-R2-md01	GGCATTCTGCTGAACCGCTTCCGATCTNNNNNTCGTAGCatgcattcTCCTTGAGCTGASTCAGGASCC
DB-NGS-VI13-Nsil-R2-md01	GGCATTCTGCTGAACCGCTTCCGATCTNNNNNTCGTAGCatgcattcCAGTCTGYYCTGAYTCAGCCT
DB-NGS-VI15-Nsil-R2-md01	GGCATTCTGCTGAACCGCTTCCGATCTNNNNNTCGTAGCatgcattcAATTTATGCTGACTCAGCCCC
DB-NGS-Jk1-NotI-R1-md01	ACACTTTCCCTACACGACGCTTCCGATCTNNNNNTCGTAGCGCGGCCGACGTTGATTCACCTGGTCCC
DB-NGS-Jk2-NotI-R1-md01	ACACTTTCCCTACACGACGCTTCCGATCTNNNNNTCGTAGCGCGGCCGACGTTGATCTCAGCTGGTCCC
DB-NGS-Jk3-NotI-R1-md01	ACACTTTCCCTACACGACGCTTCCGATCTNNNNNTCGTAGCGCGGCCGACGTTGATATCCACTTGGTCCC
DB-NGS-Jk4-NotI-R1-md01	ACACTTTCCCTACACGACGCTTCCGATCTNNNNNTCGTAGCGCGGCCGACGTTGATCTCACCTGGTCCC
DB-NGS-Jk5-NotI-R1-md01	ACACTTTCCCTACACGACGCTTCCGATCTNNNNNTCGTAGCGCGGCCGACGTTAATCTCAGCTGGTCCC
DB-NGS-JI1-NotI-R1-md01	ACACTTTCCCTACACGACGCTTCCGATCTNNNNNTCGTAGCGCGGCCGACCTAGGACGGTGACCTTGGTCCC
DB-NGS-JI2-NotI-R1-md01	ACACTTTCCCTACACGACGCTTCCGATCTNNNNNTCGTAGCGCGGCCGACCTAGGACGGTCAGCTGGTCCC
DB-NGS-JI45-NotI-R1-md01	ACACTTTCCCTACACGACGCTTCCGATCTNNNNNTCGTAGCGCGGCCGACCTAAAACGGTGAGCTGGTCCC
DB-NGS-Jh1-Bmtl-R1-md01	ACACTTTCCCTACACGACGCTTCCGATCTNNNNNTCGTAGCGTAGCTGAGGGAGACGGTGACCGGGTCCC
DB-NGS-Jh3-Bmtl-R1-md01	ACACTTTCCCTACACGACGCTTCCGATCTNNNNNTCGTAGCGCTAGCTGAGGGAGACGGTGACCGGGTCCC
DB-NGS-Jh4.5-Bmtl-R1-md01	ACACTTTCCCTACACGACGCTTCCGATCTNNNNNTCGTAGCGCTAGCTGAGGGAGACGGTGACCGGGTCCC
DB-NGS-Jh6-Bmtl-R1-md01	ACACTTTCCCTACACGACGCTTCCGATCTNNNNNTCGTAGCGCTAGCTGAGGGAGACGGTGACCGTGGTCCC
DB-NGS-Vh1-Ncol-R2-md14	GGCATTCTGCTGAACCGCTTCCGATCTNNNNACTGAGTACCATGGCCAGGTGCACTGGTCAAGTCTGG
DB-NGS-Vh2-Ncol-R2-md14	GGCATTCTGCTGAACCGCTTCCGATCTNNNNACTGAGTACCATGGCCAGGTGCACTGGTCAAGTCTGG
DB-NGS-Vh3-Ncol-R2-md14	GGCATTCTGCTGAACCGCTTCCGATCTNNNNACTGAGTACCATGGCCAGGTGCACTGGTCAAGTCTGG
DB-NGS-Vh4-Ncol-R2-md14	GGCATTCTGCTGAACCGCTTCCGATCTNNNNACTGAGTACCATGGCCAGGTGCACTGGTCAAGTCTGG
DB-NGS-Vh5-Ncol-R2-md14	GGCATTCTGCTGAACCGCTTCCGATCTNNNNACTGAGTACCATGGCCAGGTGCACTGGTCAAGTCTGG
DB-NGS-Vh6-Ncol-R2-md14	GGCATTCTGCTGAACCGCTTCCGATCTNNNNACTGAGTACCATGGCCAGGTACAGCTGCAGCAGTCAGG

**Table S1. Multiplex HTX+Display primer sets, related to Figure 1**

Multiplex, dephasing, cloning restriction site embedded, MiSeq flapped-end adapted primer sets for generation of VH, VK, VL amplicons for both high-throughput sequencing and phage display.

**Table S2. ELISA – screening for broadly-reactive anti-LNX clones, related to Figure 1**

cloneID	Taipan	Mamba	Cobra	Krait	VH	CDR-H1	CDR-H2	CDR-H3	VK	CDR-L1	CDR-L2	CDR-L3
SNEURO_P01_D01	37.794085	7.9843924	15.909953	8.173366834	IGHV3-13	FTFSNFDMH	SGLDHSGGAHYA	CVRGTLHYHTSGSYYSDAFDIW	IGKV1-39	RASQSISSYLN	AASSLQS	CQQSYSTHTF
SNEURO_P01_D06	37.776561	12.169454	17.736967	6.41959799	IGHV3-13	FTFSNFDMH	SGLDHSGGAHYA	CVRGTLHYHTSGSYYSDAFDIW	IGKV1-39	RASQSISSYLN	AASSLQS	CQQSYSTHTF
SNEURO_P01_H10	36.389923	12.334448	17.945498	7.77638191	IGHV3-13	FTFSNFDMH	SGLDHSGGAHYA	CVRGTLHYHTSGSYYSDAFDIW	IGKV1-39	RASQSISSYLN	AASSLQS	CQQSYSTHTF
SNEURO_P01_B09	35.483023	10.198439	16.954976	5.613065327	IGHV3-13	FTFSNFDMH	SGLDHSGGAHYA	CVRGTLHYHTSGSYYSDAFDIW	IGKV1-39	RASQSISSFLN	AASSLQS	CQQSYSPPLTF
SNEURO_P01_F03	34.913472	11.558528	15.943128	6.542713568	IGHV3-13	FTFSNFDMH	SGLDHSGGAHYA	CVRGTLHYHTSGSYYSDAFDIW	IGKV1-39	RASQSISSYLN	AASSLQS	CQQSYSTPLTF
SNEURO_P01_A08	33.822563	9.9598662	15.21327	6.914572864	IGHV3-13	FTFSNFDMH	SGLDHSGGAHYA	CVRGTLHYHTSGSYYSDAFDIW	IGKV1-39	RASQSISSYLN	AASSLQS	CQQSYSTHTF
SNEURO_P01_A04	31.732749	10.169454	7.5853081	7.987437186	IGHV3-13	FTFSNFDMH	SGLDHSGGAHYA	CVRGTLHYHTSGSYYSDAFDIW	IGKV1-39	RASQSISSYLN	AASSLQS	CQQSYSTPLTF
SNEURO_P01_D09	28.311062	11.2026423	13.533175	7.26381905	IGHV3-13	FTFSNFDMH	SGLDHSGGAHYA	CVRGTLHYHTSGSYYSDAFDIW	IGKV1-39	QASQDISNYLN	AASSLES	CQQQANSFPYTF
SNEURO_P01_F04	28.028478	11.168339	13.947867	6.015075377	IGHV3-13	FTFSNFDMH	SGLDHSGGAHYA	CVRGTLHYHTSGSYYSDAFDIW	IGKV1-39	QASQDISNYLN	AASSLES	CQQQANSFPYTF
SNEURO_P01_E08	27.060241	10.684504	12.478673	6.233668342	IGHV3-13	FTFSNFDMH	SGLDHSGGAHYA	CVRGTLHYHTSGSYYSDAFDIW	IGKV1-39	QASQDISNYLN	AASSLES	CQQQANSFPYTF
SNEURO_P01_D02	26.326397	10.439242	13.618483	7.545226131	IGHV3-13	FTFSNFDMH	SGLDHSGGAHYA	CVRGTLHYHTSGSYYSDAFDIW	IGKV1-39	QASQDISNYLN	AASSLES	CQQQANSFPYTF
SNEURO_P01_B12	25.840088	9.7212932	12.521327	6.135678392	IGHV3-13	FTFSNFDMH	SGLDHSGGAHYA	CVRGTLHYHTSGSYYSDAFDIW	IGKV1-39	QASQDISNYLN	AASSLES	CQQQANSFPYTF
SNEURO_P01_C03	24.955093	11.235229	16.824645	7.452261307	IGHV3-13	FTFSNFDMH	SGLDHSGGAHYA	CVRGTLHYHTSGSYYSDAFDIW	IGKV1-39	RASQSISSYLN	AASSLQS	CQQSYSTPLTF
SNEURO_P01_G10	22.75356	9.6655518	12.018957	5.175879397	IGHV3-13	FTFSNFDMH	SGLDHSGGAHYA	CVRGTLHYHTSGSYYSDAFDIW	IGKV1-39	QASQDISNYLN	AASSLES	CQQQANSFPYTF
SNEURO_P01_B06	22.278204	9.328874	11.64455	7.25879397	IGHV3-13	FTFSNFDMH	SGLDHSGGAHYA	CVRGTLHYHTSGSYYSDAFDIW	IGKV1-39	QASQDISNYLN	AASSLES	CQQQANSFPYTF
SNEURO_P01_B05	21.715225	10.06466	14.848341	7.002512563	IGHV3-13	FTFSNFDMH	SGLDHSGGAHYA	CVRGTLHYHTSGSYYSDAFDIW	IGKV1-39	RASQSISSFLN	AASSLQS	CQQQSYSPPLTF
SNEURO_P01_B11	21.463308	7.9442586	13.822275	6.005025126	IGHV3-13	FTFSNFDMH	SGLDHSGGAHYA	CVRGTLHYHTSGSYYSDAFDIW	IGKV1	RASQG1SDNLN	AASTLQS	CQQQANSFPPLTF
SNEURO_P01_A03	20.197152	7.8305463	9.4336493	6.140703518	IGHV3-13	FTFSNFDMH	SGLDHSGGAHYA	CVRGTLHYHTSGSYYSDAFDIW	IGKV1-39	QASQDISNYLN	AASSLES	CQQQANSFPYTF
SNEURO_P01_G05	17.423877	10.229654	14.111374	5.613065327	IGHV3-13	FTFSNFDMH	SGLDHSGGAHYA	CVRGTLHYHTSGSYYSDAFDIW	IGKV1-39	RASQSISSYLN	AASSLQS	CQQSYSTPWTF
SNEURO_P01_E05	17.353779	9.9041249	14.827014	6.43718593	IGHV3-13	FTFSNFDMH	SGLDHSGGAHYA	CVRGTLHYHTSGSYYSDAFDIW	IGKV1-39	RASETISIYLN	AASSLQS	CQQSYSTPWTF
SNEURO_P01_E07	16.216867	10.015608	13.473934	6.472361809	IGHV3-13	FTFSNFDMH	SGLDHSGGAHYA	CVRGTLHYHTSGSYYSDAFDIW	IGKV1-39	RASETISIYLN	AASSLQS	CQQSYSTPWTF
SNEURO_P01_E03	16.116101	10.809365	13.99763	7.221105528	IGHV3-13	FTFSNFDMH	SGLDHSGGAHYA	CVRGTLHYHTSGSYYSDAFDIW	IGKV1-39	RASETISIYLN	AASSLQS	CQQSYSTPWTF
SNEURO_P01_E06	15.542169	9.94783924	12.988152	6.035175879	IGHV3-13	FTFSNFDMH	SGLDHSGGAHYA	CVRGTLHYHTSGSYYSDAFDIW	IGKV1-39	RASETISIYLN	AASSLQS	CQQSYSTPWTF
SNEURO_P01_H09	15.064622	9.4202899	12.940758	5.947236181	IGHV3-13	FTFSNFDMH	SGLDHSGGAHYA	CVRGTLHYHTSGSYYSDAFDIW	IGKV1-39	RASETISIYLN	AASSLQS	CQQSYSTPWTF
SNEURO_P01_G03	14.760131	9.7346711	12.43128	5.889447236	IGHV3-13	FTFSNFDMH	SGLDHSGGAHYA	CVRGTLHYHTSGSYYSDAFDIW	IGKV1-39	QASQDISNYLN	AASSLES	CQQQANSFPYTF
SNEURO_P01_H08	14.236583	9.2374582	12.734597	5.939698492	IGHV3-13	FTFSNFDMH	SGLDHSGGAHYA	CVRGTLHYHTSGSYYSDAFDIW	IGKV1-39	RASETISIYLN	AASSLQS	CQQSYSTPWTF
SNEURO_P01_F11	14.223439	8.9476031	12.414692	6.605527638	IGHV3-13	FTFSNFDMH	SGLDHSGGAHYA	CVRGTLHYHTSGSYYSDAFDIW	IGKV1-39	RASETISIYLN	AASSLQS	CQQSYSTPWTF
SNEURO_P01_F05	14.133625	8.6020067	11.518957	6.522613065	IGHV3-13	FTFSNFDMH	SGLDHSGGAHYA	CVRGTLHYHTSGSYYSDAFDIW	IGKV1-39	RASETISIYLN	AASSLQS	CQQSYSTPWTF
SNEURO_P01_B01	14.109529	7.2753623	11.760664	7.33919598	IGHV3-13	FTFSNFDMH	SGLDHSGGAHYA	CVRGTLHYHTSGSYYSDAFDIW	IGKV1-39	RASETISIYLN	AASSLQS	CQQSYSTPWTF
SNEURO_P01_B02	13.81161	8.5395764	12.175355	7.409547739	IGHV3-13	FTFSNFDMH	SGLDHSGGAHYA	CVRGTLHYHTSGSYYSDAFDIW	IGKV1-39	RASETISIYLN	AASSLQS	CQQSYSTPWTF
SNEURO_P01_A09	13.54655	7.8818283	11.308057	6.168341709	IGHV3-13	FTFSNFDMH	SGLDHSGGAHYA	CVRGTLHYHTSGSYYSDAFDIW	IGKV1-39	RASETISIYLN	AASSLQS	CQQSYSTPWTF
SNEURO_P01_H01	13.020811	7.6365663	11.040284	6.675879397	IGHV3-13	FTFSNFDMH	SGLDHSGGAHYA	CVRGTLHYHTSGSYYSDAFDIW	IGKV1-39	RASETISIYLN	AASSLQS	CQQSYSTPWTF
SNEURO_P01_G02	12.863089	8.5529543	11.414692	6.721105528	IGHV3-13	FTFSNFDMH	SGLDHSGGAHYA	CVRGTLHYHTSGSYYSDAFDIW	IGKV1-39	RASETISIYLN	AASSLQS	CQQSYSTPWTF
SNEURO_P01_D04	12.841183	9.0345596	12.611374	5.947236181	IGHV3-13	FTFSNFDMH	SGLDHSGGAHYA	CVRGTLHYHTSGSYYSDAFDIW	IGKV1-39	RASETISIYLN	AASSLQS	CQQSYSTPWTF
SNEURO_P01_F02	12.672508	8.3522854	11.393365	6.63819055	IGHV3-13	FTFSNFDMH	SGLDHSGGAHYA	CVRGTLHYHTSGSYYSDAFDIW	IGKV1-39	RASETISIYLN	AASSLQS	CQQSYSTPWTF
SNEURO_P01_F09	12.582694	8.2898551	12.082938	4.570351759	IGHV3-13	FTFSNFDMH	SGLDHSGGAHYA	CVRGTLHYHTSGSYYSDAFDIW	IGKV1-5	RASQSISSWLA	AASSLQS	CQQSYSTITF
SNEURO_P01_D03	12.175246	9.3979933	13.386256	7	IGHV3-13	FTFSNFDMH	SGLDHSGGAHYA	CVRGTLHYHTSGSYYSDAFDIW	IGKV1-39	RASETISIYLN	AASSLQS	CQQSYSTPWTF
SNEURO_P01_C07	11.336254	8.4860647	18.13981	5.510050251	IGHV3-13	FTFSNFDMH	SGLDHSGGAHYA	CVRGTLHYHTSGSYYSDAFDIW	IGKV1-12	RASQGISSWLA	AASNLMQ	CQQSYTTPPLTF
SNEURO_P01_B04	8.8959474	8.6332219	11.263033	7.83919598	IGHV3-13	FTFSNFDMH	SGLDHSGGAHYA	CVRGTLHYHTSGSYYSDAFDIW	IGKV1-39	RASETISIYLN	AASSLQS	CQQSYSTPWTF
SNEURO_P01_H02	7.2157722	5.2820513	9.1587678	3.587939698	IGHV3-13	FTFSNFDMH	SGLDHSGGAHYA	CARGLTYHYHTSGSYYSDAFDIW	IGKV1-12	RASQGISSWLA	AASNLMQ	CQQANSFPPLTF
SNEURO_P01_E09	7.0711939	7.2575251	14.64455	4.869346734	IGHV3-13	FTFSNFDMH	SGLDHSGGAHYA	CVRGTLHYHTSGSYYSDAFDIW	IGKV1-12	RASQGISSWLA	AASNLMQ	CQQSYTTPPLTF
SNEURO_P01_D12	6.0219058	6.7469342	8.2037915	6.138190955	IGHV3-13	FTFSNFDMH	SGLDHSGGAHYA	CVRGTLHYHTSGSYYSDAFDIW	IGKV1-39	RASETISIYLN	AASSLQS	CQQSYTTPPLTF
SNEURO_P01_B07	5.822563	6.5574136	13.770142	4.359296482	IGHV3-13	FTFSNFDMH	SGLDHSGGAHYA	CVRGTLHYHTSGSYYSDAFDIW	IGKV1-12	RASQGISSWLA	AASNLMQ	CQQSYTTPPLTF
SNEURO_P01_F07	5.5465498	9.0590858	12.232227	4.648241206	IGHV3-13	FTFSNFDMH	SGLDHSGGAHYA	CVRGTLHYHTSGSYYSDAFDIW	IGKV1-39	RASQDIRNDLG	GASTLQS	CQQSYTTPPLTF
SNEURO_P01_H06	4.4622125	5.9955407	12.561611	3.708542714	IGHV3-13	FTFSNFDMH	SGLDHSGGAHYA	CVRGTLHYHTSGSYYSDAFDIW	IGKV1-12	RASQGISSWLA	AASNLMQ	CQQSYTTPPLTF
SNEURO_P01_D08	4.3986857	6.0624303	13.689573	3.879396985	IGHV3-13	FTFSNFDMH	SGLDHSGGAHYA	CVRGTLHYHTSGSYYSDAFDIW	IGKV1-12	RASQGISSWLA	AASNLMQ	CQQSYTTPPLTF
SNEURO_P01_C12	4.2672508	5.7948718	12.194313	4.91959799	IGHV3-13	FTFSNFDMH	SGLDHSGGAHYA	CVRGTLHYHTSGSYYSDAFDIW	IGKV1-12	RASQGISSWLA	AASNLMQ	CQQSYTTPPLTF
SNEURO_P01_D05	4.1796276	6.4124861	13.281991	3.718592965	IGHV3-13	FTFSNFDMH	SGLDHSGGAHYA	CVRGTLHYHTSGSYYSDAFDIW	IGKV1-12	RASQGISSWLA	AASNLMQ	CQQSYTTPPLTF
SNEURO_P01_A06	4.0438116	4.06466	11.521327	3.987437186	IGHV3-13	FTFSNFDMH	SGLDHSGGAHYA	CVRGTLHYHTSGSYYSDAFDIW	IGKV1-12	RASQGISSWLA	AASNLMQ	CQQSYTTPPLTF
SNEURO_P01_D07	3.7502738	5.8305463	13.199052	3.414572864	IGHV3-13	FTFSNFDMH	SGLDHSGGAHYA	CVRGTLHYHTSGSYYSDAFDIW	IGKV1-12	RASQGISSWLA	AASNLMQ	CQQSYTTPPLTF
SNEURO_P01_E10	3.5991238	5.5986622	12.308057	3.914572864	IGHV3-13	FTFSNFDMH	SGLDHSGGAHYA	CVRGTLHYHTSGSYYSDAFDIW	IGKV1-12	RASQGISSWLA	AASNLMQ	CQQSYTTPPLTF
SNEURO_P01_B03	3.32092	5.386845	12.556872	4.281407035	IGHV3-13	FTFSNFDMH	SGLDHSGGAHYA	CVRGTLHYHTSGSYYSDAFDIW	IGKV1-12	RASQGISSWLA	AASNLMQ	CQQSYTTPPLTF

**Table S2. ELISA – screening for broadly-reactive anti-LNX clones, related to Figure 1**

Broadly-reactive anti-LNX clone panel. Screening of periplasmic-extract derived soluble myc tagged scFv vs versus recombinant avi-his tagged LNX from his-avi tagged recombinant *D. polylepis*, *O. scutellatus*, *B. caeruleus*, and *N. nivea*. ELISA max OD450 signal, fold over negative control background reported. Yellow: higher binding signal, Red: lower binding signal, colors relative to within-species ELISA scores. Framework and CDR boundaries by VDJFasta<sup>37</sup>.

**Table S3. Mass spectrometry of LNX-D09 and SNX-B03-eluted proteins from snake venom – related to Figures 2, 5**

	Species of snake (venom)	Uniprot ID#	Protein name	Amino-acid sequence*	Calculated M. W. (Da)	Number of amino acids
LNX-D09-identified protein	<i>D. polylepis</i>	P01397	Alpha-elapitoxin-Dpp2c	RTCNKTFSDQS <ins>KICPPGENICYTKT</ins> WCDAFCSQRGKRVNLGG <ins>AATCPKV</ins> KAGVEIKCCSTDNCNK <ins>TQFGKPR**</ins>	8002	72
		P25674	Long neurotoxin 1	IRCFITPDVTSQACP <ins>DGHVCYT</ins> KWCDNF <ins>CGMIGKR</ins> RVDLGCA <ins>ATCP</ins> TVKPGVDI <ins>KCCSTDNCNPFPTRKRS</ins>	7821	71
	<i>N. annulifera</i>	P01388	Long neurotoxin 2	IRCFITPDVTSQI <ins>CADGHVCYT</ins> WCDNF <ins>CASRGK</ins> RVDLGCA <ins>ATCP</ins> TVKPGVN <ins>I</ins> KCCSTDNCNPFPTRNRP	7771	71
		P01389	Long neurotoxin 1	IRCFITPDVTSQACP <ins>DGQNICYTKT</ins> WCDNF <ins>CGMIGKR</ins> RVDLGCA <ins>AATCP</ins> TVKPGVDI <ins>KCCSTDNCNPFPTRERS</ins>	7911	72
	<i>N. naja</i>	P25669	Long neurotoxin 2	IRCFITPDITSKDCP <ins>GNGHVCYT</ins> WCDGF <ins>CSRGK</ins> RVDLGCA <ins>ATCP</ins> TV <ins>T</ins> GVDIQC <ins>CSTD</ins> CDCPFPTRKRP	7821	71
		P25672	Long neurotoxin 4	IRCFITPDITSKDCP <ins>GNGHVCYT</ins> WCDGF <ins>CRIRGER</ins> RVDLGCA <ins>ATCP</ins> TV <ins>T</ins> GVDIQC <ins>CSTD</ins> CDCPFPTRKRP	7889	71
	<i>N. haje</i>	P01389	Long neurotoxin 1	IRCFITPDVTSQACP <ins>DGQNICYTKT</ins> WCDNF <ins>CGMIGKR</ins> RVDLGCA <ins>AATCP</ins> TVKPGVDI <ins>KCCSTDNCNPFPTRERS</ins>	7911	72
		P01388	Long neurotoxin 2	IRCFITPDVTSQI <ins>CADGHVCYT</ins> WCDNF <ins>CASRGK</ins> RVDLGCA <ins>ATCP</ins> TVKPGVN <ins>I</ins> KCCSTDNCNPFPTRNRP	7772	71
SNX-B03-identified protein	<i>N. arabica</i>	P25674	Long neurotoxin 1	IRCFITPDVTSQACP <ins>DGHVCYT</ins> WCDNF <ins>CGMIGKR</ins> RVDLGCA <ins>ATCP</ins> TVKPGVDI <ins>KCCSTDNCNPFPTRKRS</ins>	7821	71
		P68419	Short neurotoxin 1	LECHNQQSSQ <ins>PPPTTKTCPGET</ins> NCYKKRWRDHRGSITERGCC PSVKKGIEINCC <ins>TT</ins> DKCNN	6844	60
	<i>N. arabica</i>	P0CAR1	Short neurotoxin D1	MICYNQQSS <ins>OPPTTKTCSEGQCYKKT</ins> WSDH <ins>HRTISERGCAC</ins> P NVKPGVKISCCSDKCNN	6533	60
		P01424	Short neurotoxin 1	MECHNQQSS <ins>OPPTTKTCPGET</ins> NCYKKWSDH <ins>HRTI</ins> IERGCGC PSVKKGVKINCC <ins>TT</ins> DRCNN	6804	61
	<i>N. Sputatrix</i>	Q9PSN6	Neurotoxin 3	LECHNQQSS <ins>OPPTTKTCSEGQCYKKT</ins> WSDH <ins>HRTI</ins> IERGCG CPSVKNGIEINCC <ins>TT</ins> DRCNN	6958	62
	<i>L. colubrina</i>	Q9YGW8	Short neurotoxin VAN-29†	RRCFNQQSSE <ins>PQT</ins> NKSC <ins>PPGENSCYNN</ins> QWRDH <ins>HRTI</ins> IERGCG CPQVKSGIKLTCQSDKCNN	7008	62
	<i>A. antarcticus</i>	P01434	Short neurotoxin 1	MQCCNQQSS <ins>OPKTTTCPGGVSSCYK</ins> TW <ins>DHRGTI</ins> IERGCC CPRVKPGIR <ins>LICCKTDECNN</ins>	6880	62
	<i>N. oxiana</i>	P01427	Short neurotoxin 1	LECHNQQSS <ins>OPPTTKTCSEG</ins> NCYKKWSDH <ins>HRTI</ins> IERGCGC PKVKEGVNLNC <ins>CC</ins> SDKCNN	6885	61
<i>D. viridis</i>		P01418	Short neurotoxin 1	RICYNHQ <ins>STTPATT</ins> SCGENSCYKKTWS <ins>DHRGTI</ins> IERGCGC KVKRGVHLHCCQSDKCNN	6743	60
		P01417	Short neurotoxin 1	RICYNHQ <ins>STTPATT</ins> SCGENSCYKKTWS <ins>DHRGTI</ins> IERGCGC KVKQGIHLHCCQSDKCNN	6729	60

\* Sequence segments highlighted in green were identified by mass spectrometry.

\*\* A putative single amino E39N acid polymorphism allele variant identified by mass spectrometry relative to reference P01397, is marked in grey

† This Uniprot sequence contained a signal peptide, which was removed from the mature amino-acid sequence presented above.

**Table S4. Interface analysis for LNX-Fab complexes, related to Figure 3**

nAChR	Krait	D09 fab	Taipan	Cobra	Mamba	Krait
Loop C analogue		Heavy chain	115 contacts within 4A	116 contacts within 4A	122 contacts within 4A	100 contacts within 4A
		T28		D8	D9, Q10	
		N31	S8, R10	D8	D9	
		F32	P7	P7		
		R94	P7			
W187	T6, A7, S9	L97	P7	P7	F7	S9
Y189	T6, T8, S9, I11, V39, V40	H99	T6, P7, V9, R37, V38, F67	T6, P7, V9, R36, V37, F65	T6, F7, R37, V38	T6, T8, I11, V39, V40
Y190	D30, R36, G37, K38, V39, H68	Y100	D28, R34, G35, K36, R37, F67	D27, R33, G34, K35, R36, V37, F65	D28, R34, G35, K36, R37	D30, R36, G37, K38, V39, V40
T191	R36, K38, V40, H68, K70	T100A	R34, G35, K36, V38	M24, R33, G34, K35, V37	R34, G35, K36	R36, K38, V40, H68
C192	R36	S100B S100D	R34	R33	R34	R36
Y198	R36	Y100E	R34	R33	R34	R36
		D100H	H30, R34	F29, R33	F30, R34	F32, R36
		Light chain	32 contacts within 4A	47 contacts within 4A	37 contacts within 4A	34 contacts within 4A
		N31	G29, H30	D28, F29, M32	A29, F30	A31, F32
		Y32	H30, R34	F29, R33	F30, Q33, R34	F32, R36
		Y49	D28, R37	D27, R36	D28, R37	D30
		A50	H30	N28, F29	A29, F30	A31, F32
		S52		N28	A29	
		S53	D28, G29	D27, N28	D28, A29	D30, A31

**Table S5. Interface analysis for acetylcholine receptor–LNX neurotoxin complex, related to Figure 3**

nAChR	Krait
Subunit	134 contacts within 4A
W187	T6, A7, S9
V188	V39
Y189	T6, T8, S9, I11, V39, V40
Y190	D30, R36, G37, K38, V39, H68
T191	R36, K38, V40, H68, K70
C192	R36, K70
P194	I11, H68, Q71
P197	S9
Y198	R36
MAN7	A7
MAN10	T6, A7
Subunit	23 contacts within 4A
T38	A31
W57	F32
L121	F32
D165	S34
I178	A31
D180	D30
P181	C29, Y54
E182	W28, Y54, E55

**Table S6. Interface analysis for SNX-Fab complex, related to Figure 6**

B03 fab	Black mamba SNX
Heavy chain	88 contacts within 4A
S31	R31
A33	H30, R31
A50	H30
S52	H30
Y58	H30
E95	H30
G96	D29, R31
D97	W27, D29, R31
Y98	W27, D29
D99	D29, H30
Light chain	44 contacts within 4A
G29	K45
S30	K45, P46
K31	K45
D51	K45
N66	K45
W91	W27, R28, D29, V48
N93	W27, R28, G47
D95	H30
V96	H30

**Table S7. Interface analysis for acetylcholine receptor–SNX neurotoxin complex, related to Figure 6**

nAChR	Black mamba SNX
Subunit	69 contacts within 4A
Y93	R31
W187	Q7
V188	I34
Y189	Q7, S8, Q10
Y190	S8, D29, R31, T33, I34
T191	S8, T33, I35
P194	S9, Q10
Y198	R31
Subunit	47 contacts within 4A
T38	H30
W57	H30
L121	H30
D165	R28
Y172	R28
D180	W27, R28, D29
P181	R28, K45, P46, G47, I48
E182	K25, W27, K45, I48
F184	K45
T185	K45

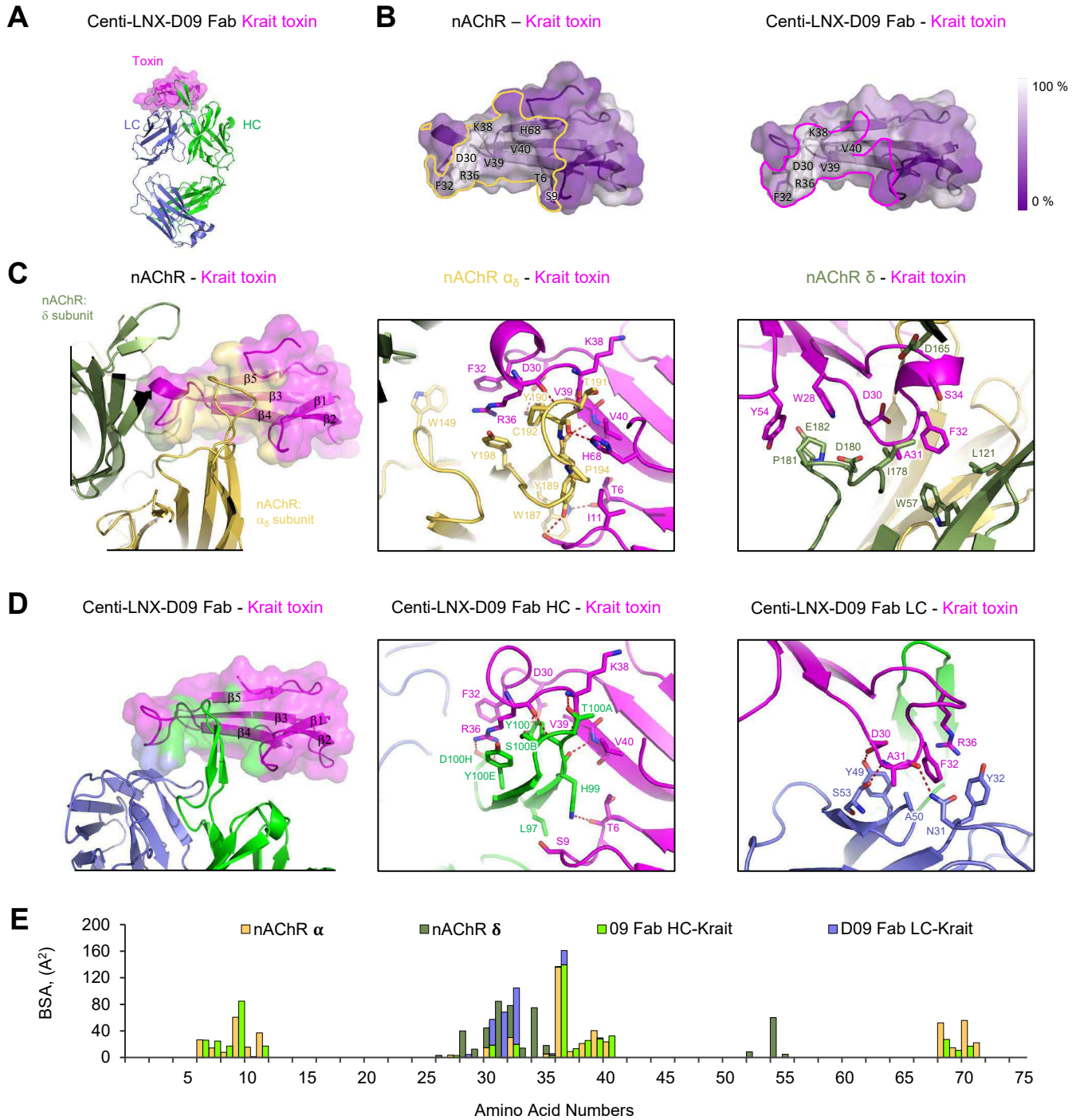
# **Data S1. X-ray data collection, refinement statistics, and Fab-toxin interface details, related to Figures 3 and 6**

	Page
<b>Table of contents</b>	1
<b>A. X-ray data statistics and structure analyses</b>	
X-ray data collection and refinement statistics, related to Figures 3 and 6	2
Crystal structure of Centi-LNX-D09 with Krait LNX, related to Figure 3	3
Crystal structure of Centi-LNX-D09 with Taipan LNX, related to Figure 3	4
Crystal structure of Centi-LNX-D09 with Cobra LNX, related to Figure 3	5
Crystal structure of Centi-LNX-D09 with Mamba LNX, related to Figure 3	6
<b>B. Interface PISA-based analyses</b>	
Interface analysis of AChR-alpha-bungarotoxin (PDB: 6UWZ), related to Figure 3	7
Interface analysis of Centi-LNX-D09 with Krait LNX, related to Figure 3	8
Interface analysis of Centi-LNX-D09 with Taipan LNX, related to Figure 3	9
Interface analysis of Centi-LNX-D09 with Cobra LNX, related to Figure 3	10
Interface analysis of Centi-LNX-D09 with Mamba LNX, related to Figure 3	11
Interface analysis of AChR-short chain neurotoxin (PDB: 7Z14), related to Figure 6	12
Interface analysis of Centi-SNX-B03 with Black mamba SNX, related to Figure 6	13

**Data S1. X-ray crystallography data collection and refinement statistics, related to Figures 3 and 6**

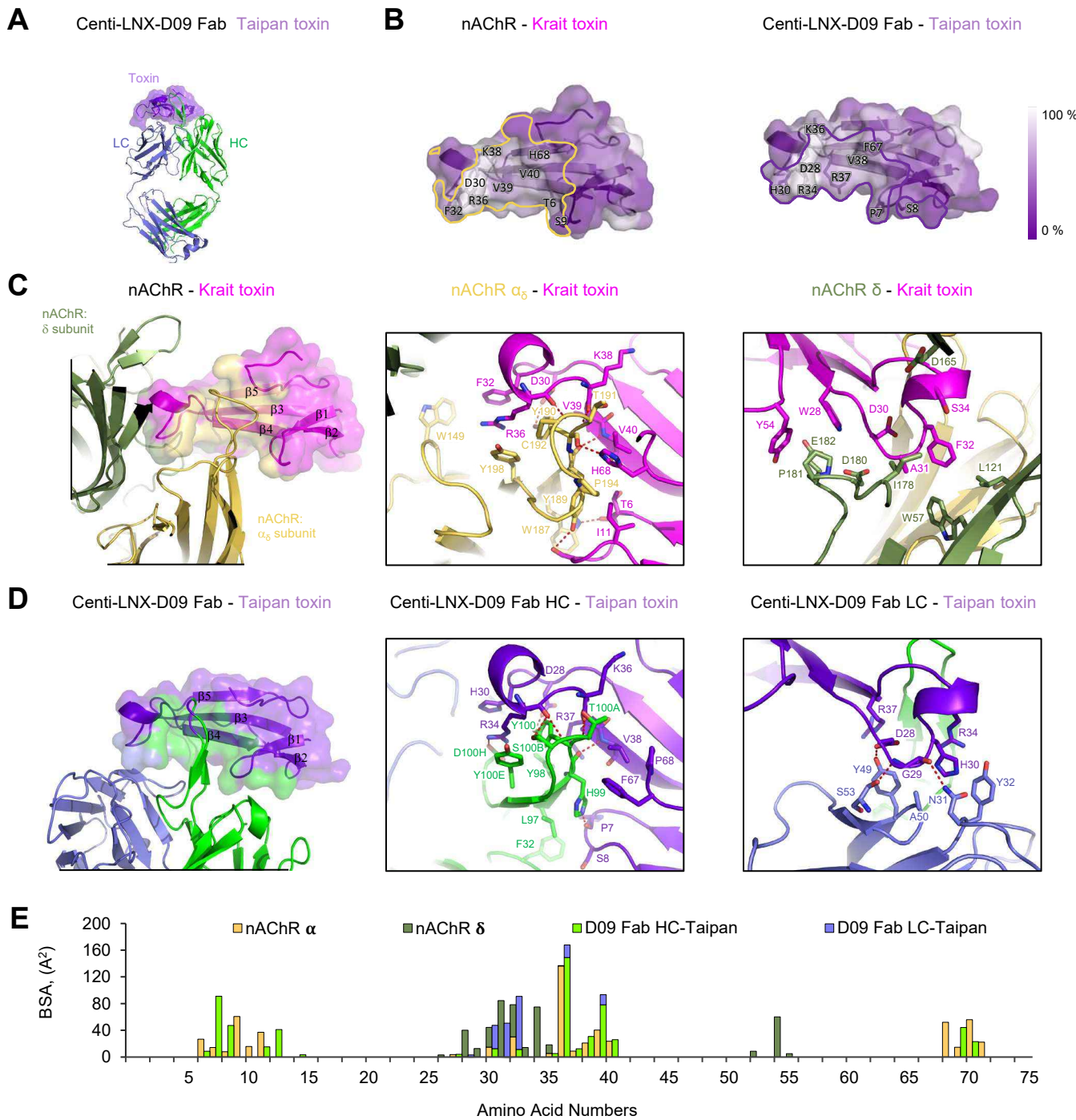
	Taipan-D09 PDB ID: 8D9Y	Cobra-D09 PDB ID: 8D9Z	Mamba-D09 PDB ID: 8DA0	Krait-D09 PDB ID: 8DA1	Black mamba-B03 PDB ID: 8V13
<b>Data collection</b>					
Space group	P1	P3 <sub>2</sub> 1	P2 <sub>1</sub>	C2	C2
Cell dimensions					
<i>a, b, c</i> (Å)	77.8, 87.2, 101.3	61.3, 61.3, 260.1	59.7, 145.5, 64.2	148.3, 63.9, 77.4	103.5, 72.3, 179.7
<i>, ,</i> (°)	109.3, 104.3, 106.5	90.0, 90.0, 90.0	90.0, 104.9, 90.0	90.0, 101.6, 90.0	90.0, 92.0, 90.0
Resolution (Å)	30.00–2.20 (2.28– 2.20)*	30.0–1.80 (1.86– 1.80)*	30.0–2.20 (2.28– 2.20)*	30.0–2.7 (2.80– 2.70)*	30.0–1.80 (1.86– 1.80)*
<i>R</i> <sub>merge</sub>	0.074 (0.400)*	0.118 (1.052)*	0.241 (0.630)*	0.248 (1.601)*	0.047 (0.809)*
<i>I</i> / <i>I</i>	8.6 (1.2)*	16.2 (1.3)*	5.9 (1.36)*	11.7 (1.5)*	22.3 (1.6)*
Completeness (%)	86.8 (76.1)*	98.8 (99.0)*	94.7 (80.8)*	98.7 (97.3)*	98.8 (98.0)*
Redundancy	2.0 (2.0)*	8.8 (7.6)*	2.8 (1.7)*	6.7 (4.2)*	3.7 (3.8)*
<b>Refinement</b>					
Resolution (Å)	30.0–2.2	30.0–1.8	30.0–2.2	30.0–2.7	30.0–1.80
No. reflections	98,262	52,273	49,249	18,010	119,970
<i>R</i> <sub>work</sub> / <i>R</i> <sub>free</sub>	0.209 / 0.262	0.165 / 0.198	0.196 / 0.249	0.185 / 0.241	0.181 / 0.229
No. atoms					
Protein	15,193	3,925	7,456	3,879	7,455
Ligand/ion	52	64	66	-	2
Water	955	351	544	-	863
<i>B</i> -factors (Å <sup>2</sup> )					
Protein	52.1	31.3	31.6	81.7	43.1
Ligand/ion	63.3	45.9	34.6	-	26.4
Water	47.9	41.9	29.6	-	44.9
R.m.s. deviations					
Bond lengths (Å)	0.003	0.012	0.008	0.007	0.012
Bond angles (°)	0.7	1.7	1.5	1.0	1.7

\*Values in parentheses are for highest-resolution shell.



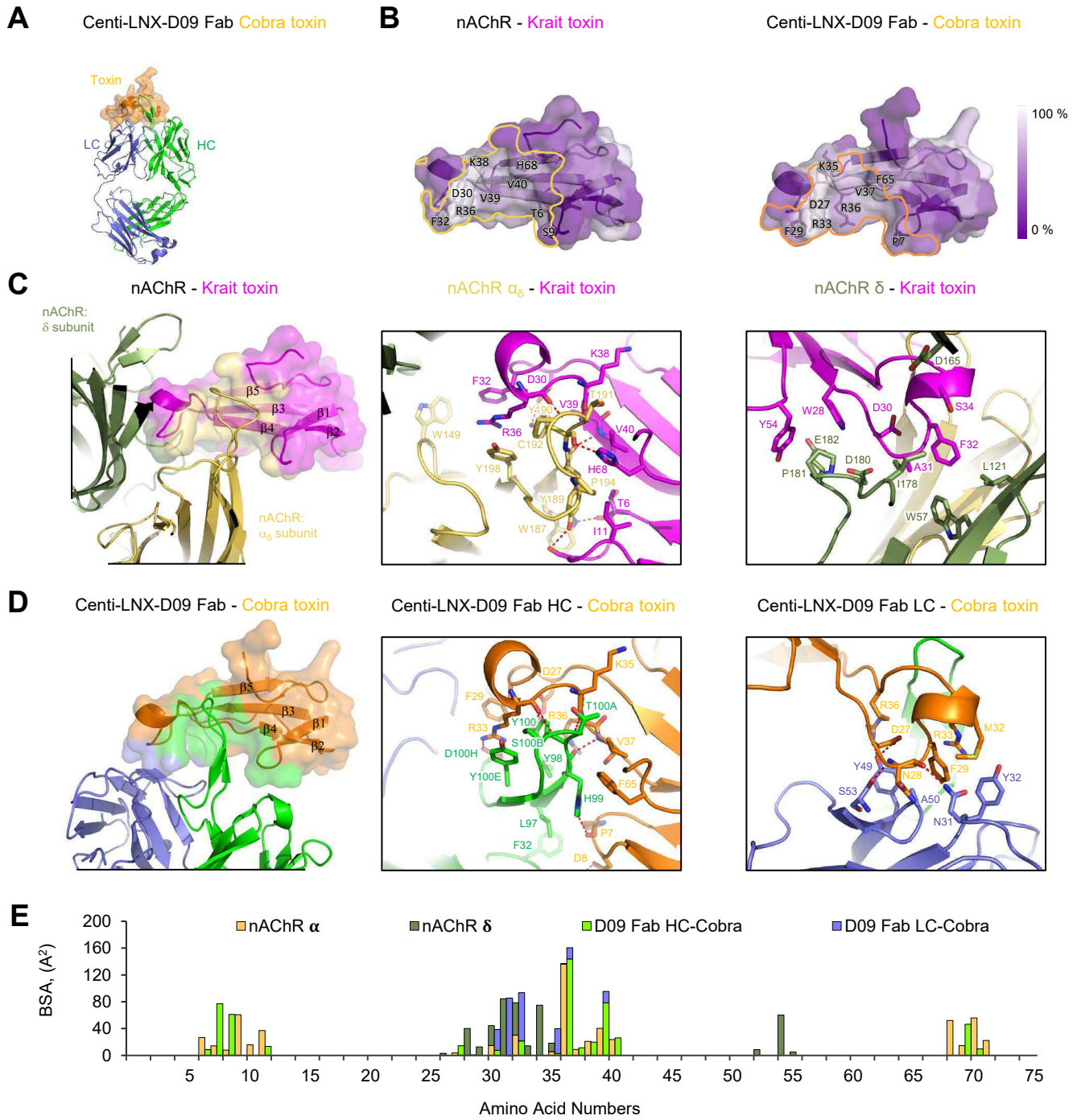
**Data S1. Complex of Fab Centi-LNX-D09 and krait toxin reveals a similar recognition pattern for antibody and nAChR, related to Figure 3**

(A) Crystal structure of Fab Centi-LNX-D09 complex with krait toxin. (B) Surface of krait toxin with its marked residues providing for binding of nAChR and Centi-LNX-D09. The surface of krait toxin is colored by sequence conservation, with white indicating 100% conservation. (C) Toxin recognition of acetylcholine receptor (PDB: 6UWZ); (left) Overview, subunits  $\alpha_5$  and  $\delta$  are shown as yellow and green cartoons. Krait toxin is shown as a semi-transparent surface with interface colored in yellow and green to indicate binding with subunits  $\alpha_5$  and  $\delta$ . Details of interactions of nAChR subunit  $\alpha_5$  (middle) and nAChR subunit  $\delta$  (right) with krait toxin. Interacting residues are shown in sticks. (D) Recognition of krait toxin by Centi-LNX-D09 (left), Overview, heavy and light chains are shown in green and slate cartoons. Krait toxin is shown as a semi-transparent surface with interface colored in green and slate to indicate binding with heavy and light chains. Details of interactions of Centi-LNX-D09 heavy (middle) and light (right) chains with krait toxin. Interacting residues are shown in sticks and numbered using Kabat system. (E) Diagram of krait toxin residues involved in binding of Centi-LNX-D09 and nAChR receptor demonstrates that they engage the same toxin residues. See also Figure 3 and Tables S3, S4.



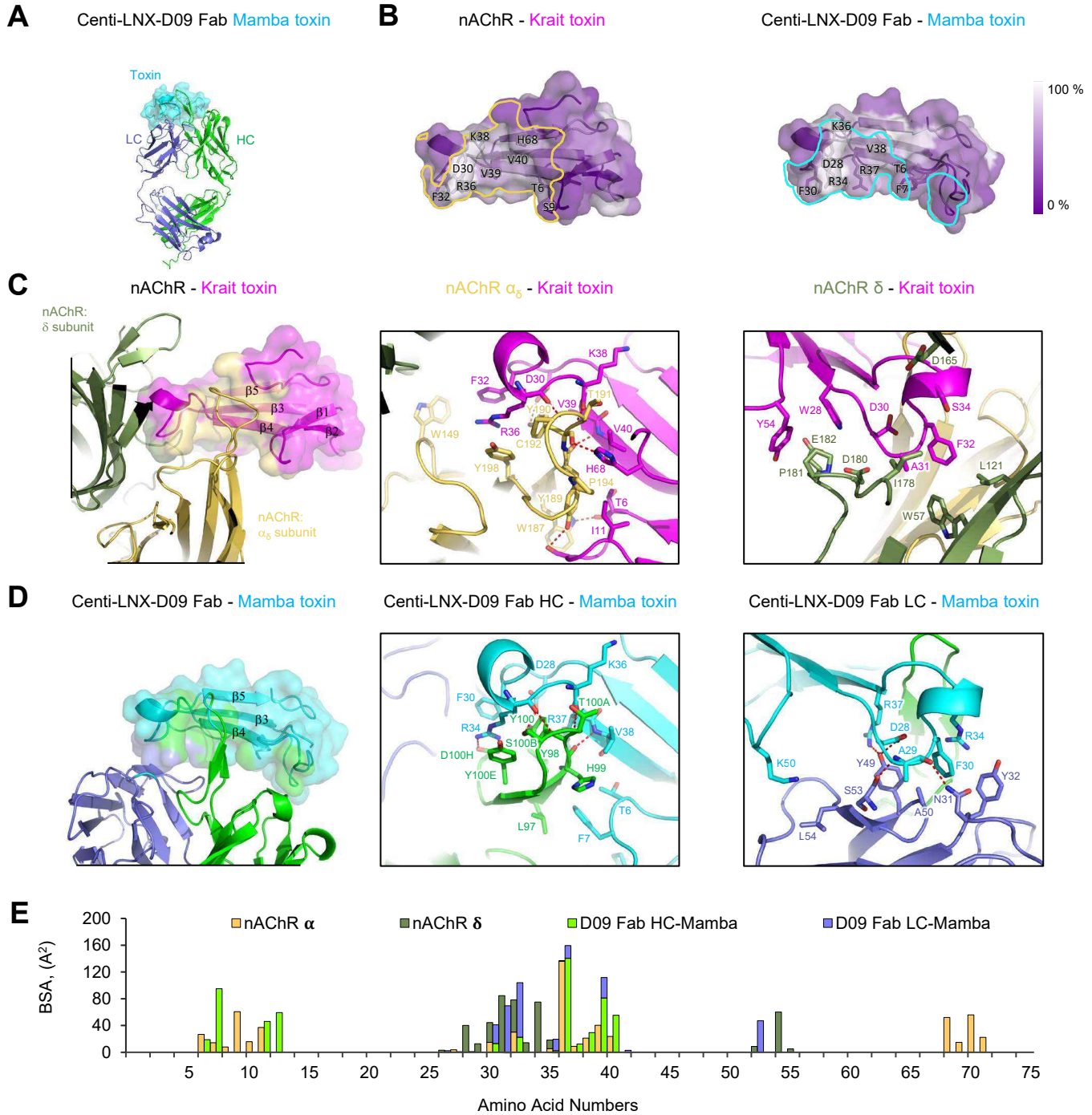
**Data S1. Complex of Fab Centi-LNX-D09 and taipan toxin reveals a similar recognition pattern for antibody and nAChR, related to Figure 3**

(A) Crystal structure of Fab Centi-LNX-D09 complex with taipan toxin. (B) Surface of krait and taipan toxins with their marked residues providing for binding of nAChR and Centi-LNX-D09, respectively. The surface of toxin is colored by sequence conservation, with white indicating 100% conservation. (C) Krait toxin recognition of acetylcholine receptor (PDB: 6UWZ); (left) Overview, subunits  $\alpha_\delta$  and  $\delta$  are shown as yellow and green cartoons. Krait toxin is shown as a semi-transparent surface with interface colored in yellow and green to indicate binding with subunits  $\alpha_\delta$  and  $\delta$ . Details of interactions of nAChR subunit  $\alpha_\delta$  (middle) and nAChR subunit  $\delta$  (right) with krait toxin. Interacting residues are shown in sticks. (D) Recognition of taipan toxin by Centi-LNX-D09 (left), Overview, heavy and light chains are shown in green and slate cartoons. Taipan toxin is shown as a semi-transparent surface with interface colored in green and slate to indicate binding with heavy and light chains. Details of interactions of Centi-LNX-D09 heavy (middle) and light (right) chains with taipan toxin. Interacting residues are shown in sticks and numbered using Kabat system. (E) Diagram of taipan and krait toxin residues involved in binding of Centi-LNX-D09 and nAChR receptor, respectively demonstrates that they engage the same toxin residues. See also Figure 3 and Tables S3, S4.



**Data S1. Complex of Fab Centi-LNX-D09 and cobra toxin reveals a similar recognition pattern for antibody and nAChR, related to Figure 3**

(A) Crystal structure of Fab Centi-LNX-D09 complex with cobra toxin. (B) Surface of krait and cobra toxins with their marked residues providing for binding of nAChR and Centi-LNX-D09, respectively. The surface of toxin is colored by sequence conservation, with white indicating 100% conservation. (C) Krait toxin recognition of acetylcholine receptor (PDB: 6UWZ); (left) Overview, subunits  $\alpha_5$  and  $\delta$  are shown as yellow and green cartoons. Krait toxin is shown as a semi-transparent surface with interface colored in yellow and green to indicate binding with subunits  $\alpha_5$  and  $\delta$ . Details of interactions of nAChR subunit  $\alpha_5$  (middle) and nAChR subunit  $\delta$  (right) with krait toxin. Interacting residues are shown in sticks. (D) Recognition of cobra toxin by Centi-LNX-D09 (left), Overview, heavy and light chains are shown in green and slate cartoons. Cobra toxin is shown as a semi-transparent surface with interface colored in green and slate to indicate binding with heavy and light chains. Details of interactions of Centi-LNX-D09 heavy (middle) and light (right) chains with cobra toxin. Interacting residues are shown in sticks and numbered using Kabat system. (E) Diagram of cobra and krait toxin residues involved in binding of Centi-LNX-D09 and nAChR receptor, respectively demonstrates that they engage the same toxin residues. See also Figure 3 and Tables S3, S4.



**Data S1. Complex of Fab Centi-LNX-D09 and mamba toxin reveals a similar recognition pattern for antibody and nAChR, related to Figure 3**

(A) Crystal structure of Fab Centi-LNX-D09 complex with mamba toxin. (B) Surface of krait and mamba toxins with their marked residues providing for binding of nAChR and Centi-LNX-D09, respectively. The surface of toxin is colored by sequence conservation, with white indicating 100% conservation. (C) Krait toxin recognition of acetylcholine receptor (PDB: 6UWZ); (left) Overview, subunits  $\alpha_\delta$  and  $\delta$  are shown as yellow and green cartoons. Krait toxin is shown as a semi-transparent surface with interface colored in yellow and green to indicate binding with subunits  $\alpha_\delta$  and  $\delta$ . Details of interactions of nAChR subunit  $\alpha_\delta$  (middle) and nAChR subunit  $\delta$  (right) with krait toxin. Interacting residues are shown in sticks. (D) Recognition of mamba toxin by Centi-LNX-D09 (left), Overview, heavy and light chains are shown in green and slate cartoons. Mamba toxin is shown as a semi-transparent surface with interface colored in green and slate to indicate binding with heavy and light chains. Details of interactions of Centi-LNX-D09 heavy (middle) and light (right) chains with mamba toxin. Interacting residues are shown in sticks and numbered using Kabat system. (E) Diagram of mamba and krait toxin residues involved in binding of Centi-LNX-D09 and nAChR receptor, respectively demonstrates that they engage the same toxin residues. See also Figure 3 and Tables S3, S4.

### Data S1. Acetylcholine receptor – alpha-bungarotoxin (PDB: 6UWZ) interface overall summary, related to Figure 3

Number of interface residues	Acetylcholine receptor	Alpha-bungarotoxin
Chain A (subunit α)	17	29
Chain B (subunit β)	16	13
Total residues	33	42

Interface, Å <sup>2</sup>	Acetylcholine receptor	Alpha-bungarotoxin
Chain A (subunit α)	812.1	739.4
Chain B (subunit β)	396.9	394.6
Total surface	1209.0	1134.0

### Data S1. Acetylcholine receptor – alpha-bungarotoxin (PDB: 6UWZ) interface details, related to Figure 3

#### H-bonds between acetylcholine receptor and alpha-bungarotoxin

	Acetylcholine receptor subunit	Distance Å	Alpha-bungarotoxin
1	A:TRP 187[ NE1]	2.58	F:THR 6[ O ]
2	A:TYR 189[ OH ]	3.05	F:SER 9[ OG ]
3	A:TYR 189[ OH ]	3.25	F:THR 8[ O ]
4	A:TYR 190[ OH ]	2.91	F:ASP 30[ OD2]
5	A:THR 191[ N ]	2.74	F:LYS 38[ O ]
6	A:THR 191[ N ]	3.49	F:ARG 36[ O ]
7	A:THR 191[ OG1]	2.94	F:LYS 38[ O ]
8	A:CYS 192[ N ]	2.73	F:ARG 36[ O ]
9	A:TYR 189[ O ]	2.98	F:VAL 40[ N ]
10	A:TYR 190[ O ]	2.64	F:HIS 68[ NE2]
11	F:THR 6[ OG1]	2.33	H:MAN 10[ O3 ]

#### Contribution of residues to the binding surface

Acetylcholine receptor			Alpha-bungarotoxin		
Residue	Bond	BSA Å <sup>2</sup>	Residue	Bond	BSA Å <sup>2</sup>
<b>Chain A subunit</b>					
A:TYR 93		11.88	F:THR 6	H	26.68
A:TRP 149		22.73	F:ALA 7		14.32
A:TRP 187	H	54.01	F:THR 8	H	7.94
A:VAL 188		19.97	F:SER 9	H	60.65
A:TYR 189	H	110.36	F:PRO 10		15.73
A:TYR 190	H	108.81	F:ILE 11		37.06
A:THR 191	H	112.85	F:MET 27		3.68
A:CYS 192	H	51.78	F:TRP 28		0.30
A:PRO 194		84.02	F:ASP 30	H	14.76
A:ASP 195		11.55	F:PHE 32		30.19
A:PRO 197		10.88	F:SER 35		5.41
A:TYR 198		42.61	F:ARG 36	H	136.24
A:LEU 199		0.50	F:GLY 37		8.95
			F:LYS 38	H	21.06
			F:VAL 39		40.40
			F:VAL 40	H	23.64
			F:HIS 68	H	52.11
			F:PRO 69		14.73
			F:LYS 70		55.89
			F:GLN 71		22.30

#### Contribution of residues to the binding surface

Acetylcholine receptor			Alpha-bungarotoxin		
Residue	Bond	BSA Å <sup>2</sup>	Residue	Bond	BSA Å <sup>2</sup>
<b>Chain H subunit</b>					
H:MAN 7		37.43	F:THR 6	H	24.15
H:MAN 8		4.17	F:ALA 7		71.62
H:MAN 9		19.02	F:THR 8		8.54
H:MAN 10	H	109.53	F:SER 9		0.73
			F:TYR 24		4.28
			F:VAL 39		1.17
			F:VAL 40		1.23
			F:GLU 41		31.90
			F:LEU 42		3.68

#### Contribution of residues to the binding surface

Acetylcholine receptor			Alpha-bungarotoxin		
Residue	Bond	BSA Å <sup>2</sup>	Residue	Bond	BSA Å <sup>2</sup>
<b>Chain B subunit</b>					
B:THR 38		16.68	F:LYS 26		3.19
B:TRP 57		30.42	F:TRP 28		39.88
B:ASP 59		11.54	F:CYS 29		12.66
B:ARG 113		5.03	F:ASP 30		29.66
B:THR 119		3.01	F:ALA 31		84.59
B:LEU 121		27.78	F:PHE 32		48.14
B:MET 163		11.25	F:CYS 33		14.26
B:THR 164		2.95	F:SER 34		74.98
B:ASP 165		42.76	F:SER 35		12.81
B:TYR 172		1.60	F:ARG 36		0.58
B:ILE 174		9.21	F:LYS 52		8.61
B:ILE 178		33.79	F:TYR 54	H	60.14
B:ILE 179		0.15	F:GLU 55		5.04
B:ASP 180		41.31			
B:PRO 181	H	77.06			
B:GLU 182		82.33			

<https://www.ebi.ac.uk/pdbe/pisa/>

**BSA** Buried Surface Area, Å<sup>2</sup>

**HSDC** Residues making Hydrogen/Disulphide bond, Salt bridge or Covalent link  
|||| Buried area percentage, one bar per 10%

### Data S1. D09 Fab – LNX interface overall summary, related to Figure 3

Number of residues for the epitope and paratope

	D09-taipan neurotoxin		D09-cobra neurotoxin		D09-mamba neurotoxin		D09-krait neurotoxin	
	Paratope	Epitope	Paratope	Epitope	Paratope	Epitope	Paratope	Epitope
Heavy chain	14	17	13	15	14	13	13	18
Light chain	7	6	9	7	11	10	6	7
Total surface	21	23	22	22	25	23	19	25

Binding surface area of the epitope and paratope (Å<sup>2</sup>)

	D09-taipan neurotoxin		D09-cobra neurotoxin		D09-mamba neurotoxin		D09-krait neurotoxin	
	Paratope	Epitope	Paratope	Epitope	Paratope	Epitope	Paratope	Epitope
Heavy chain	593.2	603.0	549.6	542.3	557.2	576.4	552.9	511.0
Light chain	198.6	202.3	256.9	260.5	280.3	299.2	198.0	221.6
Total surface	791.8	805.3	806.5	802.8	837.5	875.6	750.9	732.6

### Data S1. Krait LNX interface details, related to Figure 3

#### D09 fab – krait LNX neurotoxin hydrogen bonds

H-bonds	D09 fab	Distance Å	Krait LNX neurotoxin
<b>Heavy chain</b>			
1	B:TYR 100[ OH ]	2.49	I:ASP 30[ OD2]
2	B:THR 100A[ N ]	2.91	I:LYS 38[ O ]
3	B:THR 100A[ OG1]	3.52	I:ARG 36[ O ]
4	B:THR 100A[ OG1]	3.77	I:LYS 38[ O ]
5	B:SER 100B[ N ]	3.33	I:ARG 36[ O ]
6	B:SER 100B[ OG ]	2.64	I:ARG 36[ O ]
7	B:SER 100D[ OG ]	3.63	I:SER 9[ O ]
8	B:TYR 100F[ OH ]	2.45	I:SER 9[ OG ]
9	B:HIS 99[ O ]	2.99	I:VAL 40[ N ]
10	B:TYR 100[ O ]	3.56	I:HIS 68[ NE2]
11	B:TYR 100[ OH ]	3.49	I:ARG 36[ NH1]
12	B:THR 100A[ OG1]	3.09	I:LYS 38[ N ]
13	B:ASP 100H[ OD1]	3.04	I:ARG 36[ NH2]
14	B:ASP 100H[ OD2]	3.06	I:ARG 36[ NH1]
<b>Light chain</b>			
1	A:TYR 49[ OH ]	2.3	I:ASP 30[ OD1]
2	A:ASN 31[ ND2]	3.14	I:ALA 31[ O ]
3	A:SER 53[ OG ]	3.01	I:ALA 31[ N ]

#### Contribution of residues to the binding surface

D09 fab	Krait LNX neurotoxin				
Residue	Bond	BSA, Å <sup>2</sup>	Residue	Bond	BSA, Å <sup>2</sup>
<b>Heavy chain</b>					
B:ASN 31		28.75	I:THR 6		25.99
B:PHE 32		8.29	I:ALA 7		24.82
B:LEU 97		21.45	I:THR 8		17.25
B:TYR 98		9.28	I:SER 9	H	84.80
B:HIS 99	H	125.85	I:PRO 10		1.51
B:TYR 100	H	118.48	I:ILE 11		17.34
B:THR 100A	H	115.99	I:MET 27		2.97
B:SER 100B	H	19.13	I:ASP 30	H	18.55
B:GLY 100C		0.82	I:PHE 32		19.91
B:SER 100D	H	12.73	I:SER 35		3.20
B:TYR 100E		39.04	I:ARG 36	HS	139.74
B:TYR 100F	H	16.52	I:GLY 37		13.17
B:ASP 100H	HS	36.58	I:LYS 38	H	25.75
			I:VAL 39		28.12
			I:VAL 40	H	32.70
			I:HIS 68	H	27.32
			I:PRO 69		10.74
			I:LYS 70		17.09
<b>Light chain</b>					
A:ASN 31	H	32.88	I:TRP 28		4.53
A:TYR 32		50.80	I:ASP 30	H	38.89
A:TYR 49	H	46.71	I:ALA 31	H	68.34
A:ALA 50		31.25	I:PHE 32		84.76
A:SER 52		10.55	I:SER 35		2.58
A:SER 53	H	25.85	I:ARG 36		21.20
			I:VAL 39		1.34

<https://www.ebi.ac.uk/pdbe/pisa/>

**BSA** Buried Surface Area, Å<sup>2</sup>

**HSDC** Residues making Hydrogen/Disulphide bond, Salt bridge or Covalent link

|||| Buried area percentage, one bar per 10%

### Data S1. D09 Fab – LNX interface overall summary, related to Figure 3

Number of residues for the epitope and paratope

	D09-taipan neurotoxin		D09-cobra neurotoxin		D09-mamba neurotoxin		D09-krait neurotoxin	
	Paratope	Epitope	Paratope	Epitope	Paratope	Epitope	Paratope	Epitope
Heavy chain	14	17	13	15	14	13	13	18
Light chain	7	6	9	7	11	10	6	7
Total surface	21	23	22	22	25	23	19	25

Binding surface area of the epitope and paratope (Å<sup>2</sup>)

	D09-taipan neurotoxin		D09-cobra neurotoxin		D09-mamba neurotoxin		D09-krait neurotoxin	
	Paratope	Epitope	Paratope	Epitope	Paratope	Epitope	Paratope	Epitope
Heavy chain	593.2	603.0	549.6	542.3	557.2	576.4	552.9	511.0
Light chain	198.6	202.3	256.9	260.5	280.3	299.2	198.0	221.6
Total surface	791.8	805.3	806.5	802.8	837.5	875.6	750.9	732.6

### Data S1. Taipan LNX interface details, related to Figure 3

#### D09 fab – taipan LNX neurotoxin hydrogen bonds

H-bonds	D09 fab	Distance Å	Taipan LNX neurotoxin
<b>Heavy chain</b>			
1	B:HIS 99[ NE2]	2.21	I:PRO 7[ O ]
2	B:TYR 100[ OH ]	2.23	I:ASP 28[ OD2]
3	B:THR 100A[ OG1]	3.85	I:ARG 34[ O ]
4	B:SER 100B[ N ]	3.39	I:ARG 34[ O ]
5	B:SER 100B[ OG ]	2.68	I:ARG 34[ O ]
6	B:THR 100A[ N ]	3.11	I:LYS 36[ O ]
7	B:ASN 31[ OD1]	3.01	I:ARG 10[ NH2]
8	B:HIS 99[ O ]	2.91	I:VAL 38[ N ]
9	B:HIS 99[ O ]	3.88	I:ARG 37[ NH2]
10	B:TYR 100[ OH ]	3.31	I:ARG 34[ NH1]
11	B:THR 100A[ OG1]	3.86	I:LYS 36[ N ]
12	B:ASP 100H[ OD2]	2.79	I:ARG 34[ NH1]
13	B:ASP 100H[ OD1]	2.93	I:ARG 34[ NH1]
14	B:ASP 100H[ OD1]	3.42	I:ARG 34[ NH2]
<b>Light chain</b>			
1	A:TYR 49[ OH ]	2.24	I:ASP 28[ OD1]
2	A:ASN 31[ ND2]	3.04	I:GLY 29[ O ]
3	A:ASN 31[ OD1]	3.23	I:HIS 30[ NE2]
4	A:TYR 32[ OH ]	3.32	I:ARG 34[ NH2]
5	A:TYR 49[ OH ]	3.78	I:ARG 37[ NE ]
6	A:SER 53[ OG ]	3.07	I:GLY 29[ N ]

#### Contribution of residues to the binding surface

D09 fab		Taipan LNX neurotoxin			
Residue	Bond	BSA, Å <sup>2</sup>	Residue	Bond	BSA, Å <sup>2</sup>
<b>Heavy chain</b>					
B:GLY 26	H	3.32	I:THR 6	H	8.65
B:THR 28	H	14.05	I:PRO 7	H	90.93
B:ASN 31	H	43.96	I:SER 8	H	47.26
B:PHE 32	H	23.64	I:VAL 9	H	15.22
B:ARG 94	H	18.65	I:ARG 10	H	41.16
B:LEU 97	H	27.46	I:GLU 12	H	3.32
B:TYR 98	H	35.53	I:THR 25	H	4.02
B:HIS 99	H	127.64	I:ASP 28	H	12.50
B:TYR 100	H	110.09	I:HIS 30	H	11.41
B:THR 100A	H	90.52	I:SER 33	H	5.16
B:SER 100B	H	20.83	I:ARG 34	HS	149.03
B:GLY 100C	H	5.51	I:GLY 35	H	12.28
B:TYR 100E	H	40.15	I:LYS 36	H	30.78
B:ASP 100H	HS	31.90	I:ARG 37	H	78.11
			I:VAL 38	H	25.95
			I:PHE 67		44.19
			I:PRO 68		23.04
<b>Light chain</b>					
A:ASN 31	H	37.87	I:TRP 26	H	3.16
A:TYR 32	H	45.26	I:ASP 28	H	34.91
A:TYR 49	H	49.53	I:GLY 29	H	50.81
A:ALA 50	H	26.58	I:HIS 30	H	79.48
A:SER 52	H	7.86	I:ARG 34	H	18.82
A:SER 53	H	25.08	I:ARG 37	H	15.16
A:GLU 55	H	6.38			

<https://www.ebi.ac.uk/pdbe/pisa/>

**BSA** Buried Surface Area, Å<sup>2</sup>

**HSDC** Residues making Hydrogen/Disulphide bond, Salt bridge or Covalent link

||| Buried area percentage, one bar per 10%

### Data S1. D09 Fab – LNX interface overall summary, related to Figure 3

Number of residues for the epitope and paratope								
	D09-taipan neurotoxin		D09-cobra neurotoxin		D09-mamba neurotoxin		D09-krait neurotoxin	
	Paratope	Epitope	Paratope	Epitope	Paratope	Epitope	Paratope	Epitope
Heavy chain	14	17	13	15	14	13	13	18
Light chain	7	6	9	7	11	10	6	7
Total surface	21	23	22	22	25	23	19	25

Binding surface area of the epitope and paratope (Å²)								
	D09-taipan neurotoxin		D09-cobra neurotoxin		D09-mamba neurotoxin		D09-krait neurotoxin	
	Paratope	Epitope	Paratope	Epitope	Paratope	Epitope	Paratope	Epitope
Heavy chain	593.2	603.0	549.6	542.3	557.2	576.4	552.9	511.0
Light chain	198.6	202.3	256.9	260.5	280.3	299.2	198.0	221.6
Total surface	791.8	805.3	806.5	802.8	837.5	875.6	750.9	732.6

### Data S1. Cobra LNX interface details, related to Figure 3

#### D09 fab – cobra LNX neurotoxin hydrogen bonds

H-bonds	D09 fab	Distance Å	Cobra LNX neurotoxin
<b>Heavy chain</b>			
1	B:THR 28[ OG1]	2.49	D:ASP 8[ OD2]
2	B:ASN 31[ ND2]	2.96	D:ASP 8[ OD1]
3	B:TYR 100[ OH ]	2.71	D:ASP 27[ OD2]
4	B:THR 100A[ N ]	3.03	D:LYS 35[ O ]
5	B:THR 100A[ OG1]	3.77	D:ARG 33[ O ]
6	B:SER 100B[ N ]	3.4	D:ARG 33[ O ]
7	B:SER 100B[ OG ]	2.51	D:ARG 33[ O ]
8	B:HIS 99[ O ]	2.92	D:VAL 37[ N ]
9	B:THR 100A[ OG1]	3.8	D:LYS 35[ N ]
10	B:ASP 100H[ OD1]	2.76	D:ARG 33[ NH2]
11	B:ASP 100H[ OD2]	2.78	D:ARG 33[ NH1]
12	B:ASP 100H[ OD1]	3.5	D:ARG 33[ NH1]
13	B:ASP 100H[ OD1]	2.76	D:ARG 33[ NH2]
14	B:ASP 100H[ OD2]	2.78	D:ARG 33[ NH1]
15	B:ASP 100H[ OD2]	3.52	D:ARG 33[ NH2]
<b>Light chain</b>			
1	A:TYR 49[ OH ]	2.65	D:ASP 27[ OD2]
2	A:ASN 31[ ND2]	2.91	D:ASN 28[ O ]
3	A:TYR 49[ OH ]	3.01	D:ARG 36[ NH2]
4	A:ALA 50[ O ]	2.87	D:ASN 28[ ND2]
5	A:SER 53[ OG ]	2.9	D:ASN 28[ N ]

#### Contribution of residues to the binding surface

D09 fab			Cobra LNX neurotoxin		
Residue	Bond	BSA, Å²	Residue	Bond	BSA, Å²
<b>Heavy chain</b>					
B:PHE 27		0.84	D:THR 6		8.71
B:THR 28	H	23.51	D:PRO 7		77.03
B:ASN 31	H	28.50	D:ASP 8	H	61.11
B:PHE 32		23.48	D:VAL 9		13.56
B:LEU 97		19.04	D:MET 24		14.55
B:TYR 98		36.27	D:ASP 27	H	7.57
B:HIS 99	H	120.69	D:PHE 29		21.50
B:TYR 100	H	111.03	D:MET 32		2.70
B:THR 100A	H	89.44	D:ARG 33	HS	143.72
B:SER 100B	H	20.37	D:GLY 34		11.36
B:GLY 100C		2.18	D:LYS 35	H	19.83
B:TYR 100E		35.63	D:ARG 36		78.31
B:ASP 100H	HS	38.61	D:VAL 37	H	26.12
			D:PHE 65		46.56
			D:PRO 66		9.67
<b>Light chain</b>					
A:SER 30		3.34	D:TRP 25		0.89
A:ASN 31	H	58.62	D:ASP 27	H	31.07
A:TYR 32		53.30	D:ASN 28	H	85.48
A:TYR 49	H	55.50	D:PHE 29		72.05
A:ALA 50	H	34.82	D:MET 32		37.06
A:ALA 51		2.23	D:ARG 33		16.73
A:SER 52		19.87	D:ARG 36	H	17.18
A:SER 53	H	26.78			
A:GLY 66		2.46			

<https://www.ebi.ac.uk/pdbe/pisa/>

**BSA** Buried Surface Area, Å²

**HSDC** Residues making Hydrogen/Disulphide bond, Salt bridge or Covalent link  
||| Buried area percentage, one bar per 10%

### Data S1. D09 Fab – LNX interface overall summary, related to Figure 3

Number of residues for the epitope and paratope								
	D09-taipan neurotoxin		D09-cobra neurotoxin		D09-mamba neurotoxin		D09-krait neurotoxin	
	Paratope	Epitope	Paratope	Epitope	Paratope	Epitope	Paratope	Epitope
Heavy chain	14	17	13	15	14	13	13	18
Light chain	7	6	9	7	11	10	6	7
Total surface	21	23	22	22	25	23	19	25

Binding surface area of the epitope and paratope (Å²)								
	D09-taipan neurotoxin		D09-cobra neurotoxin		D09-mamba neurotoxin		D09-krait neurotoxin	
	Paratope	Epitope	Paratope	Epitope	Paratope	Epitope	Paratope	Epitope
Heavy chain	593.2	603.0	549.6	542.3	557.2	576.4	552.9	511.0
Light chain	198.6	202.3	256.9	260.5	280.3	299.2	198.0	221.6
Total surface	791.8	805.3	806.5	802.8	837.5	875.6	750.9	732.6

### Data S1. Mamba LNX interface details, related to Figure 3

#### D09 fab – mamba LNX neurotoxin hydrogen bonds

H-bonds	D09 fab	Distance Å	Mamba LNX neurotoxin
<b>Heavy chain</b>			
1	B:TYR 100[ OH ]	2.52	E:ASP 28[ OD2]
2	B:THR 100A[ OG1]	3.8	E:ARG 34[ O ]
3	B:SER 100B[ N ]	3.42	E:ARG 34[ O ]
4	B:THR 100A[ N ]	3.19	E:LYS 36[ O ]
5	B:THR 28[ OG1]	3.23	E:GLN 10[ NE2]
6	B:HIS 99[ O ]	2.77	E:VAL 38[ N ]
7	B:TYR 100[ OH ]	3.64	E:ARG 34[ NH1]
8	B:THR 100A[ OG1]	3.76	E:LYS 36[ N ]
9	B:ASP 100H[ OD1]	3.06	E:ARG 34[ NH2]
10	B:ASP 100H[ OD2]	2.61	E:ARG 34[ NH1]
11	B:ASP 100H[ OD1]	3.06	E:ARG 34[ NH2]
12	B:ASP 100H[ OD1]	3.51	E:ARG 34[ NH1]
13	B:ASP 100H[ OD2]	3.67	E:ARG 34[ NH2]
14	B:ASP 100H[ OD2]	2.61	E:ARG 34[ NH1]
<b>Light chain</b>			
1	A:TYR 49[ OH ]	2.59	E:ASP 28[ OD2]
2	A:ASN 31[ ND2]	3.1	E:ALA 29[ O ]
3	A:TYR 32[ OH ]	3.46	E:GLN 33[ OE1]
4	A:TYR 49[ OH ]	3	E:ARG 37[ NH1]
5	A:SER 53[ OG ]	2.97	E:ALA 29[ N ]

#### Contribution of residues to the binding surface

D09 fab			Mamba LNX neurotoxin		
Residue	Bond	BSA, Å²	Residue	Bond	BSA, Å²
<b>Heavy chain</b>					
B:GLY 26		10.23	E:THR 6		18.87
B:PHE 27		19.53	E:PHE 7		94.98
B:THR 28	H	51.27	E:ASP 9		46.06
B:ASN 31		36.11	E:GLN 10	H	59.33
B:PHE 32		11.09	E:THR 25		0.84
B:LEU 97		30.87	E:ASP 28	H	13.04
B:TYR 98		43.18	E:PHE 30		22.41
B:HIS 99	H	98.62	E:GLN 33		2.26
B:TYR 100	H	99.03	E:ARG 34	HS	140.43
B:THR 100A	H	53.01	E:GLY 35		12.31
B:SER 100B	H	20.15	E:LYS 36	H	29.32
B:SER 100D		7.73	E:ARG 37		81.26
B:TYR 100E		37.66	E:VAL 38	H	55.30
B:ASP 100H	HS	38.72			
<b>Light chain</b>					
A:ASN 31	H	34.66	E:LYS 24		2.37
A:TYR 32	H	60.57	E:TRP 26		1.02
A:TYR 49	H	57.68	E:ASP 28	H	27.96
A:ALA 50		31.84	E:ALA 29	H	69.49
A:SER 52		11.66	E:PHE 30		81.70
A:SER 53	H	28.27	E:GLN 33	H	17.12
A:LEU 54		24.57	E:ARG 34		19.06
A:GLU 55		10.43	E:ARG 37	H	30.45
A:SER 56		4.72	E:GLU 39		2.82
A:VAL 58		5.03	E:LYS 50		47.20
A:SER 60		10.89			

<https://www.ebi.ac.uk/pdbe/pisa/>

**BSA** Buried Surface Area, Å²

**HSDC** Residues making Hydrogen/Disulphide bond, Salt bridge or Covalent link  
|||| Buried area percentage, one bar per 10%

### Data S1. Acetylcholine receptor – SNX interface overall summary, related to Figure 6

Number of interface residues	Acetylcholine receptor	SNX
Chain C	17	10
Chain D	12	13
Total residues	29	23

Interface, Å <sup>2</sup>	Acetylcholine receptor	SNX
Chain C	430.0	442.1
Chain D	501.0	480.7
Total surface	943.1	910.7

### Data S1. Acetylcholine receptor – SNX (PDB: 7Z14) interface details, related to Figure 6

#### H-bonds between acetylcholine receptor and SNX

	Acetylcholine receptor	Distance Å	SNX
<b>Chain C subunit</b>			
1	C:GLU 182[ OE1]	2.98	F:LYS 25[ NZ ]
2	C:ASP 165[ OD2]	2.84	F:ARG 28[ NH1 ]
3	C:PHE 184[ O ]	2.44	F:LYS 45[ NZ ]
4	C:GLU 182[ O ]	3.00	F:LYS 45[ NZ ]
5	C:GLU 182[ OE1]	2.98	F:LYS 25[ NZ ]
6	C:GLU 182[ OE2]	3.32	F:LYS 25[ NZ ]
7	C:ASP 165[ OD2]	2.84	F:ARG 28[ NH1 ]
8	C:ASP 165[ OD2]	3.25	F:ARG 28[ NH2 ]
<b>Chain D subunit</b>			
1	D:TYR 190[ OH ]	3.05	F:ASP 29[ OD1 ]
2	D:THR 191[ N ]	3.12	F:THR 33[ O ]
3	D:THR 191[ OG1 ]	3.25	F:THR 33[ O ]
4	D:TRP 187[ O ]	3.39	F:GLN 7[ NE2 ]
5	D:TYR 190[ OH ]	3.33	F:ARG 31[ NH2 ]
6	D:TYR 190[ OH ]	3.15	F:ARG 31[ NE ]
7	D:PRO 194[ O ]	2.25	F:GLN 10[ NE2 ]

#### Contribution of residues to the binding surface

Acetylcholine receptor			SNX		
Residue	Bond	BSA Å <sup>2</sup>	Residue	Bond	BSA Å <sup>2</sup>
<b>Chain C subunit</b>					
C:THR 38		16.45	F:LYS 25	HS	19.10
C:TRP 57		31.70	F:TRP 27		41.85
C:LEU 121		29.96	F:ARG 28	HS	97.92
C:ASP 165	HS	25.79	F:ASP 29		34.45
C:THR 166		1.73	F:HIS 30		114.22
C:ILE 167		3.01	F:ARG 31		1.17
C:TYR 172	H	7.61	F:LYS 45	H	87.82
C:ILE 174		7.70	F:PRO 46		11.16
C:ILE 178		42.35	F:GLY 47		14.63
C:ILE 179		2.19	F:ILE 48		19.75
C:ASP 180		45.28			
C:PRO 181		99.94			
C:GLU 182	HS	92.83			
C:PHE 184	H	10.81			
C:THR 185		10.88			
C:GLU 186		0.15			
C:ASP 496		1.60			
<b>Chain D subunit</b>					
D:TYR 93		36.67	F:GLN7	H	65.61
D:ILE 148		0.37	F:SER8	H	41.13
D:TRP 149		23.57	F:SER9		55.19
D:TRP 187	H	18.34	F:GLN 10	H	72.24
D:VAL 188		31.47	F:PRO 11		4.19
D:TYR 189		82.03	F:TRP 27		0.31
D:TYR 190	H	102.62	F:ASP 29	H	10.70
D:THR 191	H	84.80	F:HIS 30		20.89
D:CYS 192		7.10	F:ARG 31	H	115.33
D:PRO 194	H	49.27	F:GLY 32		18.23
D:ASP 195		8.94	F:THR 33	H	38.13
D:TYR 198		35.54	F:ILE 34		43.87
			F:ILE 35		15.16

<https://www.ebi.ac.uk/pdbe/pisa/>

**BSA** Buried Surface Area, Å<sup>2</sup>

**HSDC** Residues making Hydrogen/Disulphide bond, Salt bridge or Covalent link  
|||| Buried area percentage, one bar per 10%

### Data S1. B03 – Black mamba SNX interface overall summary, related to Figure 6

Number of interface residues	Paratope	Epitope
Heavy chain	15	11
Light chain	13	9
Total residues	28	20

Interface, Å <sup>2</sup>	Paratope	Epitope
Heavy chain	384.6	391.4
Light chain	332.2	355.4
Total surface	716.8	746.8

### Data S1. Black mamba SNX interface details, related to Figure 6

#### B03 fab – black mamba SNX hydrogen bonds

	B03 fab	Distance Å	Black mamba SNX
<b>Heavy chain</b>			
1	H:TYR 98[N ]	3.09	T:ASP 29[ OD2]
2	H:TYR 58[ OH ]	3.09	T:HIS 30[ O ]
3	H:ASP 99[ OD1]	2.83	T:HIS 30[ N ]
4	H:GLU 95[ OE1]	2.77	T:HIS 30[ ND1]
5	H:ASP 97[ OD1]	2.80	T:ARG 31[ NH2]
6	H:GLU 95[ OE2]	3.06	T:HIS 30[ ND1]
7	H:ASP 99[ OD2]	3.28	T:HIS 30[ NE2]
<b>Light chain</b>			
1	L:TRP 91[ NE1]	3.06	T:ARG 28[ O ]
2	L:ASN 93[ ND2]	2.98	T:GLY 47[ O ]
3	L:ASN 93[ OD1]	2.84	T:ARG 28[ N ]
4	L:ASP 95A[ O ]	2.83	T:HIS 30[ NE2]
5	L:GLY 29[ O ]	2.96	T:LYS 45[ NZ ]
6	L:ASP 51[ OD2]	2.68	T:LYS 45[ NZ ]

#### Contribution of residues to the binding surface

B03 fab	Black mamba SNX neurotoxin				
Residue	Bond	BSA Å <sup>2</sup>	Residue	Bond	BSA Å <sup>2</sup>
<b>Heavy chain</b>					
H:SER 31		17.04	T:GLN 7		9.01
H:TYR 32		11.63	T:LYS 25		15.85
H:ALA 33		30.36	T:TRP 27		43.37
H:TRP 47		12.22	T:ARG 38		10.77
H:ALA 50		6.55	T:ASP 29	H	38.61
H:SER 52		18.58	T:HIS 30	HS	148.92
H:GLY 52A		4.97	T:ARG 31	HS	112.93
H:SER 56		2.95	T:GLY 32		1.15
H:TYR 58	H	53.37	T:ILE 34		0.16
H:GLU 95	HS	7.71	T:GLU 36		7.00
H:GLY 96		19.56	T:VAL 48		3.66
H:ASP 97	HS	57.59			
H:TYR 98	H	91.21			
H:ASP 99	HS	49.79			
H:MET 100A		1.06			
<b>Light chain</b>					
L:GLY 29	H	9.81	T:LYS 25		10.21
L:SER 30		53.06	T:TRP 27		19.06
L:LYS 31		7.20	T:ARG 28	H	44.23
L:SER 32		5.70	T:ASP 29		13.61
L:ASP 50		15.27	T:HIS 30	H	53.14
L:ASP 51	HS	14.40	T:LYS 45	HS	115.00
L:ASN 66		0.74	T:PRO 46		42.79
L:TRP 91	H	67.51	T:GLY 47	H	35.68
L:ASP 92		0.25	T:VAL 48		21.68
L:ASN 93	H	91.33			
L:ASN 94		17.89			
L:ASP 95A	H	28.95			
L:VAL 96		20.12			

<https://www.ebi.ac.uk/pdbe/pisa/>

**BSA** Buried Surface Area, Å<sup>2</sup>

**HSDC** Residues making Hydrogen/Disulphide bond, Salt bridge or Covalent link

|||| Buried area percentage, one bar per 10%